



The Quenching and Steam Explosions of Drops of Molten Silicon Released into Water

L.S. Nelson, P.W. Brooks, R. Bonazza,
M.L. Corradini, K. Hildal

November 2004

UWFDM-1229

FUSION TECHNOLOGY INSTITUTE
UNIVERSITY OF WISCONSIN
MADISON WISCONSIN

The Quenching and Steam Explosions of Drops of Molten Silicon Released into Water

L.S. Nelson, P.W. Brooks, R. Bonazza, M.L.
Corradini, K. Hildal*

Fusion Technology Institute
University of Wisconsin
1500 Engineering Drive
Madison, WI 53706

<http://fti.neep.wisc.edu>

November 2004

UWFDM-1229

*Institute of Metallurgy, Norwegian University of Science and Technology,
N-7491 Trondheim, Norway

ABSTRACT

The release of 9 mm-diameter drops of molten silicon into water at room temperature was compared with the release of 9 mm-diameter drops of molten ferrosilicon studied previously. No catastrophic effects or spontaneous explosions occurred with either material. Drops of molten silicon generate bubbles of hydrogen as they quench in water; ferrosilicon drops do not. Also, silicon drops fall through the water more slowly than ferrosilicon drops.

Steam explosions of drops of both materials can be triggered with pressure transients generated in the water with a mechanical impactor. Stronger pressure transients are required to initiate the explosions of the silicon drops than for the ferrosilicon drops. Silicon drops cannot be triggered at depths as great as the comparable ferrosilicon drops.

Drops of molten silicon 9 mm in diameter that quench quiescently in water at room temperature generate about 1 ml of hydrogen per gram of melt; those triggered to explode, not more than 6 ml/g (both STP). At most, only about 0.4% of the silicon oxidizes during even the most vigorous explosions, indicating that combustion does not add significantly to the energy release or generation of colloid during explosive molten silicon-water interactions.

Small amounts of calcium (0.04 w/o) and/or aluminum (0.4 w/o) alloyed with the silicon seem to reduce the tendency for drops of melt to explode and to deposit colloid in the water during triggered interactions. Also, less hydrogen seemed to be generated when the alloy contained only the calcium additive.

Alloyed silicon drops fell through the water more than twice as fast as the non-alloyed drops.

In a calibration experiment, a drop of non-alloyed molten silicon was triggered to explode a known distance from a transducer. The explosion produced a steam bubble that collapsed and generated a pressure transient as strong as the original triggering pulse.

INTRODUCTION

This report summarizes the quenching and steam explosion studies performed with drops of molten silicon at the University of Wisconsin-Madison during 1999. We performed these studies with the apparatus and procedures largely as developed during 1996-1998 to study the steam explosions of drops of molten ferrosilicon (75 wt.% Si) (Nelson et al., 1996-1999; also see the compilation of reports in Appendix A).

We performed the 1999 work by releasing 9 mm-diameter drops of molten silicon with and without added Al and Ca into water at room temperature. This allowed us to compare the new observations directly with the previous studies of 9 mm- and 11 mm-diameter drops of molten ferrosilicon.

In the earliest stages of the 1999 work, we made the following comparisons between 9 mm-diameter drops of molten pure silicon and 9 mm-diameter drops of molten ferrosilicon:

- There are no catastrophic effects when drops of either molten silicon or ferrosilicon fall onto ice or into liquid water.
- Drops of molten silicon or ferrosilicon do not explode spontaneously when released into water at room temperature.
- Drops of molten silicon generate a train of small hydrogen bubbles as they fall through the water; drops of molten ferrosilicon do not.
- Silicon drops fall more slowly through the water than ferrosilicon drops.
- Steam explosions of both silicon and ferrosilicon drops can be triggered by generating pressure transients in the water with a mechanical impactor.
- Silicon drops seem to require stronger pressure transients for initiation of the explosions than the ferrosilicon drops.
- Silicon drops cannot be triggered at depths as great as the ferrosilicon drops.

As we gained experience with drops of molten silicon, we realized that in order to trigger their steam explosions, it was necessary for the drops to fall very close to the surface of the pneumatic piston impactor developed in 1998 (now called Impactor 2). This closeness not only makes it difficult to image the explosions properly but also to accurately measure the threshold pressures required to achieve triggering. We have, therefore, built and tested a new slug-type device (Impactor 3) with heavier construction, also driven by gas at high pressure. With this new impactor, pulses strong enough to trigger the explosions of drops of molten silicon can now be achieved well above its surface, producing better imaging and more accurate measurements of threshold pressures.

In order to understand the chemistry and energetics of the quenching and steam explosions and to assess granulation plant safety related to gaseous explosions, it is important to know how much hydrogen is generated when drops of molten silicon interact with water. We observed the hydrogen to form as follows: Without a trigger, a drop generates a train of small bubbles that rise continuously in the water. With a mild trigger, the drop fragments coarsely and usually generates several large luminous bubbles that have particles of silicon burning inside. And if the drop produces a vigorous explosion with a strong trigger, a swarm of tiny hydrogen bubbles is generated, each of which rises independently and eventually bursts through the water surface without coalescing with its neighbors.

We tried to estimate the volumes of hydrogen bubbles from their video images, but achieved poor results due to great inaccuracies inherent in the procedure. We have, therefore, added to our apparatus a system for collecting and measuring the volume of hydrogen generated in a given interaction.

By adding Impactor 3 and the hydrogen measuring system to our original apparatus, we have been able to:

- Improve our estimates of threshold trigger pressures required for explosions of drops of molten silicon at fixed depths.
- Make better determinations of the energetics of the explosions of drops of molten silicon.
- Better understand the chemistry and amounts of the colloidal material generated during the explosions of drops of molten silicon.

We also investigated the effects of small alloyed additions of Al and Ca on the quenching and steam explosions of drops of molten silicon. When compared to drops of pure silicon, drops that had been alloyed with 0.4 w/o Al, 0.04 w/o Ca or 0.4 w/o Al + 0.04 w/o Ca showed:

- A reduced tendency to explode with a given trigger.
- Strongly reduced deposition of colloidal material in the water during the explosions.
- Somewhat reduced amounts of hydrogen generated during the triggered interactions.
- Velocities of fall through the water more than twice those of the nonalloyed drops.

We performed one exploratory experiment in which a drop of nonalloyed molten silicon was triggered to explode at a known distance from a transducer. The energy released by the explosion generated a steam bubble that collapsed and produced a strong pressure transient equivalent to the original triggering pulse. Even stronger pressure pulses may be generated from the explosions under other triggering conditions.

During the 1999 experiments, we experienced several failures of the furnace used to prepare and release the drops of molten silicon. The failures are described and corrective measures are proposed.

EXPERIMENTAL

The procedures used for generating, releasing and triggering the drops of molten silicon, for imaging their behavior in the water and for examining the solids before and after the interactions are based on those used with drops of molten ferrosilicon described previously (Nelson et al., 1996-1999; also see the compilation of reports in Appendix A).

Materials

Silicon Rods

For these experiments, we prepared drops of molten silicon from 10 mm-diameter rods prepared by Mr. Kjetil Hildal of the Institute of Metallurgy, Norwegian University of Science and Technology, Trondheim, Norway. The rods had the following compositions:

- Composition A. These rods are not alloyed, that is, they have low Al and Ca contents. These rods were received in a postal shipment that consisted of batches of two or three rods each, with the designations A-1, A-2, A-3, etc., through A-8. A second shipment of about 10 rods packed as several batches was received by express; we could see no separate designations other than an overall “A”. We grouped these “express” rods together with our designation D-36-4. Later, however, we learned these rods had been taken from Batches A-9 and A-10, and they were then designated A-9,10.
- Composition B. These rods are alloyed with 0.4 weight percent Al.
- Composition C. These rods are alloyed with 0.04 weight percent Ca.
- Composition D. These rods are alloyed with 0.4 weight percent Al and 0.04 weight percent Ca.

Analyses of the three batches of alloyed rods are given in Table E-1 in Appendix E.

Support of the Rods in the Furnace

Due to the brittleness of the silicon rods, breakage occurred often during normal handling. As a result, most rods were no longer than about 50 mm when received.

In our earlier experiments with ferrosilicon drops (Nelson et al., 1996-1999), we supported the rods in the furnace with 0.5 mm-diameter Type 316 stainless steel wire either wound around a groove at the upper end of the rod or passed through a hole drilled horizontally through the upper end of the rod. Unfortunately, we learned that this procedure could not be used with ferrosilicon rods shorter than about 50 mm because the wire comes too close to the hot zone of the furnace and fails. Therefore we did not attempt to use the wire as a support material during the 1999 studies because (a) the silicon rods were mostly shorter than 50 mm, and (b) the furnace is operated at a temperature higher than in the previous studies because of the higher melting temperature of the silicon.

Instead of using the wire as a support, we used a 3 mm-diameter graphite pin inserted through a hole drilled with a diamond core drill through the upper end of each 10 mm-diameter silicon rod, perpendicular to its axis. In turn, the graphite pin was supported between a pair of holes in the lower end of a graphite tube, the upper end of which was attached with a second graphite pin to the stainless steel tube normally used to position the rods in the furnace.

The graphite support worked well, allowing us to release drops from silicon rods as short as 30 mm. There was never any sign of interaction between the graphite and the silicon as long as the furnace temperature did not exceed ≈ 1500 °C. (There was an interaction during an overheating failure of the furnace, however; see description of experiment D-77-1 in Appendix C.)

Water

In the previous experiments with ferrosilicon, we used deionized water obtained in 20 L bottles from a local commercial source. Not only were the bottles difficult to handle, but the quality of the water seemed to vary from batch to batch. For the 1999 experiments, we leased a deionization system that supplies water of high quality at roughly the same cost as the bottled water, with considerably greater convenience and reliability.

Ice

A commercial block of ice was used as a catcher for the initial experiment with molten drops of silicon. It was obtained from a local supplier.

Gases

We flushed the furnace and the fall path of the drops between the furnace outlet and the water with a mixture of 1% hydrogen in argon obtained from a high pressure cylinder. We prepared the mixture from commercial grade gases.

Generation of Drops of Molten Silicon

These experiments were performed with the pendant drop generation and release technique used in the previous studies (Nelson et al., 1996-1999). All drops were allowed to fall spontaneously from the tip of the heated silicon rods. It should be noted that the pendant drop technique inherently produces drops at the melting temperature of the metal (1410 °C). Consequently, all experiments reported here were performed with drops at or below the melting temperature, that is, with supercooled silicon.

Time-Resolved Imaging

Video Imaging

We used the video imaging and playback techniques described in the earlier work (Nelson et al., 1996-1999). These techniques involved recording images with a video camera, either in a darkened room using the self-luminosity of the drops, or in reflected light provided by a bank of three fluorescent tube lamps placed at the left side of the water chamber. We viewed the tapes with a video cassette recorder either in continuous mode or in frame-by-frame mode with a time resolution of 30 frames per second (0.033 s per frame).

35 mm Photography

We also used time-exposed 35 mm photography in a darkened room to record the behavior of the molten silicon drops as they fell through water. We used two 35 mm cameras: One is placed 380 mm from the chamber to produce high quality streak images of the falling drop and the bubble growth associated with its explosion. The second camera, placed about 2 m from the chamber, records time-exposed images by viewing the luminous drops through a rotating shutter wheel. These images show “dotted” tracks for the main drop as well as for any secondary drops produced during the experiment. With this procedure, we obtain a time resolution of 12 chops per second (0.083 s per chop).

Initiation of Steam Explosions with Pressure Transients

Because neither drops of molten ferrosilicon nor molten silicon explode spontaneously, we have initiated their explosions with pressure transients applied to the water by submerged mechanical impactors. During the program sponsored by SINTEF Materials Technology at the University of Wisconsin, we have developed and tested three impactors: Impactor 1, a solenoid-driven device (Nelson et al., 1998, 1999a); Impactor 2, a device driven by a pneumatic piston (Nelson et al., 1999); and Impactor 3, a new device that employs an air-driven slug. Each device generates a pressure transient in the water by the upward impact of a metallic element on the underside of the steel cover of a watertight canister in which the impactor is mounted. Impactors 2 and 3 were used for triggering explosions during the 1999 experiments described in this report. Impactor 1 was retired during 1998.

Tourmaline Pressure Transducer

To measure the pressure transients generated by Impactors 2 and 3, we used the tourmaline underwater blast transducer-oscilloscope combination described previously (Nelson et al., 1999). For both sets of measurements, we placed the surface of the impactor at a depth of 400 mm in the water, and the tourmaline transducer 100 mm above at a depth of 300 mm.

Pressure Transients Generated by Impactor 2

In the initial phases of the 1999 work, we generated pressure transients for triggering the steam explosions of drops of molten silicon with the encapsulated submerged impactor described in our 1998 work (Nelson et al., 1999). This submerged unit generates nominally 0.3 MPa pressure transients at a distance of 100 mm above its surface, as measured with the tourmaline underwater blast transducer-oscilloscope combination. As the early work progressed, we realized that these pressure transients were not strong enough for the quantitative studies desired for the silicon drops.

Pressure Transients Generated by Impactor 3

To generate the stronger pressure transients needed to initiate explosions of the silicon drops, we have built an entirely new encapsulated impactor, designated Impactor 3. A drawing of this device is shown in Figure 1. Photographs of the impactor before and after assembly are shown in Figures 2a-e. Note that Impactor 3 has heavier construction and a larger gas inlet than Impactor 2. Impactor 3 also has a cleaner, smoother exterior to make recovery of debris easier and more quantitative.

Impactor 3 operates when a 60 g, 15 mm-diameter X 39 mm-tall steel slug is driven upward in a rifle-like barrel by gas at high pressure.¹ The pressure transient is generated in the water when the slug strikes the underside of the cover of a welded carbon steel canister. The impactor is fired by electrically opening a solenoid valve backed by a ballast volume of about 2 L that is connected with 6 mm polyethylene tubing to a commercial cylinder of gaseous argon at high pressure. An appropriate regulator and a high quality dial-type bourdon gauge are used to determine the pressure of the driving gas, usually 1.3 MPa (185 psi). When the solenoid valve opens, the sudden pressurization at the base of the barrel drives the slug upward to strike the under-surface of the canister and generate the pressure transient.

After it had been fired and the driving gas had been vented, we learned that we could not rely on gravity to reseal the slug at the bottom of the barrel between shots; instead, we applied a back-pressure to the canister to drive the slug down again. We found this procedure significantly increased the reproducibility of the pressure transients generated by the impactor in repeated shots.

Triggering with a Submerged Photodetector

The 110 VAC electrical signal that operates the solenoid valve to fire the impactor is supplied by a time-delay relay switched by a control relay activated when a submerged photodetector (No. 1²) senses the passage of the luminous silicon drop. The submerged photodetector and its placement in the water a fixed distance above the surface of the impactor have been described earlier (Nelson et al., 1999).

The sensor and control relay are the Skan-a-Matic P33001 photodetector switched with the R40100 control, both obtained from Clarostat Controls and Sensors, Richardson, TX. This photosensor is filtered optically

¹Anticipating the possible need for still larger pressure transients, we also fabricated a second slug and gun barrel with a larger diameter that can be installed interchangeably in Impactor 3. This slug weighs 150 g and is 25 mm in diameter X 39 mm tall. As yet, the second slug and gun barrel have not been tested.

²Because two identical photodetectors are used in these experiments, we distinguish them as No.1 and No. 2. Photodetector No. 2 is used in the operation of the hydrogen collector.

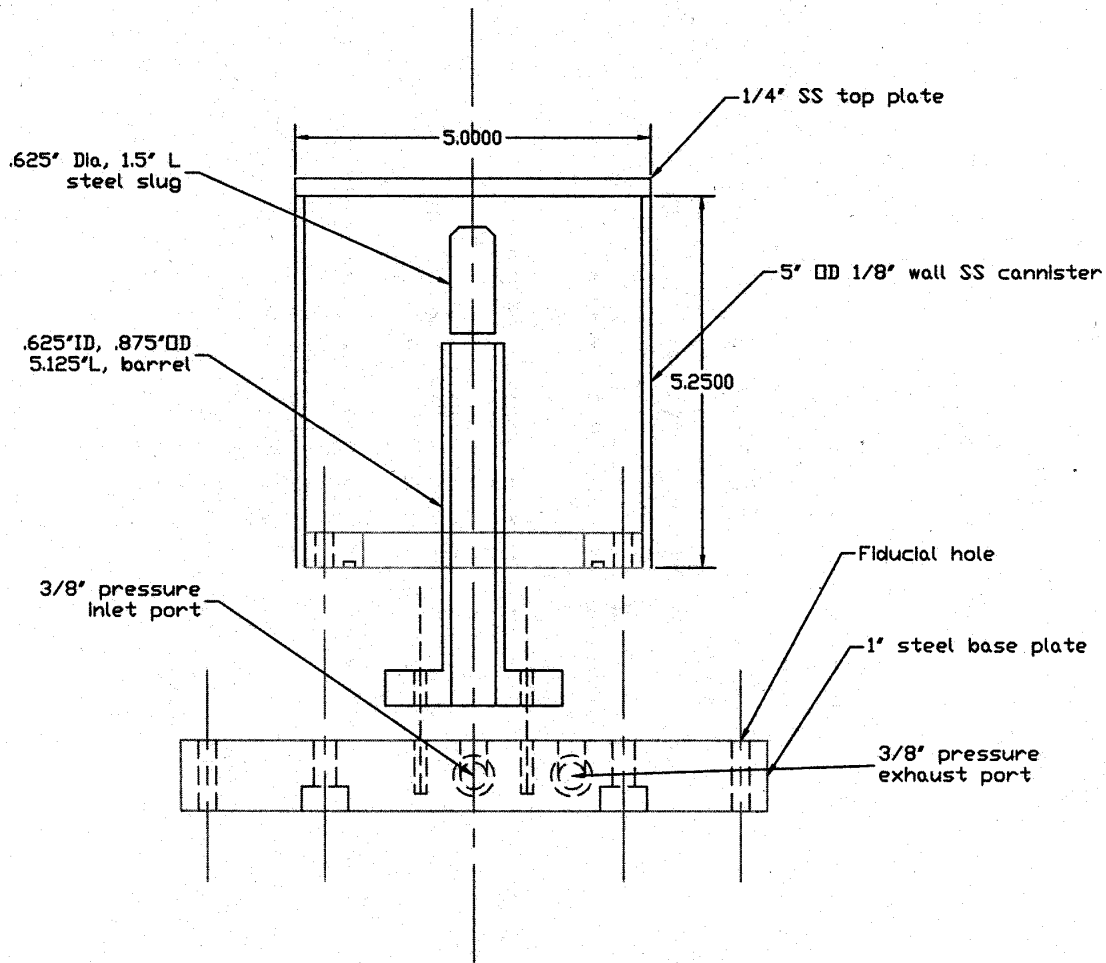


Figure 1. Schematic drawing of Impactor 3 (exploded view). All dimensions are in inches.

to be most sensitive to radiation generated by an infrared light-emitting diode (IR LED), that is, light emitted in the near infrared, at about 900 nm, as shown in Figure 3. Operation of this photodetector in the near infrared is advantageous when photographic and video images are being recorded with reflected light generated by fluorescent tube lamps. Since fluorescent lamps emit very little radiation in this part of the spectrum, there is minimal interference between the illumination source and the photodetector. The practical advantage of using this wavelength region, then, is that switching the fluorescent light sources on and off will not activate the photodetector. It will be activated, however, by incandescent light sources, which emit strongly in the infrared. These sources include the luminous silicon drops and filament lamps, for example, hand-held flashlights.

The output of this photodetector-activated control system is a short 110 VAC pulse fed via a latching relay to switch a time-delay relay (Dayton, Model 6A855, with a range of delays from 50 ms to 999 minutes). We used variable small delays to fire the impactor with the submerged photodetector.

In the experiments with drops of molten silicon, it was necessary to place small plates above and below the photodetector—"blinders"—to achieve triggering at the proper depths in the water. These plates formed a horizontal slit that prevented premature triggering by the reflection of the luminosity of the drop from the walls of the chamber. These plates were not required in the earlier experiments with the less luminous drops of molten ferrosilicon (Nelson et al., 1999).



Figure 2a. Photograph of Impactor 3 during assembly.

Hydrogen Collector

The hydrogen collection concept used here is based on the apparatus used by Nelson et al. (1994) to estimate hydrogen generated when single drops of a molten aluminum-lithium alloy were released into water. In that system, the drop of melt fell from the furnace through a fast-acting valve that closed just after the drop passed through it. This allowed the volume of gas in the headspace of the closed apparatus to be collected quantitatively in an inverted water-filled graduated cylinder. Because the headspace of the apparatus had been flushed with argon to prevent oxidation of the alloy, the gases collected were mixtures of hydrogen and argon that had to be analyzed by mass spectrometry.

In the experiments described here, we simplified the approach for estimating the amounts of hydrogen—coalescence and gathering of the bubbles in a conical collector at the top of the water chamber and directly measuring their combined volume by displacement of water contained in a graduated cylinder.

The hydrogen bubbles generated by the steam explosion of a single drop of melt are produced in a roughly spherical volume that may have a diameter almost as wide as our water chamber. In order to collect the many small bubbles, we placed a conical bubble collector just below the surface of the water at the top of the chamber. The base of the conical collector, made of 0.5 mm-thick transparent polycarbonate sheet, is circular and has a diameter of 295 mm, slightly smaller than the 300 mm-wide chamber. The upper end of the cone opens upward into a smaller inverted funnel that is attached to a water-filled graduate above. The graduate has a small valve at its upper end with a flexible tube that leads to a water aspirator. The evacuation produced by the aspirator allows us to draw a continuous column of water up through the funnel into the graduated volume. Once gas bubbles enter the funnel from the cone below, they will pass upward into the graduate and displace an equivalent volume of water. In order to measure various amounts of hydrogen, we prepared interchangeable graduated cylinders with five different volumes—10, 25, 50, 100 and 250 ml.

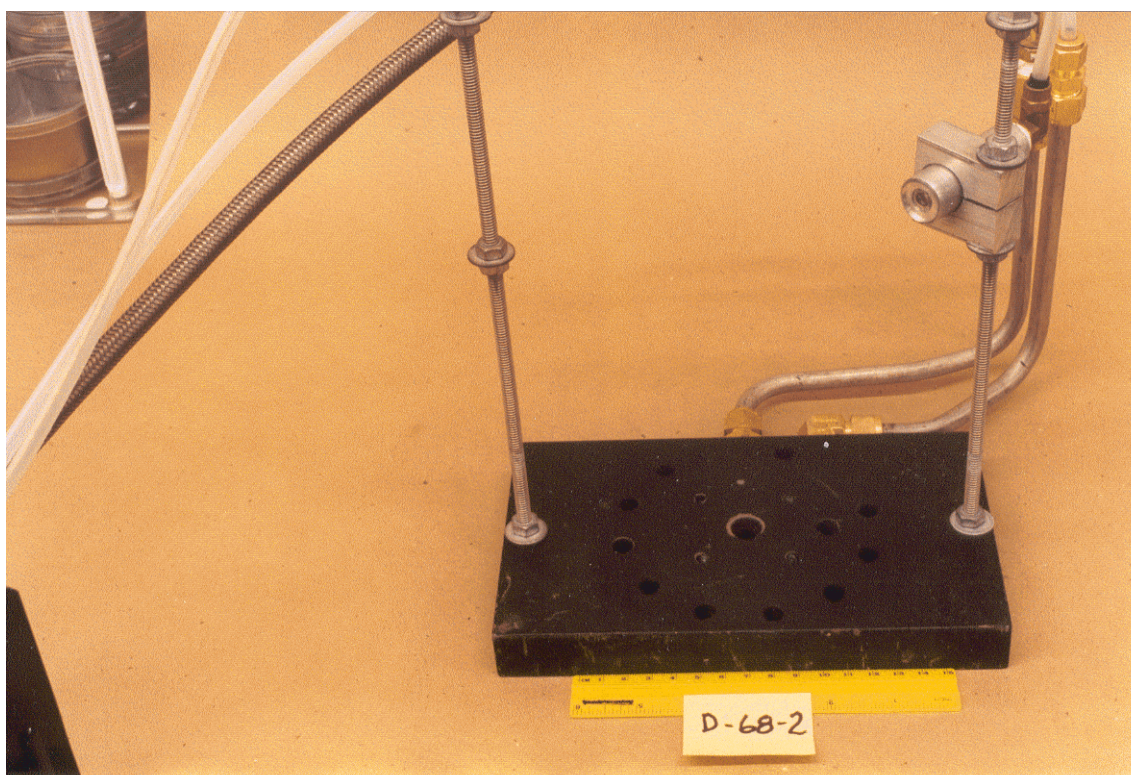


Figure 2b. Photograph of Impactor 3 during assembly.

The inverted funnel is caused to slide sideways by mounting it on a non-rotating air cylinder (29 mm bore diameter, 76 mm stroke, obtained from the Speedaire Co.). In order to provide a path for the drop to fall into the water unimpeded, the funnel is positioned initially at the right side of the chamber. When the drop falls from the furnace, a second photodetector (No. 2³) senses its release and starts a second time delay relay. After an appropriate delay to allow the drop to enter the water and fall through the open top of the cone, the relay activates the cylinder with air at a pressure of 0.6 MPa (90 psi). This activation drives the inverted funnel quickly to the left to cover the outlet of the cone and thus capture all bubbles that rise from the interaction zone.

A schematic diagram of the hydrogen collection system is shown in Figure 4 and photographs of the sliding funnel and graduated cylinder are presented in Figures 5a through e.

Gas Collection Tests

We performed two tests of the ability of the collection system to gather and measure known amounts of gas released in the water as bubbles. We released bubbles of air in the first test, and bubbles of hydrogen in the second.

Collection of Air Bubbles. These tests were performed with capped pipe nipples that had volumes of 14 ml, 91 ml or 167 ml. When one of these nipples was lowered on strings into the water with its open end down, it carried with it a known volume of trapped air. When we inverted one of these nipples in the water at a depth of about 400 mm beneath the conical bubble collector, the trapped air was released as a column of bubbles that rose into the cone and sliding funnel and ultimately coalesced into a volume of gas that was collected and measured in the graduated cylinder.

³ See footnote 2 earlier in the experimental section.



Figure 2c. Photograph of Impactor 3 during assembly.

Collection of Hydrogen Bubbles. For these tests, we used a 10 ml hypodermic syringe (± 0.1 ml accuracy) to inject known amounts of gaseous hydrogen into the water at a depth of 400 mm. The syringe was connected to a flexible tube that was initially placed over the outlet of a commercial cylinder of hydrogen. The tube and syringe were flushed thoroughly with flowing hydrogen before each filling. After tube and syringe were filled, the lower end of the tube was then placed at a depth of 400 mm in the water, where between 3 and 8 ml of gaseous hydrogen was ejected from the syringe. The gas then rose as bubbles in the water, passed through the conical bubble collector and the sliding funnel and was collected and measured in the graduated cylinder. The bubbles formed at the end of the flexible tube, the inside diameter of which was 4.2 mm.

Transducer Experiment

One experiment was performed to determine the pressurizations generated in the water by the steam explosion of a drop of molten silicon. The experimental setup is described in Appendix B.

Examination of Solids

Rods

The silicon rods were examined before and after each experiment by length measurements, by changes of weights and with 35 mm photography. We included an appropriate calibration scale in each 35 mm photograph to determine true dimensions of the rods.



Figure 2d. Photograph of Impactor 3 during assembly.

Granular Debris

The granular debris is the particulate material that can be recovered from the catcher pan within an hour or so after each experiment. These materials included solidified drops that had not exploded and coarse or fine material from drops that had completely or partially exploded. We investigated these materials by both weighing and with 35 mm photographs with calibration scales included in the images. These materials have also been archived for future studies.

Colloidal Debris

After each explosion, fine particles remain suspended in the water for hours or days as clouds of milky white or gray colloids. Their amounts were determined as the difference of between the loss of weight of the rod (that is, the amount of melt delivered to the water) and the weight of granular debris recovered. The examination of the colloidal material during the 1999 experiments has been only qualitative, with visual and video imaging.

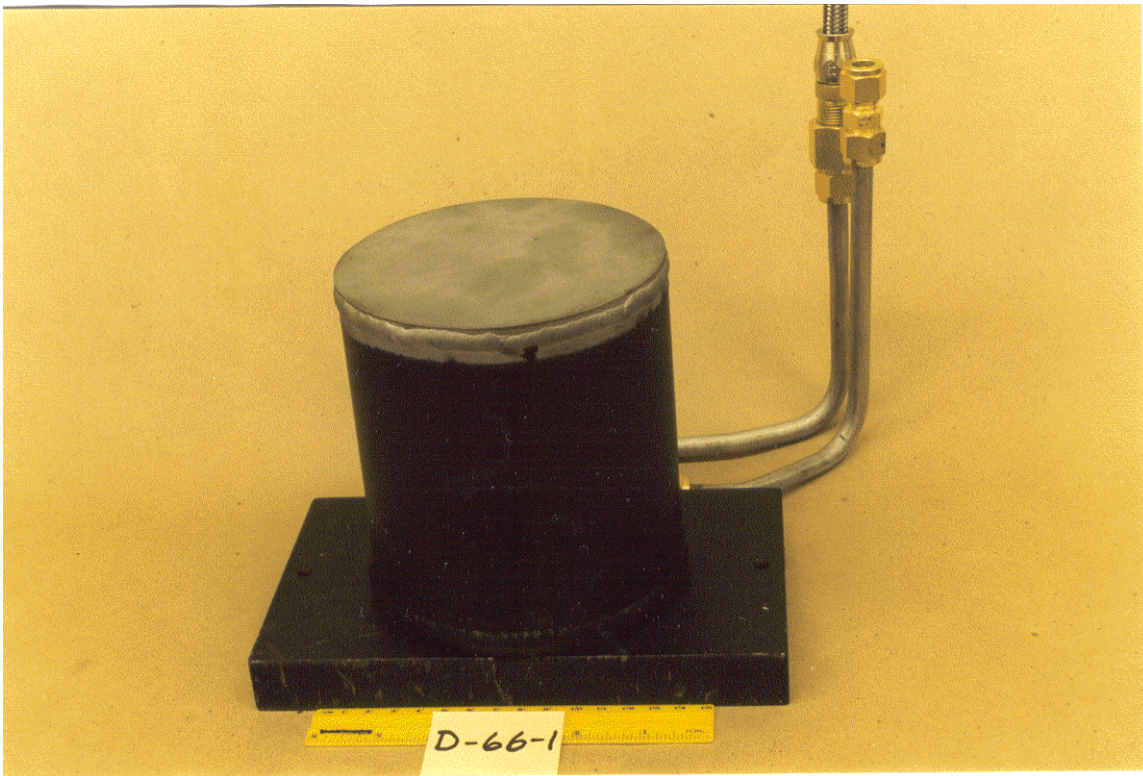
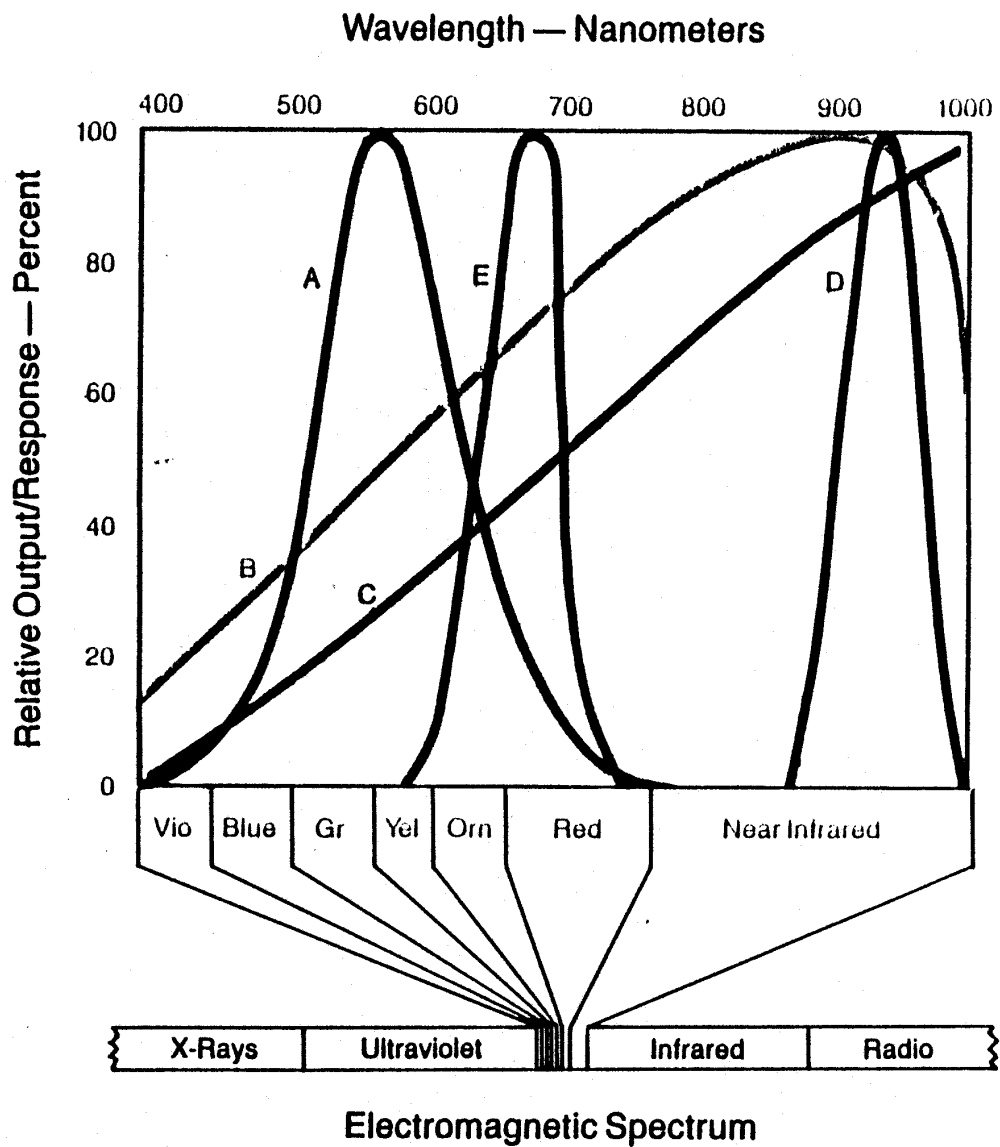


Figure 2e. Photograph of Impactor 3 during assembly.



- A Human Eye
- B Photodetector
- C Lamp
- D IR LED
- E Visible red LED

Figure 3. Outputs and responses vs. wavelength for several light sources and receptors. Our photodetector, B, is filtered to be most sensitive to the infrared light-emitting diode (IR LED), D. (Reproduced from literature supplied by Clarostat Controls and Sensors, Richardson, TX.)

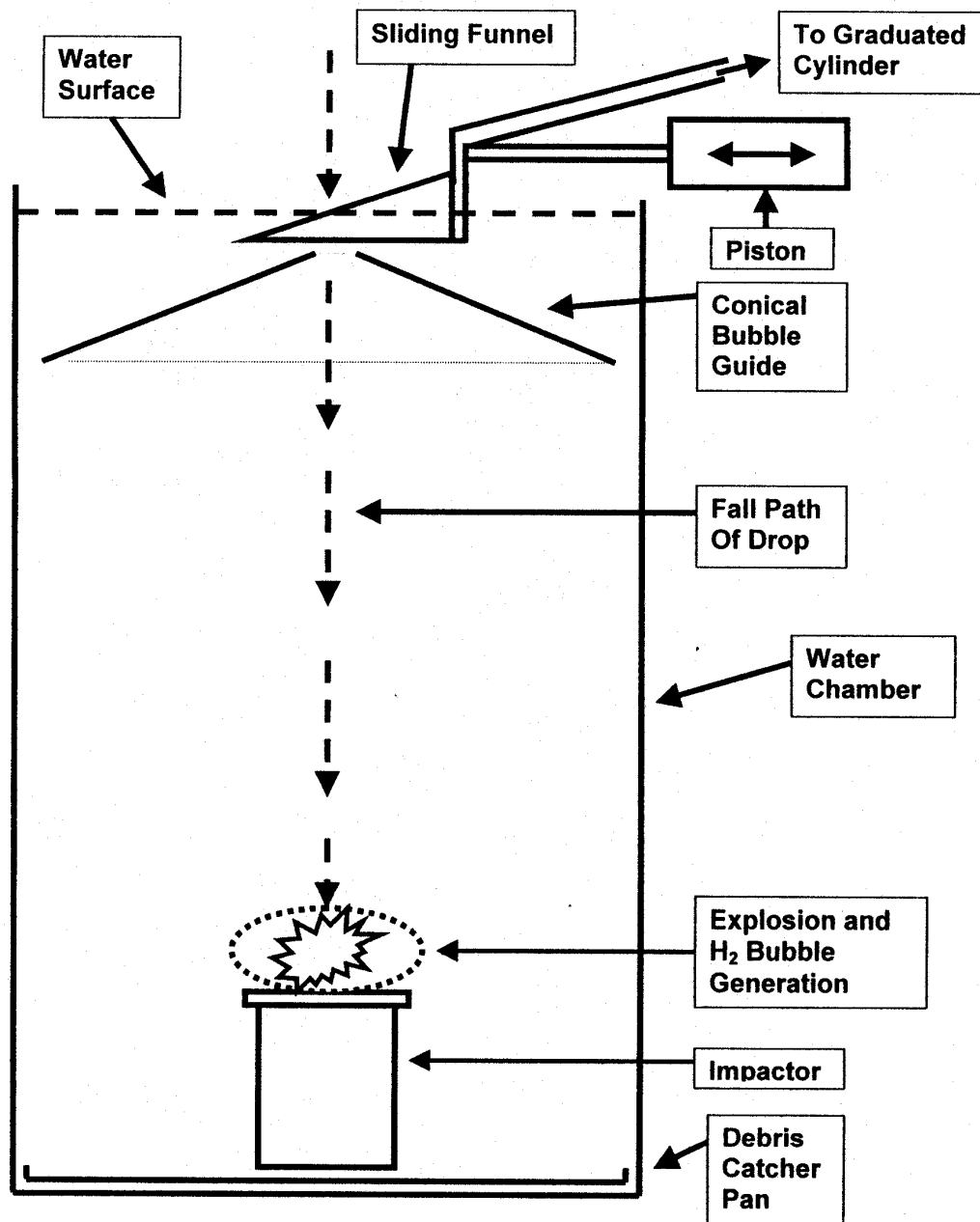


Figure 4. Schematic drawing of the hydrogen collector and its relationship to the water chamber and the explosion of a typical drop.

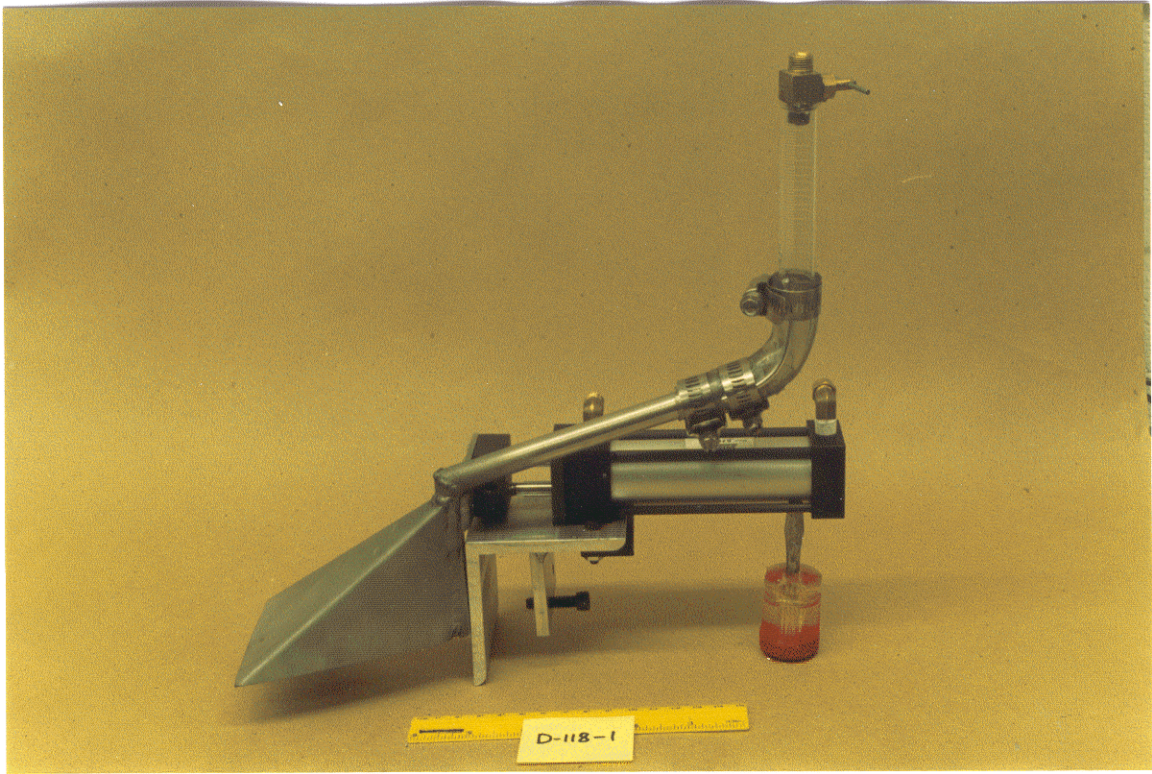


Figure 5a. Side view of the sliding funnel and graduated gas collection cylinder. Funnel is in retracted position.

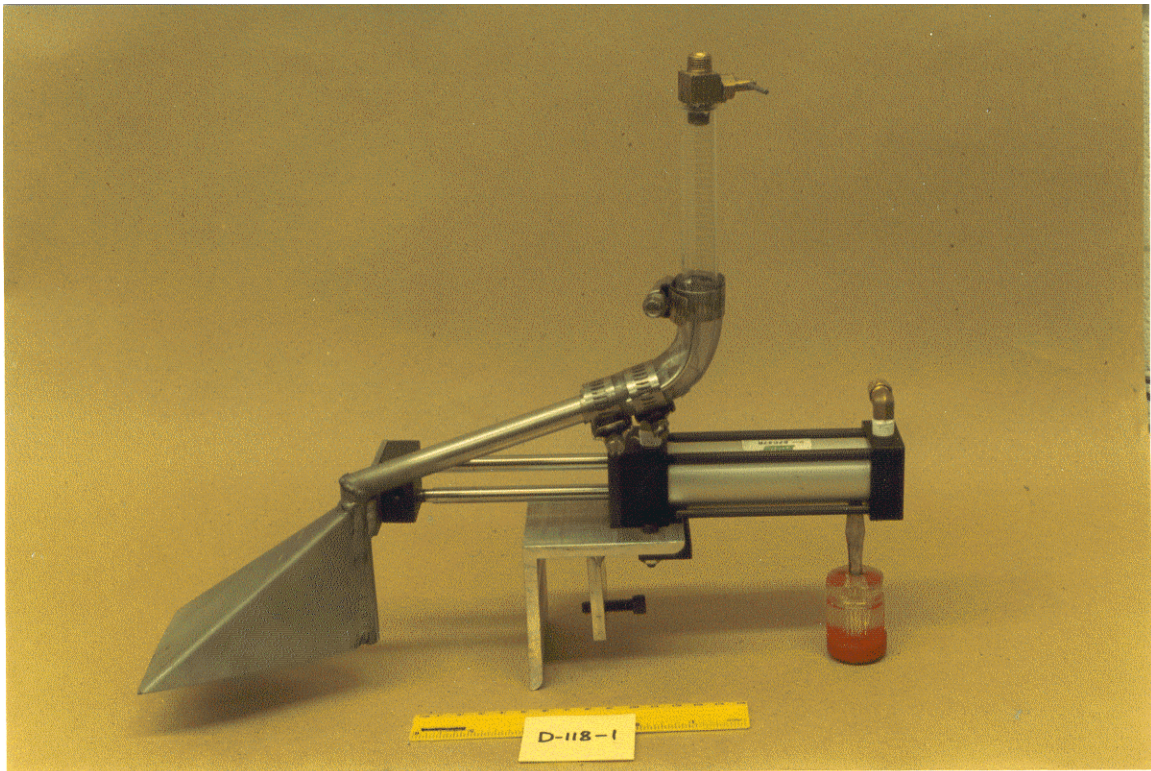


Figure 5b. Side view of the sliding funnel and graduated gas collection cylinder. Funnel is in the extended position.

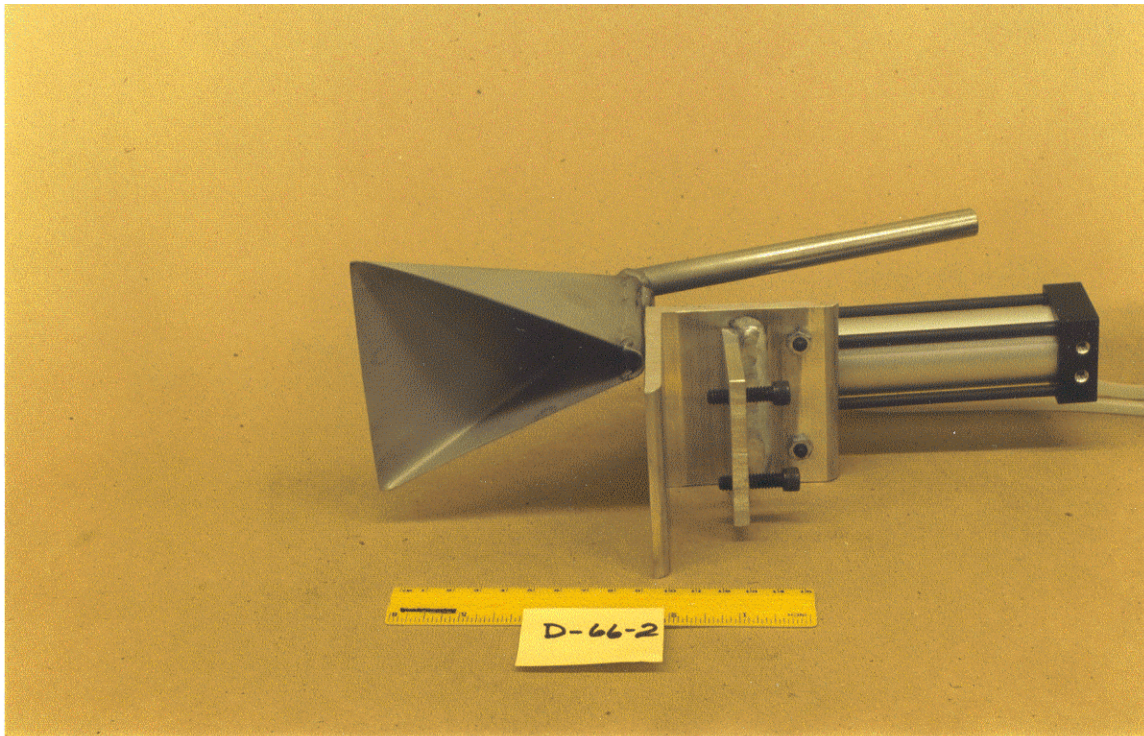


Figure 5c. Bottom view of the sliding funnel and graduated gas collection cylinder. Funnel is in the retracted position.

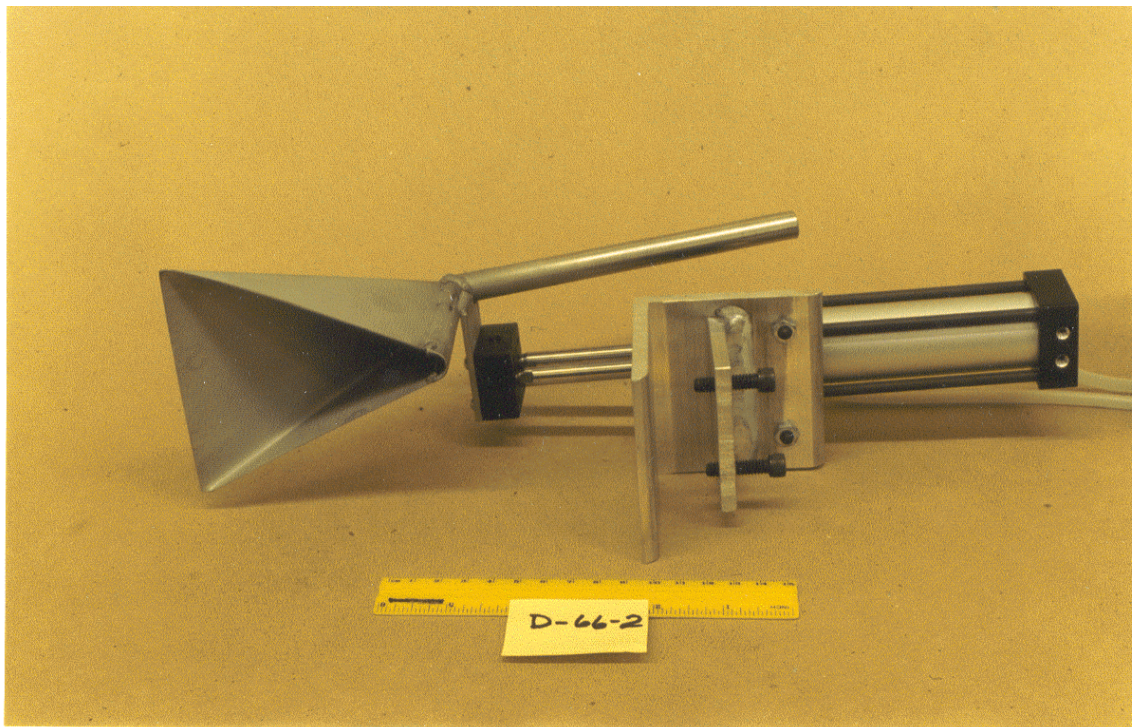


Figure 5d. Bottom view of the sliding funnel and graduated gas collection cylinder. Funnel is in the extended position.

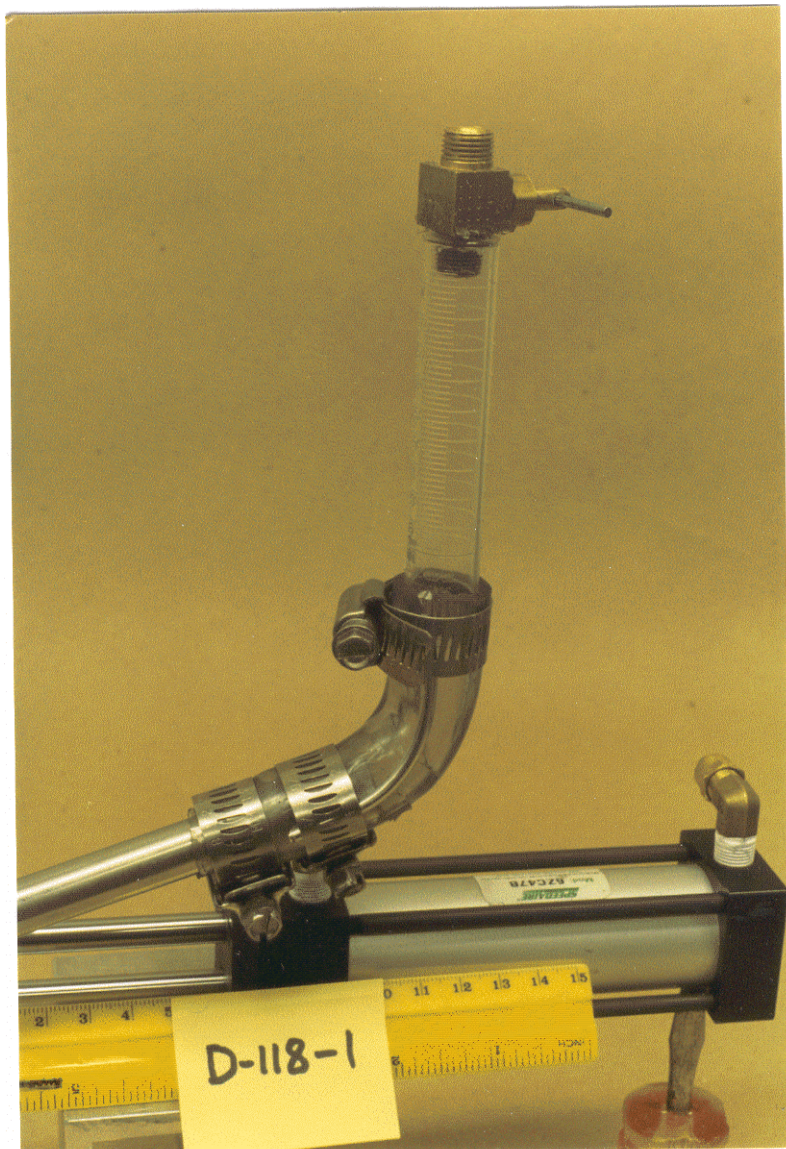


Figure 5e. Photograph of the graduated gas collection cylinder.

RESULTS

Generation of Drops of Molten Silicon

The pendant drop procedures used in the previous studies of drops of molten ferrosilicon (Nelson et al., 1996-1999; also see the compilation of reports in Appendix A) were applied with only minor modifications to the preparation and release of drops of molten silicon. Only one major experimental difference was required—using the graphite support to compensate for the shortness of the rods.

The 10 mm-diameter rods produced drops that weighed 0.8 g to 1.0 g, corresponding to 9 mm-diameter drops, as estimated from the density of molten silicon of 2.54 g/cc.

We have summarized the releases of silicon drops performed during 1999 in Tables 1A, 1B and 1C.

Release of Drops of Molten Silicon onto Ice

Because of the anecdotal reputation of molten silicon drops to be dangerous when released into water, we approached the new experiments in 1999 with caution. Therefore, we chose to use a block of ice placed just below the furnace outlet as the first catcher. As indicated in Table 1A, our first experiment was D-36-2. We used the same procedures for preparing the drops that were used during 1998, except that we raised the furnace temperature from about 1450 °C to about 1530 °C to compensate for the higher melting temperature of the silicon. As in the previous studies, we used the argon +1% hydrogen mixture to flush the furnace and drop exit path downward to very near the surface of the ice. A 25 mm-diameter hole approximately 25 mm deep was drilled into the upper surface of the ice to catch the drop. The hole was partially filled with water, and then positioned below the exit of the furnace.

The lower tip of the silicon rod was positioned in the furnace at the center of the viewing hole where we had placed the tips of the ferrosilicon rods in the earlier experiments. At this location, a drop of melt and also a chunk of solid silicon rod detached spontaneously and fell onto the ice. There were no sparks or explosions or other signs of violent interaction. This single experiment convinced us that the initial interaction of molten silicon drops with water was essentially benign and that no further experiments with ice as a catcher were warranted.

Release of Drops of Molten Silicon into Water Without Triggering

As indicated in Table 1A, our next experiment was D-38-1, in which three drops of molten silicon were released several minutes apart into our 1 m-deep chamber filled to the brim with deionized water at room temperature; the impactor was not used. Our stainless steel catcher pan was placed on the polycarbonate bottom of the chamber to prevent pyrolysis. We recorded the release and fall of the drops with the video camera and reflected light.

There were no spontaneous explosions of the drops at any level in their 1 m-fall through water, or upon impact with the stainless steel plate, or afterward as the luminosity of the drops gradually extinguished. The most obvious features of their fall were:

- The drops “whistled” as they fell through the water.
- The drops seemed to swerve from side to side as they fell through the water.
- The drops seemed to fall more slowly than the 9 mm-diameter and 11 mm-diameter ferrosilicon drops studied in 1998.
- Hydrogen bubbles were released during the fall of the drops and long after they landed on the stainless steel catcher pan. A photograph of a single frame from the video record of this experiment is shown in Figure 6. Drops 1, 2 and 3 released 20, 19 and 18 bubbles, respectively.

Table 1A. Summary of Releases of 9 mm-Diameter Drops of Nonalloyed Molten Silicon into Water ^a														
Explosions were triggered with Impactor 2; air pressure was 1.3 Mpa.														
In each experiment, the silicon rod was supported in the furnace on a graphite cross-rod.														
Drop No.	Alloy	T(water) (°C)	T(furnace) (°C)	Furnace Atm.	Rod Loss Wt (g)	Debris Wt. (g)	Difference (g)	Depths (mm)		Delay (s)	Trigger ^b (mm)	Trigger ^b (Mpa)	Imaging	Remarks
								Impactor	Photode't'r					
D-36-2 (Prelim.)	A-3	0 (Ice)	1550	Ar + 1%H ₂	3.20	2.36	0.84	None	None	None	None	None	None	A chunk of rod and some melt fell onto ice; interaction was benign.
D-38-1-1	A-4	RT	1550	Ar + 1%H ₂	3.16	3.23	0.07	None	None	None	None	None	RL, VCR	Pan at bottom, no impactor;no explosion; H ₂ bubbles.
D-38-1-2	A-4	RT	1550	Ar + 1%H ₂	See entries for D-38-1-1			None	None	None	None	None	RL, VCR	Pan at bottom, no impactor;no explosion; H ₂ bubbles.
D-38-1-3	A-4	RT	1550	Ar + 1%H ₂	See entries for D-38-1-1			None	None	None	None	None	RL, VCR	Pan at bottom, no impactor; no explosion; H ₂ bubbles.
D-40-1-1	A-4	18	1525	Ar + 1%H ₂	1.89	1.80	-0.09	400	375	None	20?	1.6?	RL, VCR	No pilot light. Drop triggered, no explosion. Small bubbles rise.
D-40-1-2	A-4	18	1525	Ar + 1%H ₂	See entries for D-40-1-1			400	375	None	80?	0.4?	RL, VCR	No pilot light. Drop triggered, no explosion. Small bubbles rise.
D-43-1-1	A-4	RT	1530	Ar + 1%H ₂	2.15	2.07	-0.08	200	175	None	50	0.6	RL, VCR	Drop triggered impactor, then fell behind it. No explosion.
D-43-1-2	A-4	RT	1530	Ar + 1%H ₂	See entries for D-43-1-1			200	175	None	50	0.6	RL, VCR	Drop triggered. Coarse fragmentation. Large luminous bubbles.
D-45-1-1	A-4	RT	1520	Ar + 1%H ₂	2.22	2.31	0.09	200	175	None	70	0.5	RL, VCR	Very coarse fragmentation. Large luminous bubbles rise.
D-45-1-2	A-4	RT	1520	Ar + 1%H ₂	See entries for D-45-1-1			200	175	None	80	0.4	RL, VCR	Very coarse fragmentation. Large luminous bubbles rise.
D-46-1-1	A-9,10	17	1525	Ar + 1%H ₂	2.00	1.98	-0.02	200	175	None	60	0.5	RL, VCR	Shield to block reflection; drops still triggered high. Coarse fragmentation.
D-46-1-2	A-9,10	17	1525	Ar + 1%H ₂	See entries for D-46-1-1			200	175	None	80	0.4	RL, VCR	No fragmentation. Only a few bubbles afterward.
D-48-1-1	A-9,10	15	1530	Ar + 1%H ₂	2.09	1.65	-0.44	200	175	0.17	25	1.3	RL, VCR	Drop triggered at edge of impactor where pressure pulse is low. Audible "pop" when bubble burst through surface of the water.
D-48-1-2	A-9,10	15	1530	Ar + 1%H₂	See entries for D-48-1-1			200	175	0.17	10	3.2	RL, VCR	Stong explosion, cloud of colloid, 1-frame flash of light.
D-50-1-1	A-9,10	RT	1530	Ar + 1%H ₂	2.05	2.19	0.14	810	785	0.17	None	None	OS, VCR	Drop fell behind the impactor, did not trigger.
D-50-1-2	A-9,10	RT	1530	Ar + 1%H ₂	See entries for D-50-1-1			810	785	0.17	0	Infinite	OS, VCR	Drop landed on the impactor, triggered 6 frames later. Coarse fragmentation.

^a Drops that exploded are indicated by this symbol: 

^b The magnitude of the triggering pulse was estimated from the distance of the drop above the impactor at the time of triggering . This distance was determined from the video image.

Table 1A (continued). Summary of Releases of 9 mm-Diameter Drops of Nonalloyed Molten Silicon into Water ^a														
Explosions were triggered with Impactor 2; air pressure was 1.3 Mpa.														
In each experiment, the silicon rod was supported in the furnace on a graphite cross-rod.														
Drop No.	Alloy	T(water) (°C)	T(furnace) (°C)	Furnace Atm.	Rod Loss Wt (g)	Debris Wt. (g)	Difference (g)	Depths (mm)		Delay (s)	Trigger ^b (mm)	Trigger ^b (Mpa)	Imaging	Remarks
								Impactor	Photode ^r					
D-52-1-1	A-9,10	RT	1530	Ar + 1%H ₂	2.98	2.90	-0.08	400	375	0.17	50	0.6	OS, VCR	Large luminous bubbles rise.
D-52-1-2	A-9,10	RT	1530	Ar + 1%H ₂	See entries for D-52-1-1			400	375	0.17	None	None	OS, VCR	Drop missed the impactor; did not trigger.
D-52-1-3	A-9,10	RT	1530	Ar + 1%H ₂	See entries for D-52-1-1			400	375	0.17	15	2.1	OS, VCR	Large flash of light in 2nd frame but no explosion.
 D-53-1-1	A-9,10	RT	1525	Ar + 1%H₂	2.00	1.83	-0.17	200	175	0.17	15	2.1	OS, VCR	Good explosion. Lost the time-exposed photo.
D-53-1-2	A-9,10	RT	1525	Ar + 1%H ₂	See entries for D-53-1-1			200	175	0.17	25	1.3	OS, VCR	No explosion. Drop triggered early
D-55-1-1	A-9,10	RT	1535	Ar + 1%H ₂	3.00	2.93	-0.07	200	175	0.17	25	1.3	OS, VCR	No explosion. Drop triggered early
D-55-1-2	A-9,10	RT	1535	Ar + 1%H ₂	See entries for D-55-1-1			200	175	0.17	25	1.3	OS, VCR	No explosion. Drop triggered early
D-55-1-3	A-9,10	RT	1535	Ar + 1%H ₂	See entries for D-55-1-1			200	175	0.17	50	0.6	OS, VCR	No explosion. Drop triggered early
D-56-1-1	A-9,10	16.5	1535	Ar + 1%H ₂	3.71	3.42	-0.29	200	175	0.17	40	0.8	OS, VCR	Fresh water filling. No explosion.
D-56-1-2	A-9,10	16.5	1535	Ar + 1%H ₂	See entries for D-56-1-1			200	175	0.15	50	0.6	OS, VCR	No explosion.
D-56-1-3	A-9,10	16.5	1535	Ar + 1%H ₂	See entries for D-56-1-1			200	175	0.19	30	1.1	OS, VCR	No explosion.
 D-56-1-4	A-9,10	16.5	1535	Ar + 1%H₂	See entries for D-56-1-1			200	175	0.25	10	3.2	OS, VCR	Explosion.
D-59-1-1	A-9,10	19.5	1540	Ar + 1%H ₂	2.28	1.86	-0.42	300	275	0.17	None	None	OS, VCR	Drop swerved and missed impactor. Did not trigger.
 D-59-1-2	A-9,10	19.5	1540	Ar + 1%H₂	See entries for D-59-1-1			300	275	0.17	15	2.1	OS, VCR	Drop fell straight down. Explosion with double bubble. Fine debris.
 D-61-1-1	A-9,10	23	1530	Ar + 1%H₂	0.87	0.68	-0.19	400	375	0.17	15	2.1	OS, VCR	Explosion with double bubble. Total time <0.1 s. Fine debris.
D-62-1-1	A-9,10	17	1525	Ar + 1%H ₂	1.5	1.36	-0.14	500	475	0.17	V. small	V. high	OS, VCR	Coarse fragments that burned inside rising bubbles.
D-64-1-1	A-9,10	19.5	1530	Ar + 1%H ₂	1.18	1.18	0	500	475	0.17	V. small	V. high	OS, VCR	Coarse fragments. burned inside rising bubbles. Pocket-like main fragment.

^a Drops that exploded are indicated by this symbol: 

^b The magnitude of the triggering pulse was estimated from the distance of the drop above the impactor at the time of triggering. This distance was determined from the video image.

Table 1B. Summary of Releases of 9 mm-Diameter Drops of Nonalloyed Molten Silicon into Water ^a															
Interactions were triggered with the Impactor 3; air pressure was 1.3 Mpa.															
In each experiment, the silicon rod was supported in the furnace on a graphite cross-rod.															
Drop No.	Alloy	T(water) (°C)	T(furnace) (°C)	Furnace Atm.	Rod Loss Wt (g)	Debris Wt. (g)	Difference (g)	Depths (mm)		Delay (s)	Trigger ^b (mm)	Trigger ^b (Mpa)	Imaging	V(H ₂) (ml)	Remarks
								Impactor	Photodetr						
D-71-1-1	A-8	25	1575	Ar + 1%H ₂	3.25	3.31	Gain 0.06	None	None	None	N. A.	N. A.	RL, VCR	1.5	1st test of H ₂ collector. Poor video. Many tiny bubbles.
D-71-1-2								None	None	None	N. A.	N. A.	RL, VCR		Funnel not retracted, drop fell on cone. Wt = 0.90 g.
D-71-1-3								None	None	None	N. A.	N. A.	RL, VCR		Drop caught on cone, deflected to left, image blocked.
D-74-1-1	A-8	24	1520	Ar + 1%H ₂	2.87	2.94	Gain 0.07	None	None	None	N. A.	N. A.	RL, VCR	0.5	H ₂ collector, V(H ₂) = 0.5 ml.
D-74-1-2								None	None	None	N. A.	N. A.	RL, VCR	0.5	H ₂ collector, V(H ₂) = 0.5 ml.
D-74-1-3								None	None	None	N. A.	N. A.	RL, VCR	1.0	H ₂ collector, V(H ₂) = 1.0 ml.
D-77-1-1	A-8	23	>>1520	Ar + 1%H ₂	Unknown	1.47	Unknown	350	325	None	200	0.51	RL, VCR	3.0	Triggered early, near bottom of cone; good generation of H ₂ .
D-77-1-2					Unknown	1.45	Unknown	350	325	0.3	50	3.54	RL, VCR		Drop fell behind the impactor.
D-77-1-X					Unknown	None	None	350	325	0.5	N. A.	N. A.	RL, VCR		No drop. Furnace overheated. Ruined furnace tube.
D-83-1-1	A-8	21	>>1520	Ar + 1%H ₂	2.14	2.21	Gain 0.07	350	325	0	In cone	Very small	RL, VCR	0.8	Trial #1 aborted. In Trial # 2, 2
D-83-1-2										0.3	120	1.64	RL, VCR	0.5	drops, photodetector activated early. No explosions.
D-86-1-1	A-8	21	>>1520	Ar + 1%H ₂	2.28	2.27	Loss 0.01	350	325	0	High	Small	RL, VCR	0.5	Photodetector activated early for each drop. No explosions.
D-86-1-2								350	325	0.3	High	Small	RL, VCR	0.5	
D-86-1-3								350	325	0.6	High	Small	RL, VCR	0.3	
D-90-1-1	A-8	22	>>1520	Ar + 1%H ₂	2.26	2.05	Loss 0.21	400	350	0.8	80	2.45	RL, VCR	2	Coarse fragmentation.
 D-90-1-2								400	350	0.9	60	3.27	RL, VCR	3	Explosion.
D-94-1-1	A-8	21.5	>>1520	Ar + 1%H ₂	2.33	1.71	Loss 0.62	400	350	0	170	1.16	RL, VCR	1.5	"Blinders" on photodetector. Large bubbles with Si particles.
 D-94-1-2								400	350	0.3	40	4.91	RL, VCR	5.0	Added delay. Strong explosion with very persistent colloid, H₂ bubbles. Gas from below impactor.
D-97-1-1	A-8	19.5	>>1520	Ar + 1%H ₂	2.15	2.02	Loss 0.13	400	350	0.3	160	1.23	RL, VCR	2.5	Triggered very early. Large luminous bubbles rose, fell.
 D-97-1-2								400	350	0.5	60	3.27	RL, VCR	1.0	Good explosion. No gas from below impactor.
D-104-1-1	A-8	22.0	1590	Ar + 1%H ₂	2.51	1.98	Loss 0.53	400	350	0.20	20 (edge)	>> 9.82	RL, VCR	1.5	"Blinders"+ 2 shims properly fired impactor; drop # 1 at edge.
 D-104-1-2								400	350	0.00	50	3.93	RL, VCR	5.5	Good explosion. Gas from below impactor.

^a Drops that exploded are indicated by this symbol: 

^b The magnitude of the triggering pulse was estimated from the distance of the drop above the impactor at the time of triggering. This distance was determined from the video image.

Table 1B (continued). Summary of Releases of 9 mm-Diameter Drops of Nonalloyed Molten Silicon into Water ^a															
Interactions were triggered with the Impactor 3; air pressure was 1.3 Mpa.															
In each experiment, the silicon rod was supported in the furnace on a graphite cross-rod.															
Drop No.	Alloy	T(water) (°C)	T(furnace) (°C)	Furnace Atm.	Rod Loss Wt (g)	Debris Wt. (g)	Difference (g)	Depths (mm)		Delay (s)	Trigger ^b (mm)	Trigger ^b (Mpa)	Imaging	V(H ₂) (ml)	Remarks
								Impactor	Photodet'r						
 D-107-1-1	A-7	20.5	1540	Ar + 1%H ₂	1.20	0.89	Loss 0.31	400	350	0.10	40	4.91	RL, VCR	3.5	"Blinders"+ 2 shims. Good explosion; granular debris in streak across impactor. No gas from below.
 D-109-1-1	A-7	21.0	1535	Ar + 1%H ₂	1.07	0.99	Loss 0.08	400	350	0.10	40	4.91	RL, VCR	1.5	"Blinders"+ 2 shims. Mild explosion, flaky debris. Little colloid. No gas from below the impactor.
D-111-1-1	A-7	21.5	1535	Ar + 1%H ₂	1.13	1.02	Loss 0.11	400	350	0.00	80	2.45	OS, VCR	3.0	"Blinders"+ 2 shims. Coarse fragmentation with burning particles in rising and falling bubbles.
 D-114-1-1	A-7	21.0	1520	Ar + 1%H ₂	1.04	0.91	Loss 0.13	400	350	0.05	35	5.61	OS, VCR	2.0	"Blinders"+ 2 shims. Good explosion with flaky debris, little colloid.
D-115-1-1	A-7	20.0	1520	Ar + 1%H ₂	0.93	0.97	Gain 0.04	400	350	0.00	60 (Edge)	3.22	OS, VCR	1.0	"Blinders"+ 2 shims. Drop fell to left rear edge of impactor. No explosion.
D-118-2-1	A-7	17.5		Ar + 1%H ₂	1.28	1.17	Loss 0.11	400	350	0	N. A.	N. A.	OS, VCR	N. M.	Drop fell onto cone. Shutter had been closed part-way.
D-120-1-1	A-7	19.0	1520	Ar + 1%H ₂	1.25	1.32	Gain 0.07	400	350	0	42 (Edge)	4.2	OS, VCR	1.6	Drop fell far to the left. Coarse fragmentaion, hydrogenbubbles.
 D-123-1-1	A-7	19.5	1579?	Ar + 1%H ₂	1.55	1.28	Loss 0.27	400	350	0	31	6.33	OS, VCR	2.6	Good explosion forward amd to left of the impactor. Threw water.

^a Drops that exploded are indicated by this symbol: 

^b The magnitude of the triggering pulse was estimated from the distance of the drop above the impactor at the time of triggering . This distance was determined from the video image.

Table 1C. Summary of Releases of 9 mm-Diameter Drops of Molten Alloyed Silicon into Water ^a																
Interactions were triggered with Impactor 3; air pressure was 1.3 Mpa.																
In each experiment, the silicon rod was supported in the furnace on a graphite cross-rod.																
Drop No.	Alloy ^c	T(water) (°C)	T(furnace) (°C)	Furnace Atm.	Rod Loss Wt (g)	Debris Wt. (g)	Difference (g)	Depths (mm)		Delay (s)	Trigger ^b (mm)	Trigger ^b (Mpa)	Imaging	V(H ₂) (ml)	Remarks	
								Impactor	Photodet'r							
D-127-1-1	B	17.5	1500	Ar + 1%H ₂	1.43	1.35	Loss 0.08	400	349	0	19	10.3	OS, VCR	6.5	Coarse fragmentation."Seaweed-like" image.	
 D-130-1-1	B	17	1500	Ar + 1%H₂	1.26	1.26	None	400	329	0	39	5	OS, VCR	6.2	Good explosion.	
D-145-1-1	B	21	1500	Ar + 1%H ₂	1.39	1.44	Gain 0.05	400	300	0	66.6	2.9	OS, VCR	2.2	Drop did not fragment or explode.	
D-147-1-1	C	17	1500	Ar + 1%H ₂	1.13	1.14	Gain 0.01	400	350	0	21	9.3	RL, VCR	4	Coarse fragmentation. Video record with reflected light	
D-133-1-1	C	17.5	1500	Ar + 1%H ₂	1.2	1.16	Loss 0.04	400	329	0	29	6.8	OS, VCR	4.0	Coarse fragmentation."Seaweed-like" image.	
D-135-1-1	C	17	1500	Ar + 1%H ₂	1.24	1.23	Loss 0.01	400	300	0	61.8	3.2	OS, VCR	2.2	Drop did not fragment or explode.	
D-137-1-1	D	17	1500	Ar + 1%H ₂	1.25	1.24	Loss 0.01	400	350	0	21.5	7.1	OS, VCR	7.6	Coarse fragmentation."Seaweed-like" image.	
D-139-1-1	D	17	1500	Ar + 1%H ₂	1.22	1.22	None	400	329	0	40.6	4.8	OS, VCR	7.3	Coarse fragmentation."Seaweed-like" image.	
D-143-1-1	D	22	1500	Ar + 1%H ₂	1.06	1.07	Gain 0.01	400	300	0	66.6	2.9	OS, VCR	2.4	Drop did not fragment or explode.	
^a Drops that exploded are indicated by this symbol: 																
^b The magnitude of the triggering pulse was estimated from the distance of the drop above the impactor at the time of triggering . This distance was determined from the video image.																
^c Alloy Compositions: A = Pure Si; B = Si + 0.4 w/o Al; C = Si + 0.04 w/o Ca; D = Si + 0.4 w/o Al + 0.04 w/o Ca.																
^d Approximate temperature.																

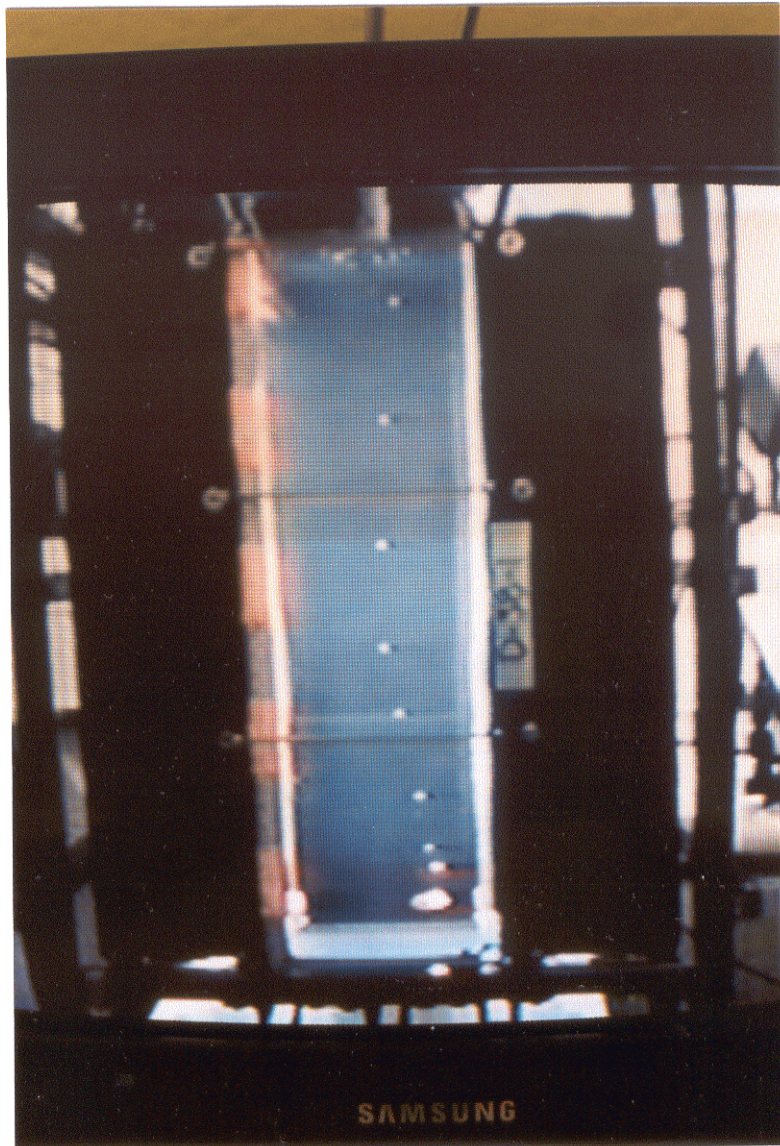


Figure 6. Photograph of a single frame from the video screen showing a continuous train of hydrogen bubbles rising from an untriggered 9 mm-diameter silicon drop in Experiment D-38-1. This image was recorded 3.66 seconds after release of the drop.

- A small “puff” of colloidal material was released into the water from each drop just after its last hydrogen bubble detached.

Release of Drops of Molten Silicon into Water With Triggering

Generation of Pressure Transients

Impactor 2. During the first two months of the 1999 experiments with drops of molten silicon, we generated pressure transients with Impactor 2 (the pneumatic impactor) used for triggering the ferrosilicon drops in the 1998 experiments. Our first effort was to check Impactor 2 for consistency of output after being unused for almost 8 months.

Table 2. Summary of Impactor Checks.

Driver gas at 185 psi; transducer is 100 mm above Impactor 2; impactor depth is 400 mm.

Date	Elapsed Time (d)	Expt. No	Average	Std. Dev	Percent
07/01/1998	0	C-265-3	0.378	0.027	7.1
09/16/1998	78	D-9-1	0.322	0.008	2.5
05/07/1999	307	D-34-1	0.292	0.040	13.8
05/10/1999	310	D-35-1	0.307	0.038	12.3

We repeated tests C-265-3 and D-9-1 with the tourmaline underwater blast transducer and the Infinium oscilloscope as described in the final report for 1998 (Nelson et al., 1999). As in 1998, we placed the surface of the impactor in the water at a depth of 400 mm with the transducer positioned 100 mm above it at 300 mm. We did two sets of tests, repeating the measurements 10 times for each set.

The results of the tests performed during a ten-month period In 1998 and 1999 are summarized in Table 2 and shown graphically in Figure 7. It can be seen that the output of Impactor 2 remained reasonably constant with time, decreasing gradually by about 5 % over this time interval. We used the most recent value of the output of Impactor 2, 0.300 ± 0.039 MPa ($\pm 13\%$) at 100 mm, for preparing the initial experiments and for their interpretation later.

Impactor 3. Before we attempted to use Impactor 3 for initiating explosive interactions, we also investigated its output with the tourmaline underwater blast transducer-oscilloscope combination used with Impactors 1 and 2 (Nelson et al., 1999). As before, we placed the surface of the impactor at a depth of 400 mm in the water, and the tourmaline transducer 100 mm above at a depth of 300 mm.

A typical pressure transient generated by Impactor 3 is shown in Figure 8. Note the double peaked pulse, about 100 μ s long, much shorter and simpler than the 1 ms- to 2 ms-long oscillatory pulses generated by Impactors 1 and 2.

As before, we checked the reproducibility of the pulses generated with a given impactor setup by making sets of 10 measurements of the maximum pressure with a driver gas pressure of 1.3 MPa (185 psi). Two sets of measurements with the slug-type impactor are shown as the upper plots in Figure 9. The earlier set, D-67-1, recorded when only gravity was used to reseal the slug, showed considerable variation between shots, with standard deviations of about $\pm 10\%$. We then discovered that if we vented the driving gas from the gun barrel and applied a backpressure to the impactor's canister after each shot to reseal the slug at the bottom of the barrel, the reproducibility between shots increased significantly. This can be seen in the plot for experiment D-89-1 in Figure 9. This latter set of measurements produced a value of 1.963 ± 0.037 MPa ($\pm 1.9\%$) for the pressure transient measured 100 mm above the center of Impactor 3. This value will be used in the discussions below.

In Figure 9, we have also compared the pulses generated by Impactor 3 with similar sets of measurements made with Impactor 2, the pneumatic impactor used for triggering ferrosilicon drops in 1998 (Nelson et al., 1999) and silicon drops early in 1999 and with Impactor 1, the original solenoid-driven impactor used for triggering ferrosilicon drops in 1997 (Nelson et al., 1998, 1999a). It should be noted in this figure that the slug-type impactor generates peak pressures at 100 mm in water at least five times greater than those produced by the pneumatic impactor and more than ten times greater than those produced by the solenoid-driven device, all measured at 100 mm.

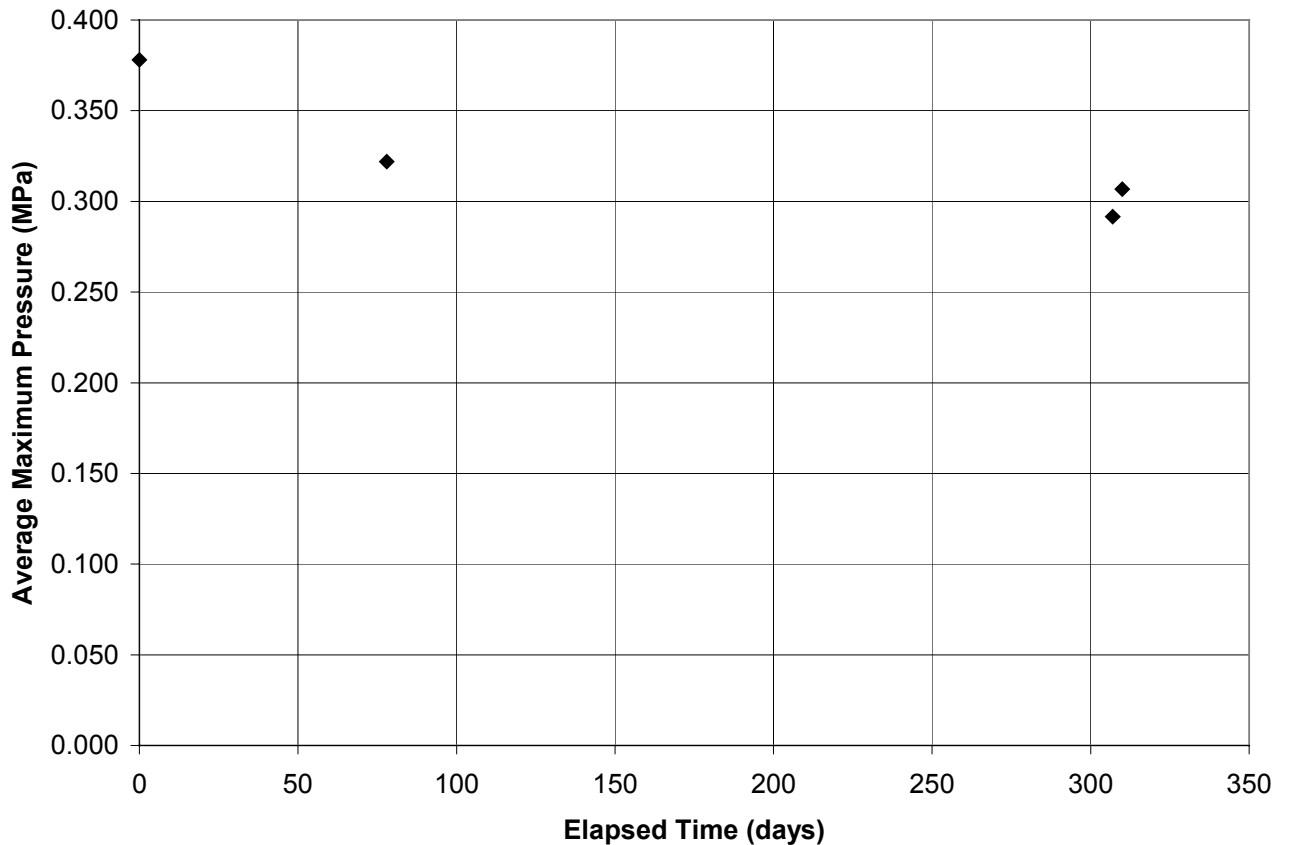


Figure 7. Output of the pneumatic impactor (Impactor 2) vs. elapsed time. (Experiments C-265-3, D-9-1, D-34-1, D-35-1).

Triggering Silicon Drops with the Submerged Photodetector

When we began the 1999 experiments, we quickly realized that there was a significant difference between the response of our photodetector to the silicon drops used in the 1999 studies and to the ferrosilicon drops used in the 1997 and 1988 studies. This difference became apparent when we tried to trigger the silicon drops as they fell past the horizontally-aimed optical axis of the submerged photodetector. The ferrosilicon drops always activated the photodetector almost exactly when they passed its axis. But the silicon drops seldom did; instead, they energized the photodetector very soon after they entered the water, far above the axis.

We attribute this behavior to the silicon drops being significantly brighter than the ferrosilicon drops at the wavelengths to which the photodetector is sensitive. This additional luminosity apparently causes reflections from the walls of the polycarbonate chamber to precede the drops as they fall and activate the photodetector early. Since the distance above the impactor at the time of activation determines the magnitude of the pressure pulse applied for triggering of the drops, and since this magnitude varies with $1/r$, early firing can greatly reduce the triggering effectiveness of the pulse.

Early in the 1999 work, we overcame this difficulty empirically by delaying the firing until the drop had fallen to the proper distance above the impactor. We had used this procedure in the 1998 work but abandoned it because of the effort required to select the proper time delay by trial and error and the uncertainty in fall velocities of the drops.

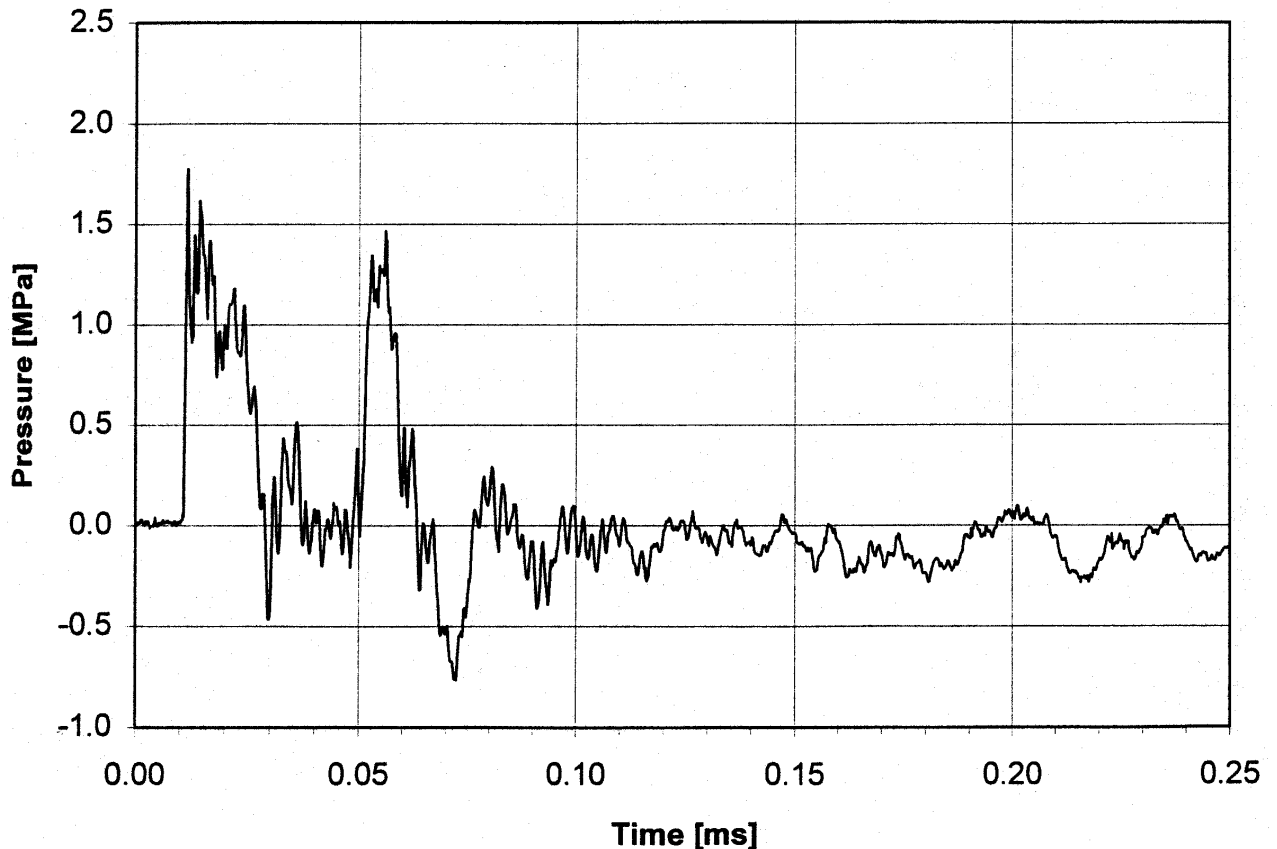


Figure 8. Pressure-time trace measured with the tourmaline transducer placed 100 mm above the surface of Impactor 3, which was 400 mm beneath the water surface. (D-69-1-3).

Later in the 1999 work, we minimized the effects of the reflections by:

- Installing small plates above and below the photodetector to produce a narrow horizontal aperture and thus reduce the reflected light that can enter from above.
- Covering the inner walls of the chamber with thin polycarbonate sheets that have nonreflective coatings (black spray paint).
- Placing nonreflective coatings on other underwater surfaces.

After these actions were taken, the luminous drops of molten silicon caused activation almost exactly at the axis of the photodetector instead of several hundred millimeters above it without these precautions.

Triggered Interactions between Drops of Molten Silicon and Water

During 1999, we performed three sets of experiments with drops of molten silicon:

1. Series A. The experiments were performed with drops prepared from rods taken from three batches of pure silicon, A-4 and A-9,⁴10⁴. These drops were triggered at various depths in the water with Impactor 2.

⁴ Due to confusion in the markings of the rods in the express shipment, we failed to distinguish between the individual rods in these batches. Therefore, batches A-9 and A-10 are treated as one batch, Batch A-9,10.

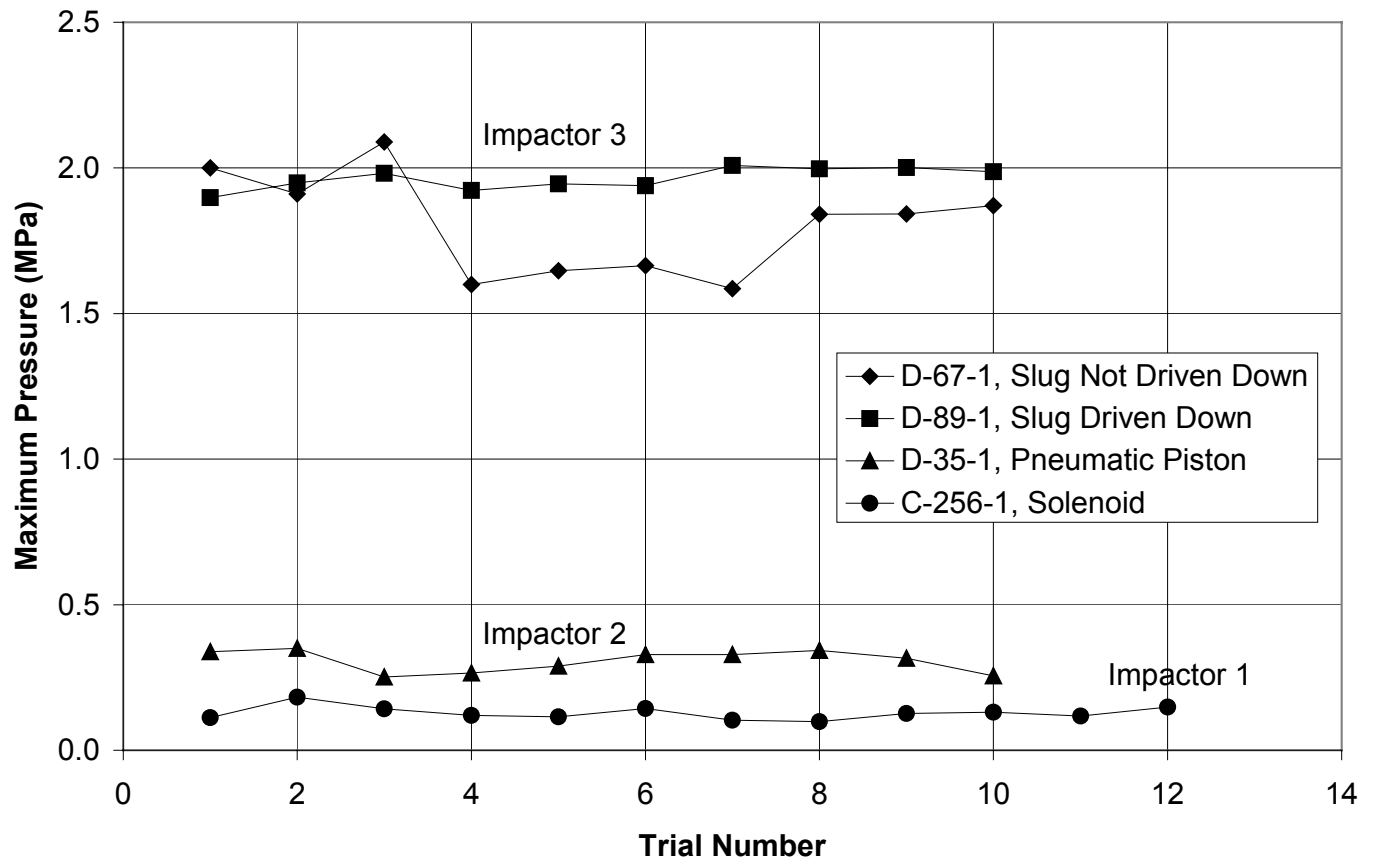


Figure 9. Comparisons of the maximum pressures generated by Impactor 1 (solenoid-driven), Impactor 2 (pneumatic piston-driven) and Impactor 3 (slug-type), measured in repetitive trials. The traces for Impactor 3 were recorded with the slug reset between trials by gravity (slug not driven down) and by applying a backpressure (slug driven down).

- Series B. The experiments were performed with drops prepared from rods taken from two different batches of pure silicon, A-7 and A-8. These drops were triggered with Impactor 3 placed at a constant depth in the water. Hydrogen was collected and measured.
- Series C. The experiments were performed with drops prepared from rods taken from three batches of alloyed silicon: B, with 0.4 w/o Al; C, with 0.04 w/o Ca; and D, with a combination of 0.4 w/o Al and 0.04 w/o Ca. These drops were triggered with Impactor 3 also placed at a constant depth in the water. Hydrogen was collected and measured.

The experiments from Series A, B and C are summarized in Tables 1A, 1B and 1C, respectively.

Series A. (May and June 1999)

When we first began the experiments with drops of molten silicon, we did not anticipate the early firing of the impactor as described above. As a result, the triggering of each drop was attempted with only a relatively small pressure pulse. This can be seen in Table 1A for experiments D-40-1 through D-46-1, where the impactor was placed at depths of 400 mm or 200 mm, with the photodetector axis aimed 25 mm above the surface of the impactor. For these experiments, the magnitude of the pressure pulse applied to the drops was determined approximately from the video records by (a) estimating the distance of the drop above the impactor at the time the impactor was activated and (b) applying the $1/r$ relationship to the value

of 0.3 MPa measured at 100 mm (see Table 2 and Figure 8). Thus, as indicated in Table 1A, if the impactor fires when the drops are 50 mm to 80 mm above its surface, the pressure transients applied to the drops will be only 0.4 to 0.6 MPa, about the same as the threshold of 0.3 MPa required for 11 mm-diameter ferrosilicon drops, but considerably lower than the threshold of 1.3 MPa required to trigger 9 mm-diameter ferrosilicon drops (Nelson et al., 1999).

In experiments D-40-1 through D-46-1, however, there were several interactions in which coarse fragmentation occurred with the lower peak pressures (see Table 1A). These fragmentations occurred when the impactor was at a depth of 200 mm. In each of these interactions, the video images recorded in reflected light showed relatively large luminous bubbles rising after the interaction. Several video records showed that the luminosity was emitted by fragments of silicon that burn and generate hydrogen as the bubbles rise. (Similar behavior was observed in the 1997 experiments when coarse fragmentation of drops of molten ferrosilicon occurred in hot water; see, for example, experiment C-203-1 in Nelson et al., (1998).)

As we examined the video records of experiments D-43-1 through D-46-1, we noted that the drops were about 5 video frames (at 30 frames/second, this corresponds to 0.17 second) above the photodetector axis when the impactor fired. In order to expose the drops to a more intense pressure transient, in experiment D-48-1 we delayed the firing of the impactor 0.17 seconds after the photodetector was activated. (The delayed firing of the impactor was achieved with the time delay relay used in the 1997 work (Nelson et al., 1998).)

When we delayed the firing of the impactor by 0.17 seconds, we achieved an energetic event but not a strong explosion in experiment D-48-1-1 and a strong explosion in experiment D-48-1-2. The impactor was at a depth of 200 mm here. Although the imaging was done only with the video camera and reflected light, we estimated that the impactor fired when the drops had descended to about 25 mm and 10 mm above the surface of the impactor, respectively. With the $1/r$ relationship, this would correspond to applied pressure transients of about 1.3 and 3 MPa, respectively. The former value is about the same as the threshold for triggering the 9 mm-diameter ferrosilicon drops, while the latter is more than twice as large.

Experiment D-48-1-1 was interesting even though there was no strong explosion. The drop in this experiment fell toward the outer edge of the impactor plate, where the pressure pulse would be expected to be lower than near the center of the plate. There was significant fragmentation, however. But also interesting was the observation that the hydrogen bubbles generated during the interaction “popped” audibly when they broke through the surface of the water. This indicates ignition and explosion of the hydrogen when it contacted the air. It also indicates that the hydrogen must have been at a temperature of at least 500 °C, the spontaneous ignition temperature of hydrogen in air (Conti and Hertzberg, 1988).

Experiment D-48-1-2 produced a strong explosion that emitted a flash of light and produced fine debris. It also generated many small hydrogen bubbles that rose afterward and burst through the surface of the water without coalescing. It also deposited a cloud of colloid in the water afterward. Photographs of frame-by-frame images on the video screen are shown in Figure 10. Note that the flash of light is visible in only one video frame, suggesting that the energy transfer in the explosion occurred in 0.033 s or less.

In the experiments performed in Series A after D-48-1, we changed our imaging from the video camera alone with reflected light to open shutter, time-exposed 35 mm photography combined with the video camera in a darkened room.

Thresholds for the Explosions

In this section, we look at the thresholds for triggered explosions of 9 mm-diameter silicon drops in Series A that were prepared from rods taken from Batches A-4 and A-9,10 and released into water at room temperature. These experiments are summarized in Table 1A.

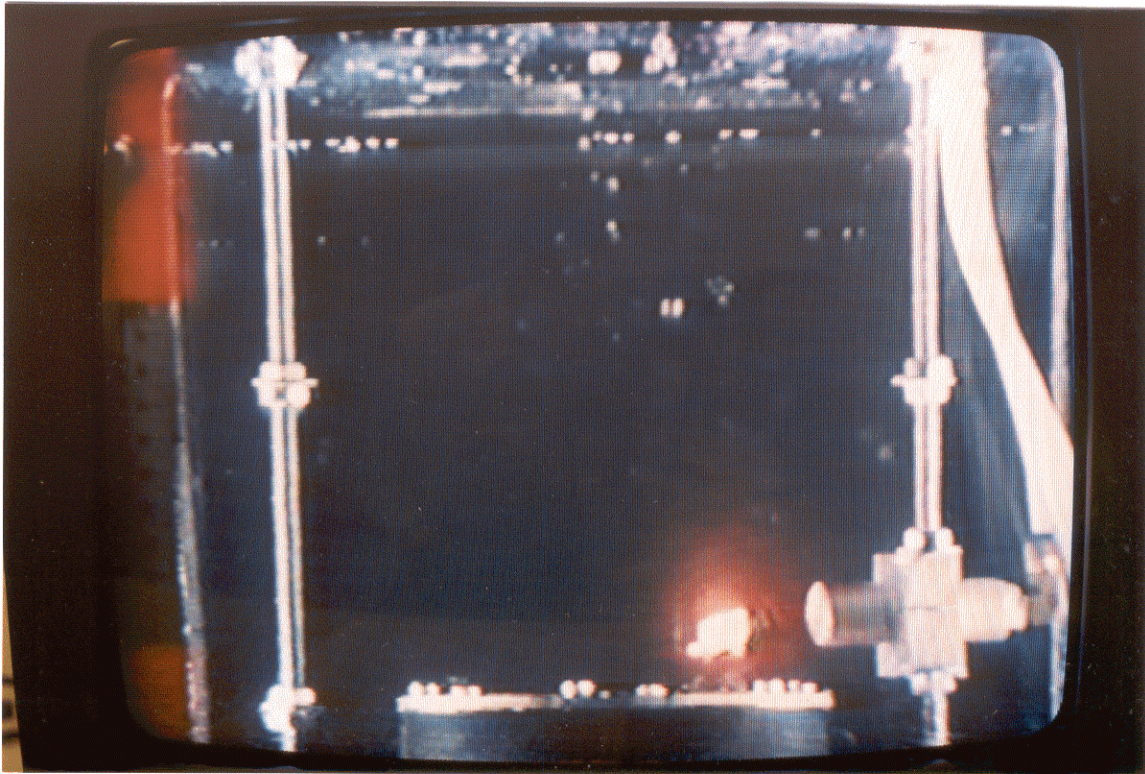


Figure 10a. The first of three photographs of frame-by-frame images on the video screen for Experiment D-48-1-2. The images are recorded (a) one frame before (-0.033 s), (b) during (0.0 s), and (c) one frame after (+ 0.033 s) the explosion. The frames are 0.033 s apart. Impactor 2 was used to trigger the explosion. The horizontal separation of the vertical fiducial bars is 185 mm.

Triggering Intensity. We noted in our discussions of experiments D-43-1 through D-46-1 in the previous section that if Impactor 2 fired when the silicon drops were too high above its surface, the drops would not explode. This was caused by the premature activation of the photodetector. Because the intensity of the pressure transients is proportional to $1/r$, where r is the distance above the impactor, these drops were exposed to triggers smaller than the threshold of 1.3 MPa produced at 25 mm above the surface of Impactor 2 that were required for initiating the explosions of the ferrosilicon drops (Nelson et al., 1999). At distances greater than 25 mm, of course, the intensity of the pulses would be considerably less than 1.3 MPa.

In experiment D-48-1-2, we learned, however, that if the impactor fired when the drop was 10 mm above the surface, there was a vigorous explosion that generated a short flash of light, fine debris, tiny hydrogen bubbles and an almost milky deposit of colloid in the water. In subsequent experiments (see Table 1A) we learned that the explosions occurred only when the drops were closer to the impactor than about 25 mm. This allows us to conclude tentatively that 9 mm-diameter silicon drops that were prepared from rods taken from Batches A-4 and A-9,10 and released into water at room temperature will not explode with pressure transients less than the 1.3 MPa transients that were sufficient to initiate the explosions of the ferrosilicon drops in the 1998 work.

In Table 3, we have summarized the experiments shown in Table 1A in which silicon drops have exploded (X) or quenched without explosion (0) as a function of the applied pressure transient. We have divided the group approximately on the basis of whether the applied transient was greater than or less than 2 MPa, estimated with the $1/r$ relationship from the distance of triggering above the impactor as determined from photographic and video images. From the data shown in Tables 1A and 3, we have made the preliminary

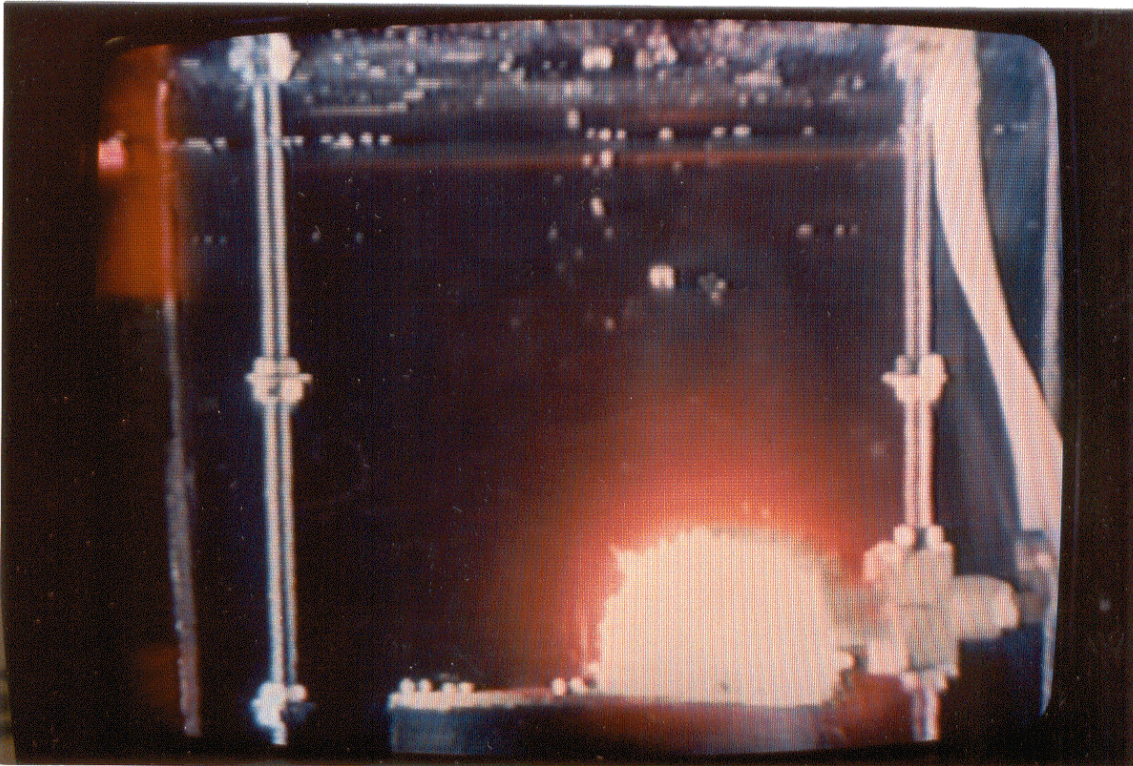


Figure 10b. The second of three photographs of frame-by-frame images on the video screen for Experiment D-48-1-2. The images are recorded (a) one frame before (-0.033 s), (b) during (0.0 s), and (c) one frame after (+ 0.033 s) the explosion. The frames are 0.033 s apart. Impactor 2 was used to trigger the explosion. The horizontal separation of the vertical fiducial bars is 185 mm.

estimate that 2 MPa is approximately the threshold for the transient needed to trigger explosions of 9 mm-diameter silicon drops in Series A that were prepared from rods in Batches A-4 and A-9,10 and released into water at room temperature.

Depth in the Water. After we learned that the approximate magnitude of the threshold pressure pulse needed to initiate the explosions is on the order of 2 MPa at an impactor depth of 200 mm, we began to look at the effect of depth in the water on the ability of the silicon drops to explode. We then increased the depth of the impactor, holding the distance of the photodetector axis above the impactor constant at 25 mm and the delay constant at 0.17 s. We lowered the impactor 100 mm between each experiment, starting at a depth of 200 mm. As shown in Table 1A, we obtained good explosions at 200 mm, 300mm and 400 mm, but not at 500 mm. The experiment at 500 mm was performed twice, and in neither experiment were explosions initiated. We also tried one experiment with the impactor at the bottom of the chamber, 785 mm deep, but there was no explosion at this depth, either. These results are also included in Table 3. We conclude tentatively then that the maximum depth at which 9 mm-diameter silicon drops in Series A that were prepared from rods taken from Batches A-4 and A-9,10 and released into water at room temperature can be triggered to explode with 2 MPa triggers is about 400 mm.

Series B. (July through September, 1999)

Threshold Trigger Pressures at Fixed Depths

For the experiments in this series, we placed the surface of Impactor 3 at the fixed depth of 400 mm and aimed the photodetector axis horizontally 50 mm above it, at a depth of 350 mm. We then varied the

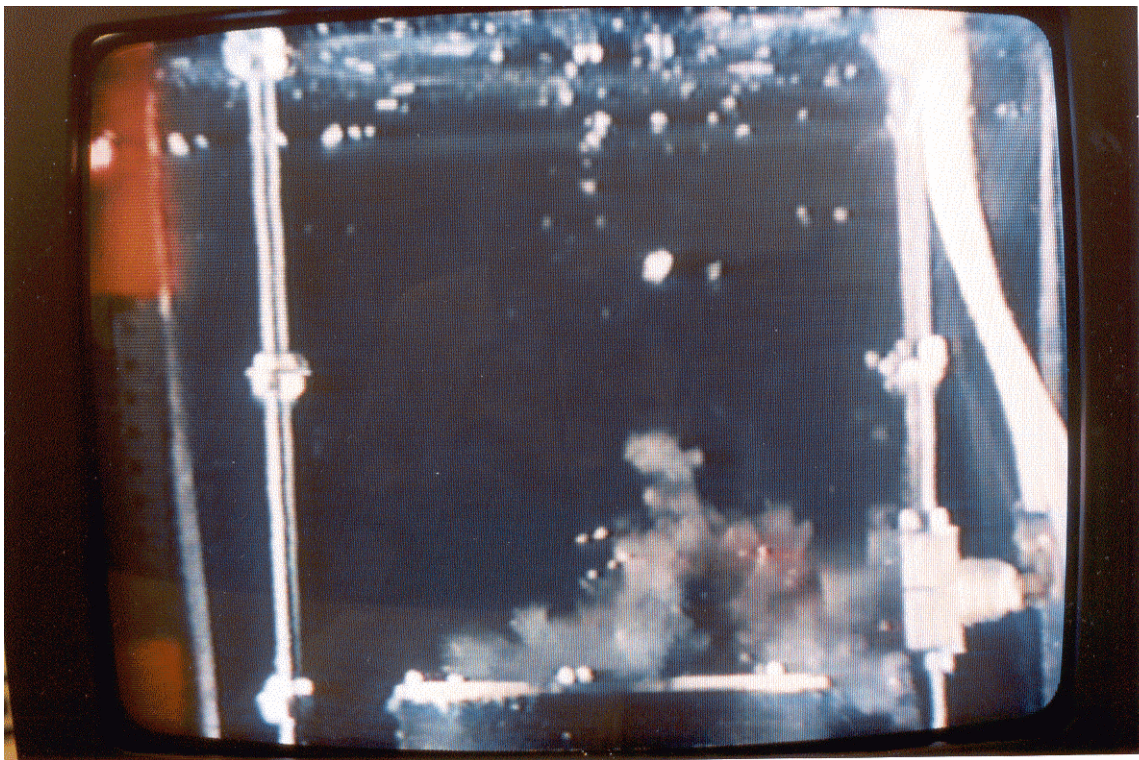


Figure 10c. The third of three photographs of frame-by-frame images on the video screen for Experiment D-48-1-2. The images are recorded (a) one frame before (-0.033 s), (b) during (0.0 s), and (c) one frame after (+ 0.033 s) the explosion. The frames are 0.033 s apart. Impactor 2 was used to trigger the explosion. The horizontal separation of the vertical fiducial bars is 185 mm.

triggering transients by adding short time delays or making small changes in the height of the photodetector axis to alter the distance of the drops above the impactor when it fired. In this way, we could employ the $1/r$ relationship to vary the triggering pressures.

The experiments performed in Series B with Impactor 3 are summarized in Table 1B. The drops were prepared from rods taken from two batches of nonalloyed silicon, A-7 and A-8. All experiments were performed in water at room temperature (nominally 20 °C).

Drops Prepared from Rods in Batch A-8

Based on the peak pressure measured to be 1.963 MPa at 100 mm above Impactor 3, we learned that when the 9 mm-diameter drops prepared from rods taken from Batch A-8 were exposed to transients with peaks of 2.45 MPa (D-90-1-1) or less, there were no explosions; instead, a few coarse particles separated from the parent drop and burned luminously inside rising hydrogen bubbles. But when the pressure transients were 3.27 MPa (D-90-1-2) or greater, there were strong explosions with fine fragmentation and deposition of significant amounts of colloid in the water. Parameters related to the explosive behavior of the drops prepared from the rods in Batch A-8 are summarized in Table 1B.

From these results, we conclude that the threshold pressure transient for triggering 9 mm-diameter silicon drops prepared from Batch A-8 rods at a depth of 400 mm lies between 2.45 MPa and 3.27 MPa, or about 2.9 MPa. This value is consistent with our preliminary estimate of somewhat greater than 2 MPa for molten

Table 3. Explosiveness of Silicon Drops vs. Fall Distance in Room Temperature Water							
(O = No Explosion; X = Explosion)							
Rods A-4 and A-9,10 (10 mm-diameter)							
9 mm-Diameter Drops Triggered with Impactor 2							
	Triggering						
	Depth						
	(mm)	$P_{max} < 2 \text{ Mpa}$			$P_{max} > 2 \text{ Mpa}$		
	0						
	50						
	100						
	150						
	200	0000000000000X			XXX		
	250						
	300					X	
	350						
	400		0			0? X	
	450						
	500					0	
	550						
	600						
	650						
	700						
	785(Bottom)					0	

silicon drops in Series A reported in the previous section. It should also be compared to the lower threshold determined to be 1.3 MPa at similar depths for 9 mm-diameter ferrosilicon drops during the 1998 work (Nelson et al., 1999a).

Drops Prepared from Rods in Batch A-7

After exhausting our supply of rods from Batch A-8, we continued the experiments with rods from Batch A-7. Both batches of rods were received as pure, nonalloyed silicon. We soon learned, however, that drops prepared from Batch A-7 rods behaved differently, requiring stronger pressure transients to initiate the explosions. When the drops were exposed to pulses of 2.45 MPa, we obtained only coarse fragments, many of which burned inside hydrogen bubbles that rose and fell as the oxidation progressed (D-111-1-1). But when the peak triggering pressure was 4.91 MPa, explosions were produced (D-107-1-1, D-109-1-1), but they were not as vigorous as those produced with the rods from Batch A-8.

Table 4. Preliminary Analysis of Silicon Rods^a

Alloy	Al content [wt%]	Ca content [wt%]	Fe content [wt%]
A-7	0.035	0.005	0.013
A-8	0.034	0.004	0.009

^aProvided by Dr. B.Andresen, Fesil, Norway.

There were other differences:

- (a) In similarly triggered experiments, less colloid was generated with drops prepared from the rods in Batch A-7 than with those prepared from the rods in Batch A-8. These lesser amounts seemed to occur both with drops that froze benignly without explosions and those that exploded moderately.
- (b) The amounts of hydrogen generated by the A-7 drops seemed to be lower than the amounts generated in similar interactions by the A-8 drops. At the time these experiments were performed, however, our measurements of hydrogen were not accurate enough to firmly substantiate these observations.

Parameters related to the explosive behavior of the drops prepared from the rods in Batch A-7 are summarized in Table 1B. We hypothesize that the differences between drops prepared from rods taken from Batches A-7 and A-8 may be due to small differences between the compositions of the melts. We are currently having these two batches of silicon analyzed to determine their compositions. A preliminary partial analysis has been received and is presented in Table 4; it indicates a somewhat higher concentration of iron in Batch A-7, but essentially identical contents of aluminum and calcium.

Series C. (October, 1999)

Effects of Alloying

In Series C, we examined how the triggering of steam explosions is affected by alloying the silicon rods from which the drops are prepared. Three experiments were performed with drops prepared from three rods each taken from one of three batches of alloyed silicon: B, with 0.4 w/o Al; C, with 0.04 w/o Ca; and D, with a combination of 0.4 w/o Al and 0.04 w/o Ca. (Analyses are presented in Table E-1 in Appendix E.) The drops prepared from alloys B, C and D were exposed to three different pulse levels: low (about 3 MPa), moderate (5 to 6 MPa) and strong (9 to 10 MPa). These pulses were generated by Impactor 3 with its upper surface placed in the water at a constant depth of 400 mm and with the optical axis of the photodetector aimed horizontally at one of three heights above it to obtain the three different triggering levels at the drop: 100 mm, 71 mm and 50 mm. We released nine drops in all, one of each alloy exposed to one of the three triggering pulses. These experiments are summarized in Table 1C.

When the pulses were strong (9 to 10 MPa), there were no explosions—only coarse fragmentation, with each of the three alloys producing “seaweed-like” time-exposed images. A typical “seaweed-like” image for the B alloy is shown in Figure 11.

When the pulses were of moderate strength (5 to 6 MPa), there was only one good explosion. It occurred with the B alloy (0.4 w/o Al) as shown in the time-exposed image in Figure 12. Drops prepared from the C and D alloys produced only coarse fragmentation that yielded “seaweed-like” time-exposed images similar to that shown in Figure 11.

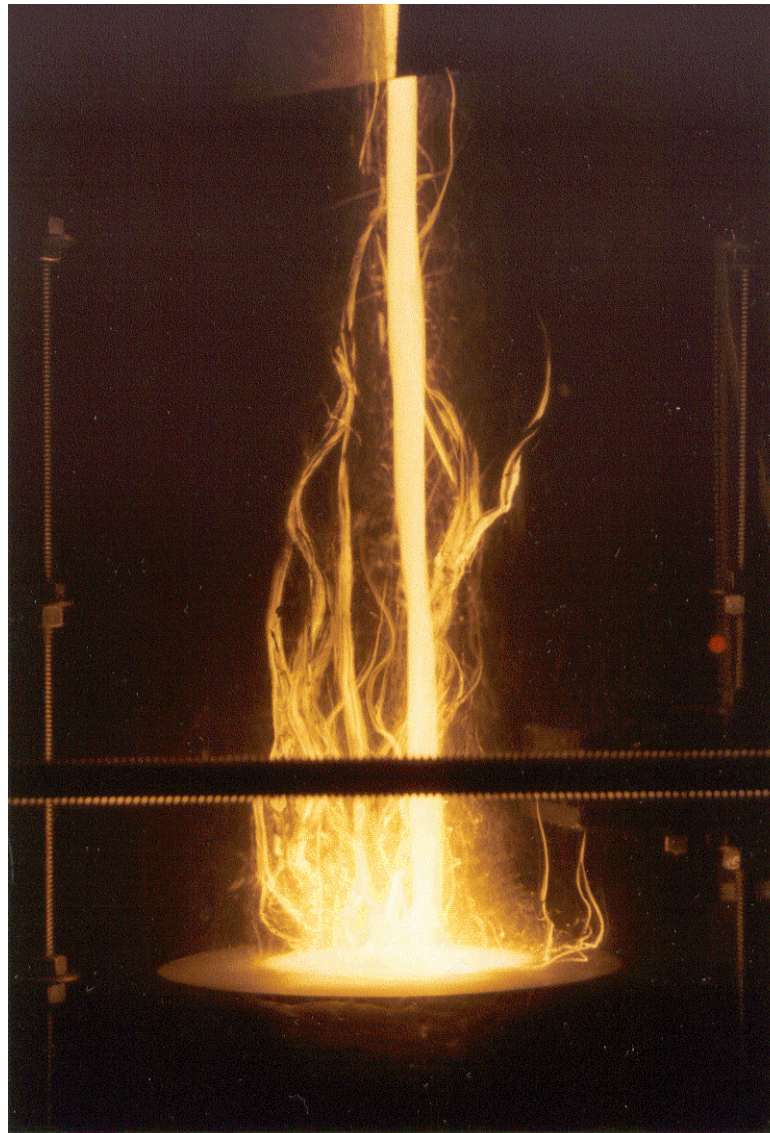


Figure 11. A typical “seaweed-like” time-exposed photograph of a drop of the molten B alloy (0.4 w/o Al) triggered with a strong pulse (10.3 MPa) generated by Impactor 3. There was no explosion, only coarse fragmentation (D-127-1-1). The horizontal separation of the vertical fiducial bars is 185 mm.

When the pulses were low (about 3 MPa), none of the drops exploded. With each alloy, the drops fell and froze without incident, each producing a single uneventful time-exposed photograph similar to the one obtained for the B alloy and shown in Figure 13.

Imaging of Drops of Molten Silicon

Because we devoted considerable effort during 1999 to the timing and sequencing required for the new melt with unexpected brightness, and for checking the new apparatus—Impactor 3 and the hydrogen collector—much of the imaging of the falling drops was done only with the video camera recording with reflected light, indicated by (RL, VCR) in Tables 1A, 1B and 1C. This reduced the quantitative knowledge of the explosions and their energetics that can be obtained from the open shutter, time-exposed photographic images (OS, VCR) and their corresponding shutter wheel images. Although (RL, VCR) images provide important information, it is difficult to use them to investigate the explosive interactions quantitatively because of the relatively low resolution and tendency toward overexposure of the video system.

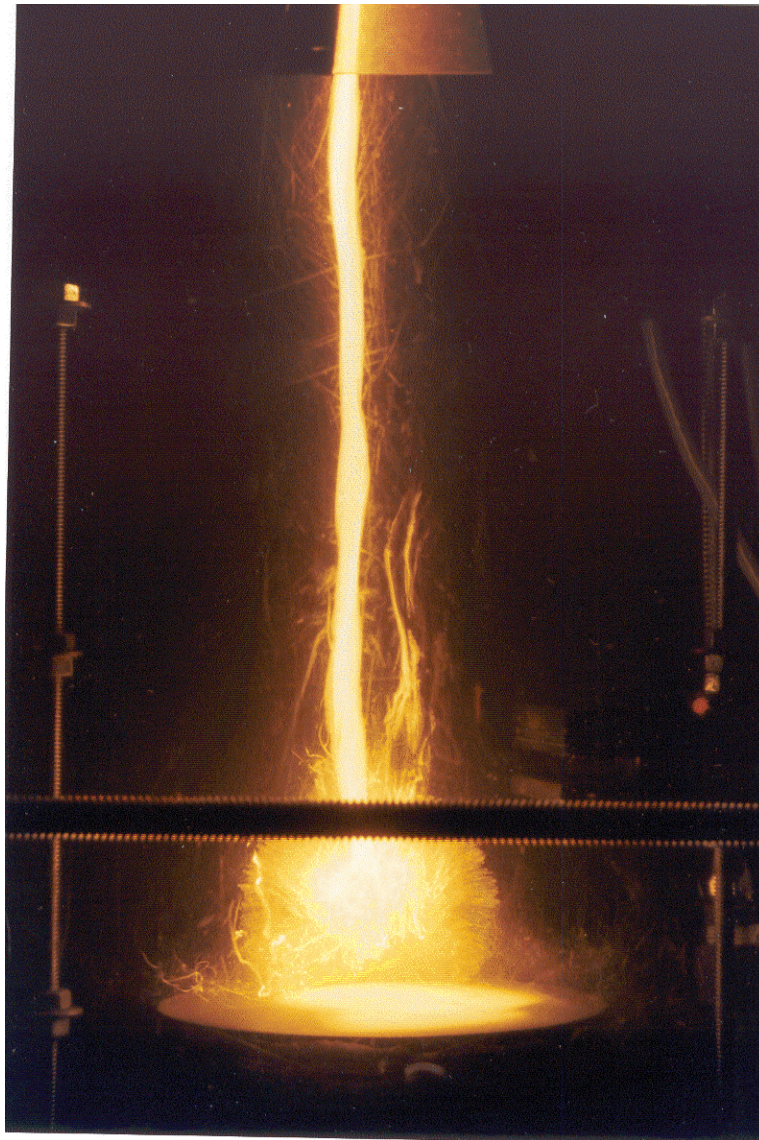


Figure 12. The time-exposed photograph of the only explosion obtained with drops of alloyed silicon. The drop was prepared from the B alloy (0.4 w/o Al) and was triggered with a moderate pulse (5 MPa) generated by Impactor 3 (D-130-1-1). The horizontal separation of the vertical fiducial bars is 185 mm.

We obtained the largest number of (OS, VCR) images in the experiments of Series A, as indicated in Table 1A. A typical image of a steam explosion obtained with a nonalloyed silicon drop prepared from a rod from Batch A-9,10 is shown in Figure 14 for experiment (D-61-1-1). This explosion was triggered with Impactor 2 placed at a depth of 400 mm in the water, with the axis of the photodetector aimed horizontally 25 mm above it, and with a delay of 0.17 seconds. (Note that this explosion occurred very close to the surface of Impactor 2. This closeness will be discussed in a later section.)

In Series B, we recorded only six (OS, VCR) images and these only with silicon drops prepared from rods from Batch A-7. We have recorded one image (experiment D-111-1-1) in which the drop fragmented coarsely and the particles burned luminously while rising and falling within bubbles. This image is shown in Figure 15. This interaction was triggered with the surface of Impactor 3 at a depth of 400 mm in the water and the axis of the photodetector aimed horizontally 50 mm above it; no delay was used.

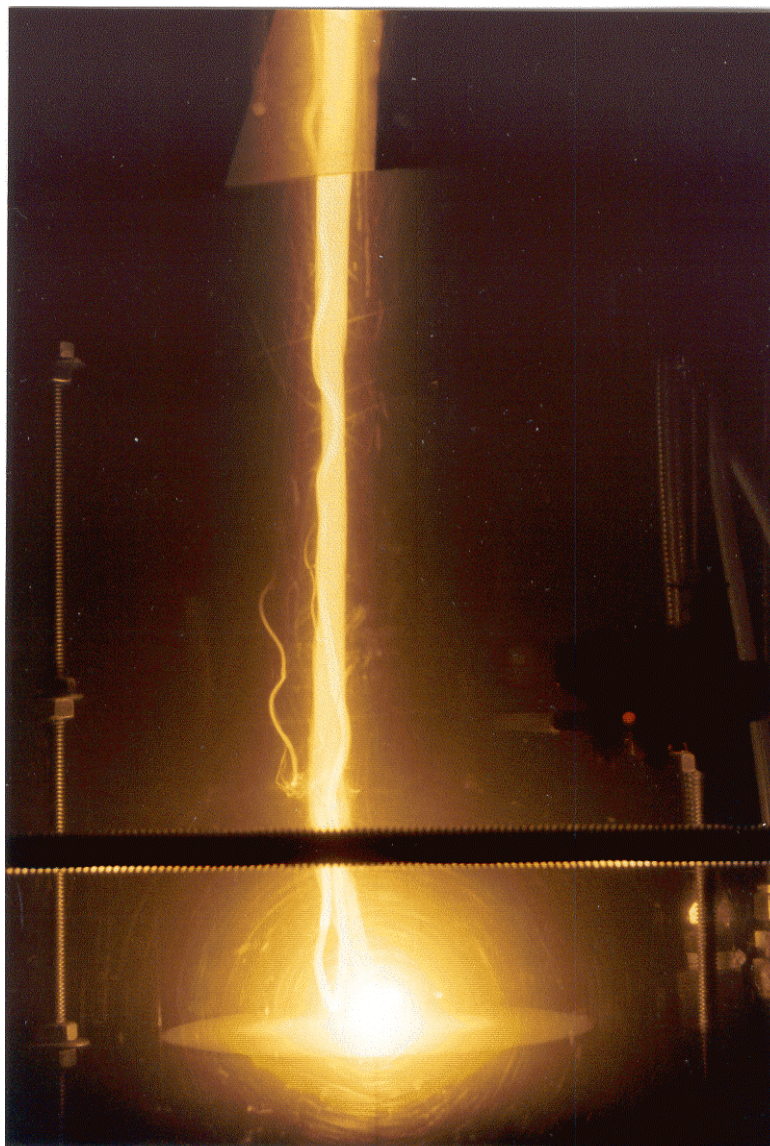


Figure 13. The time-exposed photograph of a drop prepared from the molten B alloy (0.4 w/o Al) and exposed to a low pulse (2.9 MPa) generated by Impactor 3 (Di145-1-1). When the pulses were low, none of the drops exploded; instead, the drops fell and froze without incident, each producing a single uneventful time-exposed photograph similar to the one shown here. The horizontal separation of the vertical fiducial bars is 185 mm.

Another (OS, VCR) image is shown in Figure 16. In this experiment (D-114-1-1), the drop, also prepared from a rod in Batch A-7, exploded vigorously to produce an essentially spherical bubble image. This explosion was triggered with the surface of Impactor 3 at a depth of 400 mm in the water, the axis of the photodetector aimed horizontally 50 mm above it, and with a delay of 0.05 seconds. (Note that the explosion in Figure 16, triggered with Impactor 3, occurred higher above the surface of the impactor than the explosion in Figure 14, triggered with Impactor 2. This increased separation will be discussed later.)

The images from the experiments performed with drops of alloyed silicon in Series C have already been discussed. In this series, we obtained eight (OS, VCR) images (see Figures 11,12 and 13), and one (RL, VCR) image. In each experiment, the trigger was generated by Impactor 3.

Table 4A. Fraction of the Silicon Drops Deposited in the Water as Colloid During Triggered Steam Explosions (Taken from Tables 1A, 1B and 1C.)						
Drop No.	Alloy	Rod Loss Wt (g)	Debris Wt. (g)	Colloid Wt. (g)	Colloid Fraction	
D-48-1-2	A-9,10	2.09	1.65	0.44	0.211	
D-53-1-1	A-9,10	2.00	1.83	0.17	0.085	
D-56-1-4	A-9,10	3.71	3.42	0.29	0.078	
D-59-1-2	A-9,10	2.28	1.86	0.42	0.184	
D-61-1-1	A-9,10	0.87	0.68	0.19	0.218	
D-90-1-2	A-8	2.26	2.05	0.21	0.093	
D-94-1-2	A-8	2.33	1.71	0.62	0.266	
D-97-1-2	A-8	2.15	2.02	0.13	0.060	Min.
D-104-1-2	A-8	2.51	1.98	0.62	0.247	
D-107-1-1	A-7	1.20	0.89	0.31	0.258	Max.
D-109-1-1	A-7	1.07	0.99	0.08	0.075	
D-114-1-1	A-7	1.04	0.91	0.13	0.125	
D-123-1-1	A-7	1.55	1.28	0.27	0.174	
D-130-1-1	B	1.26	1.26	0.00	0.000	

Debris

Granular Debris

The granular debris recovered from the interactions of the silicon drops resembles that recovered from the ferrosilicon drops during the 1997 and 1998 studies (Nelson et al., 1998, 1999). It is generally black, and may include lozenge-shaped frozen drops, angular and smooth chunks, material that resembles black sand and sometimes a fine powdery material. None of the granular debris appears white to the unaided eye. We have not attempted to analyze the debris recovered from the silicon drop experiments, but we have determined the weights and taken dimensionally calibrated 35 mm photographs as appropriate.

Colloidal Debris

Colloidal products are generated when molten silicon drops interact with water. The formation of this material is observed visually and with video imaging both as the drops fall and after the interactions. Sometimes the colloid appears light or dark gray, sometimes white and milky, probably depending on the illumination. The colloidal suspensions are very stable, with little change noticed many hours or even days after an experiment. The suspensions produced with the molten silicon strongly resemble those produced with molten ferrosilicon (Nelson et al., 1999), except, perhaps, that they may be more copious and longer lasting.

Our only quantitative diagnostic for the colloidal material is the difference between the weight of silicon released into the water (the loss in weight of the rod) and the weight of granular debris recovered after the experiment. As shown in Tables 1A, 1B and 1C, in experiments without explosions, this difference is very small, within the precision of the weighings. But when a vigorous explosion occurs, a significant fraction of the silicon often remains suspended in the water; this is shown in Table 4A, in which the colloid fractions for the drops that exploded have been summarized from Tables 1A, 1B and 1C. Note that as much as 27% of the original silicon remained suspended as colloid in experiment D-107-1-1.

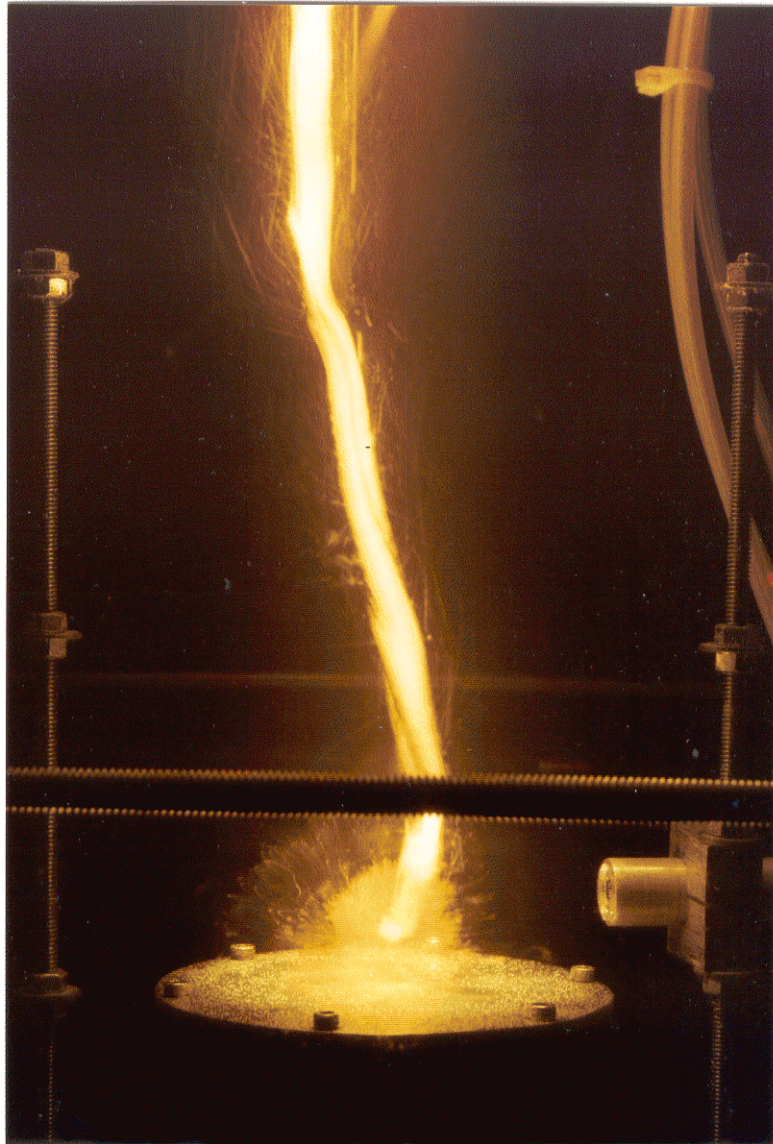


Figure 14. Time-exposed image of the explosion of Drop No. D-61-1-1. Impactor 2 was at a depth of 400 mm with the photodetector 25 mm above its surface. The horizontal separation of the vertical fiducial bars is 185 mm.

When the silicon drops did not explode or fragment (that is, with no trigger or only a very small trigger), the video records showed that colloid was not formed until very late in the quenching process. Instead, these drops began to release a train of small hydrogen bubbles soon after they entered the water and continued throughout the cooling, even after the drops landed on the impactor or the debris collector pan. These drops were usually still partially molten when they landed, and continued their solidification on the surface. Colloid started to rise as a thin wispy column only after the last few hydrogen bubbles were released and solidification seemed to be almost complete.

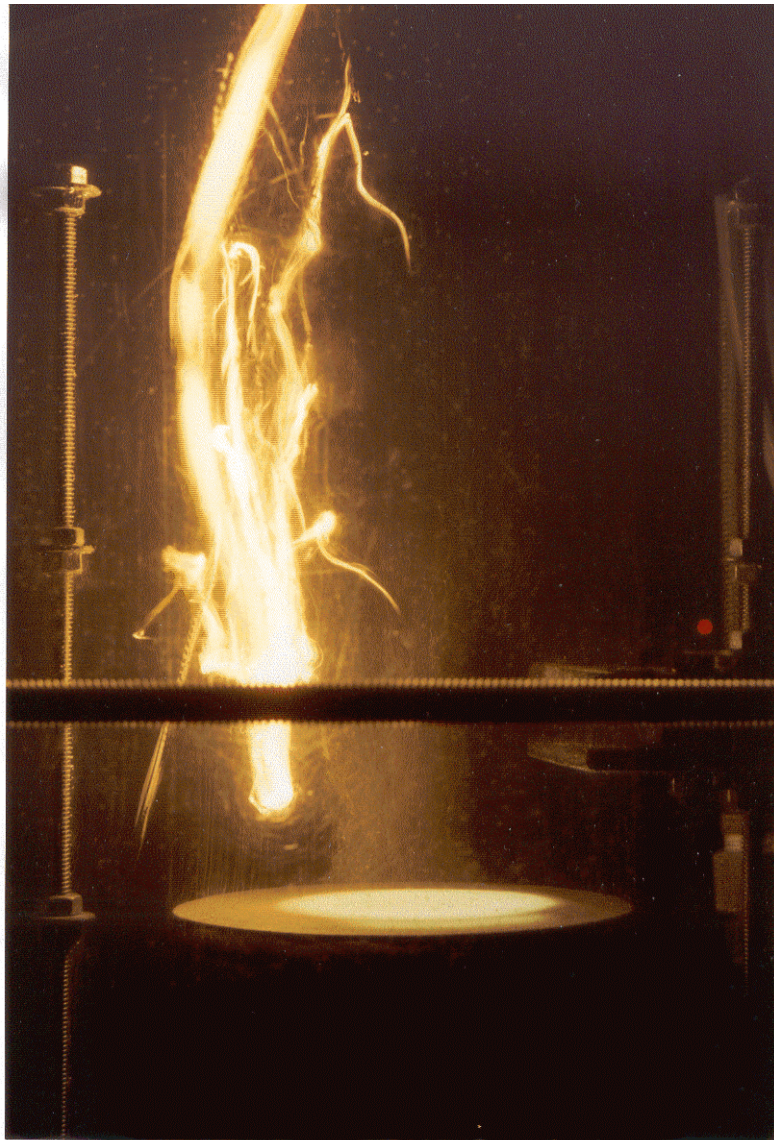


Figure 15. Photographic image of a molten silicon drop prepared from a rod in Batch A-7 that fragments coarsely and the particles burn luminously while rising and falling within hydrogen bubbles. This is an open shutter time-exposed image recorded in a darkened room. Vertical fiducial bars are 185 mm apart. (D-111-1-1). Impactor 3 was used in this experiment.

For example, in experiment D-86-1-2 (see Table 1B), where the impactor was placed 350 mm below the water surface, the drop was exposed to a very weak trigger and did not fragment or explode. The drop landed on Impactor 3 1.667 s after water entry and began to release small hydrogen bubbles at 1.867 s. These bubbles continued to rise for another 3 s before the colloid first appeared at 5.000 s. When the colloid began to appear, the rate of release of the small hydrogen bubbles seemed to drop and remain low until the last bubble was released at 5.800 s. It was difficult to tell exactly when the generation of colloid ended because the video image showed only a gradual transition to a slowly drifting cloud of colloid in the water.

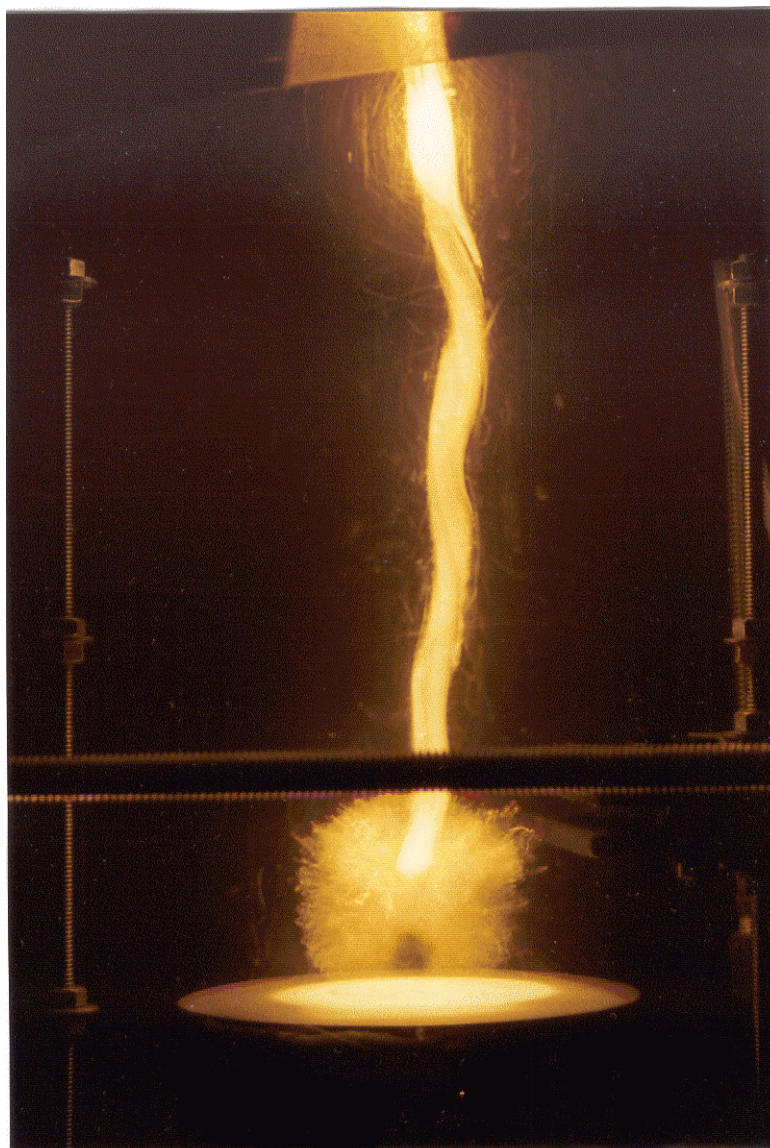


Figure 16. Photographic image of a molten silicon drop prepared from a rod in Batch A-7 that exploded vigorously to produce an essentially spherical bubble. This is an open shutter time-exposed image recorded in a darkened room. Vertical fiducial bars are 185 mm apart. (D-114-1-1). Impactor 3 was used in this experiment.

When the silicon was alloyed with small amounts of Al and/or Ca, there was an unexpected change in the deposition of the colloidal material. In our only explosion of an alloyed silicon drop, experiment D-130-1-1, described in Table 1C and included in Table 4A, there was no measurable deposition of colloid. That is, in each of the nine experiments summarized in Table 1C, either with or without an explosion, the differences between the weight of the drop of melt released into the water (the loss of weight of the rod) and the weight of the granular debris recovered were negligible, at most only a few percent. This indicates that very little colloidal material was deposited in the water during triggered interactions of the alloyed silicon. This is in contrast to the experiments performed with drops of nonalloyed silicon, in which as much as one-fourth of the molten drop remained in colloidal suspension after an explosion (see Tables 1A and B).

Generation of Hydrogen Bubbles

When 9 mm-diameter silicon drops near their melting temperature fell into water at room temperature, hydrogen bubbles were always observed. Bubbles of several appearances were generated in both triggered and untriggered interactions.

Untriggered Drops

In experiment D-38-1, three drops of molten silicon were released a minute or so apart into water at room temperature. Imaging was done with the video camera only, with reflected illumination. Because triggering was not attempted, the impactor was not in the chamber. The stainless steel catcher pan was placed on the bottom of the 1 m-deep chamber, allowing the maximum depth of unobstructed fall for the drops.

Shortly after its entry into the water, hydrogen bubbles began to rise one at a time from the drop. They continued to be generated until well after the drop had landed on the catcher pan. A photograph of a single frame from the video screen recorded 3.66 seconds after release is shown in Figure 6. Here the continuous train of bubbles can be seen rising from the drop.

Early in 1999, we attempted a “guesstimate” of the amount of hydrogen generated by measuring the diameter of the bubbles on the video images. In this way, we estimated the diameters of the bubbles to be approximately 17 mm, which corresponds to a volume per bubble of 2.6 ml. From the video records, we were also able to count the total number of bubbles emitted by each drop both during free fall and after it landed on the catcher pan. For Drops D-38-1-1, -2 and -3, we counted 20, 19 and 18 bubbles, respectively. Taking the average to be 19 bubbles, and the volume per bubble to be 2.6 ml, the “guesstimated” total amount of hydrogen was 49 ml, assuming the gas in the bubble to have equilibrated with the water at room temperature.

Based on this “guesstimate”, we calculated the extent of oxidation of the silicon from the amount of hydrogen generated. At STP, the total number of moles of hydrogen in 49 ml is $49 / 22400 = 2$ millimoles. Compared to the weight of the silicon drop of about 1 gram, which is $1/28.06 = 36$ millimoles, this approximate measurement suggests that about 6% of the silicon had oxidized during the quenching of the drop in water at room temperature.

It will be shown later that after we began to collect the hydrogen and measure its volume directly, we realized that our “guesstimate” was badly in error—about an order-of-magnitude too high.

Interactions with Coarse Fragmentation

In the triggered interactions in which mild interactions occurred, several bubbles much larger than those generated from untriggered drops formed, rose rapidly and burst through the surface of the water. Often in the early stages of the formation of these bubbles, particles of burning silicon were carried upward inside the bubbles as they rose, causing the bubbles to appear luminous. Photographs of several frames from the video screen recorded from 1 frame before to 12 frames after (-0.03 s to + 0.4 s) the trigger fired in Experiment D-43-1-2 are shown in Figures 17a through f. It is difficult to estimate either the number or the volumes of the hydrogen bubbles from these video images.

Interactions with Strong Explosions

In triggered interactions with strong explosions, many small bubbles were generated, along with a cloud of colloidal material. In experiment D-48-1-2, the first strong explosion obtained with silicon, the triggering occurred very close to Impactor 2 (about 10 mm above it), and both bubbles and colloidal material were driven rapidly outward across the surface of the impactor. Shortly afterward, a swarm of small bubbles rose separately until they broke the surface of the water without coalescing. Photographs of several frames from the video screen recorded at - 0.033, 0 and +0.033 s after the trigger fired were shown earlier in Figure 10. In Figure 18, we show another video image of this same experiment, recorded 0.7 seconds after the trigger fired. In this image, many hydrogen bubbles have risen and are about to break through the surface of the

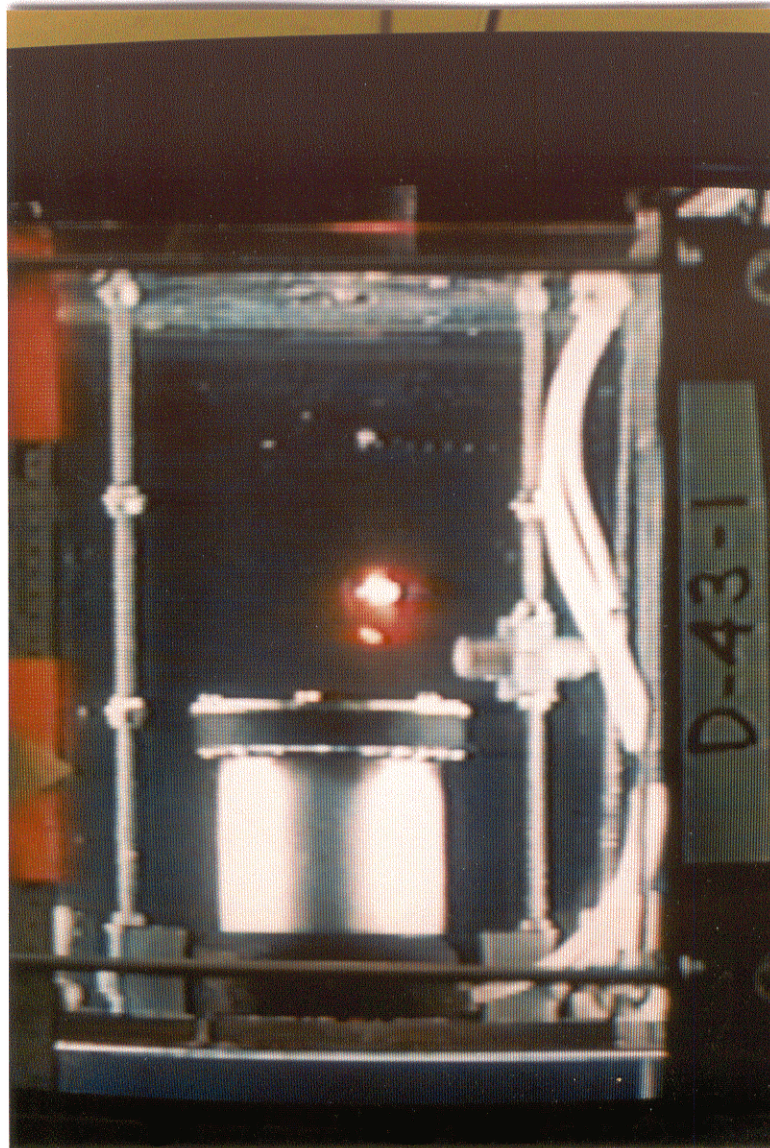


Figure 17a (- 0.033 s). First of six photographs of frames from the video screen recorded from 1 frame before to 12 frames after (-0.03 s to + 0.4 s) the trigger fired for Experiment D-43-1-2. In these images, particles of burning silicon were carried upward inside the bubbles as they rose, causing the bubbles to appear luminous. Impactor 2 was used in this experiment. Vertical fiducial bars are 185 mm apart.

water. As can be seen, it is still more difficult in Figure 18 to estimate either the number of the volumes of the bubbles than in Figure 6. It should also be noted that the bubbles in Figure 18 rise and break through the surface of the water distributed over a circular pattern almost as wide as the entire chamber, perhaps 250 mm across.

Collection and Measurement of Hydrogen

We believe it is important to know how much hydrogen is generated in these three bubble generation situations, both to understand the melt-water interactions and from the standpoint of plant safety. Therefore, we used the collection system with the conical bubble collector, sliding funnel and graduated

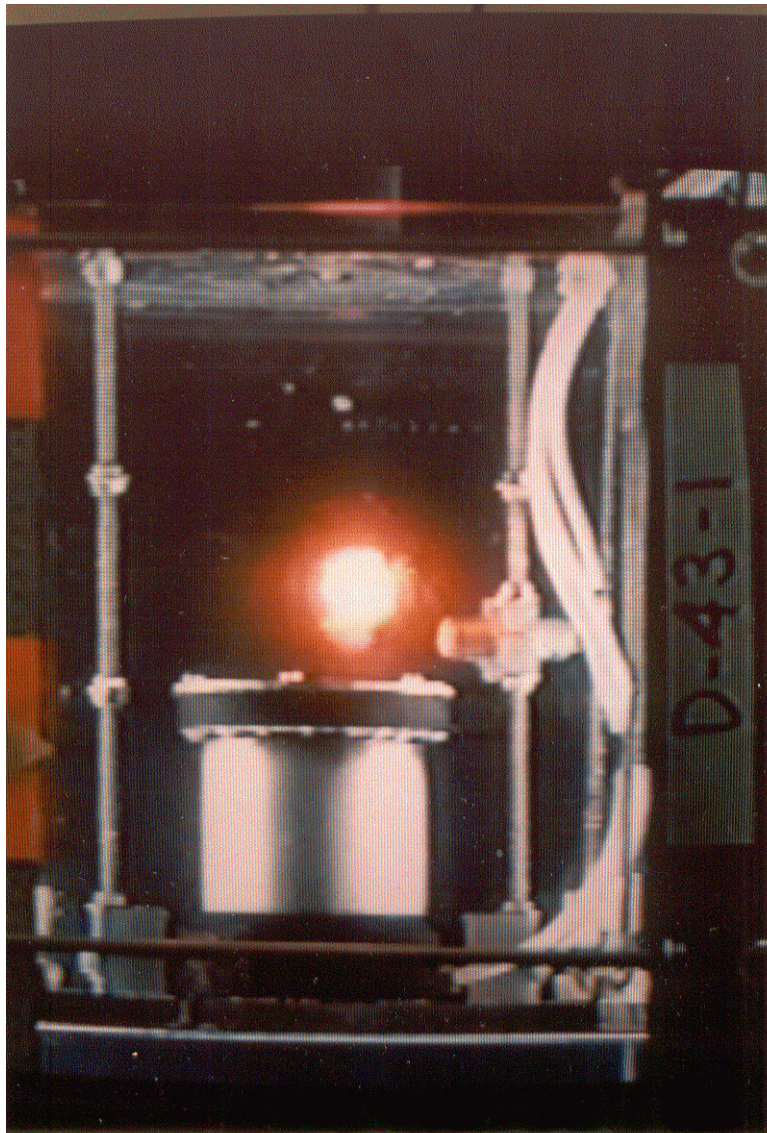


Figure 17b (0.0 s). Second of six photographs of frames from the video screen recorded from 1 frame before to 12 frames after (-0.03 s to + 0.4 s) the trigger fired for Experiment D-43-1-2. In these images, particles of burning silicon were carried upward inside the bubbles as they rose, causing the bubbles to appear luminous. Impactor 2 was used in this experiment. Vertical fiducial bars are 185 mm apart.

cylinder depicted in Figures 4 and 5 to capture and combine the bubbles and to measure the total volume of gas generated. With this technique, the gas is always measured after it equilibrates to ambient temperature, thus eliminating possible overestimation of its volume because it is hot, for example, by measuring high speed photographs of bubbles generated by metal-water reactions (Nelson et al., 1994).

Testing the Hydrogen Collector

We used video imaging time-resolved at 30 frames per second to determine the behavior of the inverted funnel as it slid over the conical bubble collector. We used air at 0.6 MPa (90 psi) to activate the piston that moved the funnel from the right side of the chamber to the center.

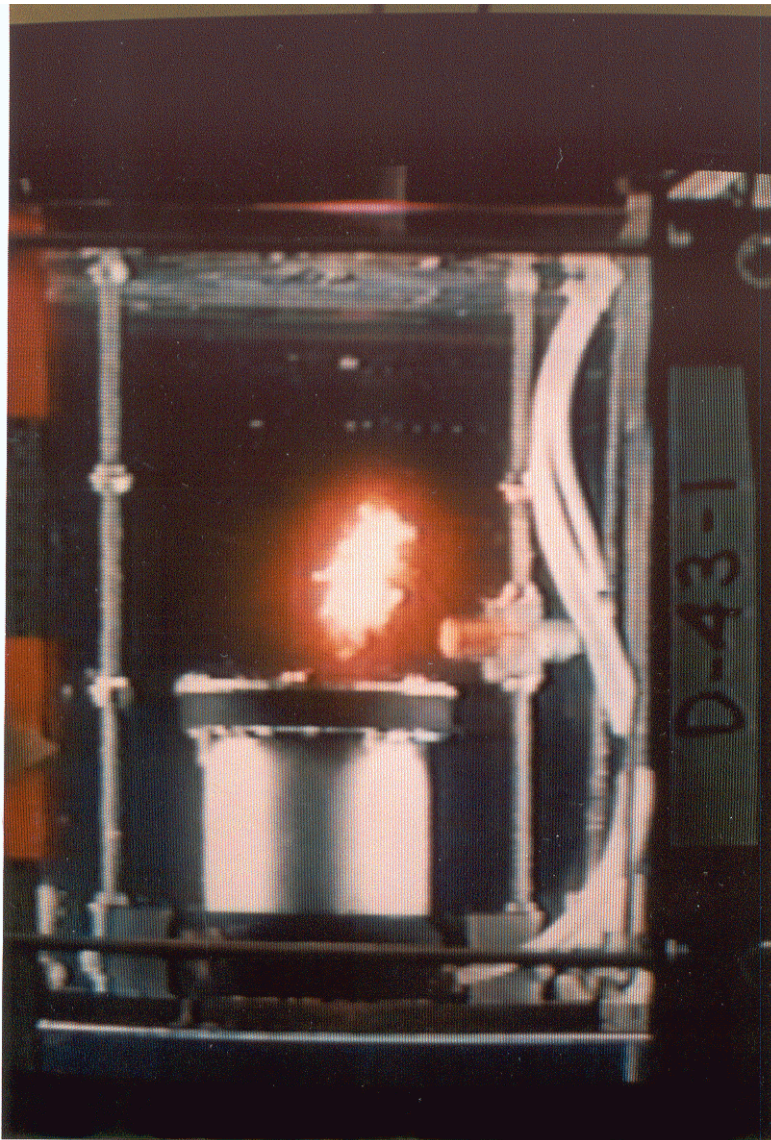


Figure 17c (+ 0.1 s). Third of six photographs of frames from the video screen recorded from 1 frame before to 12 frames after (-0.03 s to + 0.4 s) the trigger fired for Experiment D-43-1-2. In these images, particles of burning silicon were carried upward inside the bubbles as they rose, causing the bubbles to appear luminous. Impactor 2 was used in this experiment. Vertical fiducial bars are 185 mm apart.

First, we tested the closure time of the sliding funnel with video imaging. We learned that with the time-delay relay set at 0.3 s, a typical drop of molten silicon enters the cone 0.2 s after it first enters the water, and the funnel closes completely after an additional 0.3 s. Since the time required for the drop to fall to the appropriate depth and explode and for the bubbles to rise into the cone is usually at least 2 s, there is adequate time for the complete collection of the hydrogen.

We also used the video images to observe the hydrodynamic action of the funnel as it moves through the water. It is important that this motion does not disturb the continuity of the column of water drawn up through the funnel into the graduated cylinder. The video imaging showed that this continuity was not broken during the closure of the funnel and that no spurious bubbles of the ambient atmosphere above the

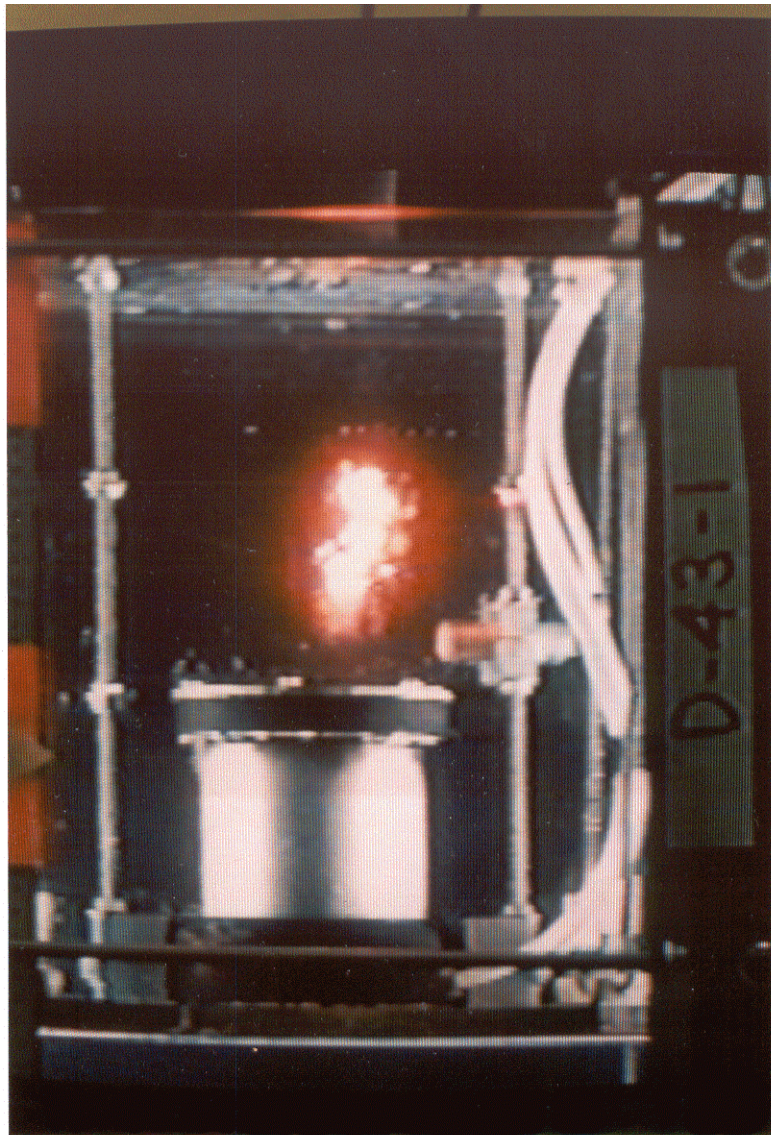


Figure 17d (+ 0.2 s). Fourth of six photographs of frames from the video screen recorded from 1 frame before to 12 frames after (-0.03 s to + 0.4 s) the trigger fired for Experiment D-43-1-2. In these images, particles of burning silicon were carried upward inside the bubbles as they rose, causing the bubbles to appear luminous. Impactor 2 was used in this experiment. Vertical fiducial bars are 185 mm apart.

water surface entered the gas collector as long as a depth of about 50 mm of water was maintained above the lower edge of the funnel.

Collection of Air Bubbles. We also tested the ability of the system to collect and measure various amounts of gas quantitatively. This was done first with capped pipe nipples that had volumes of 14 ml, 91 ml or 167 ml. When one of these nipples was lowered into the water in our chamber with open end down, it carried with it a known volume of trapped air. When one of these nipples was inverted in the water beneath the conical bubble collector, the volume of gas trapped in the nipple was released as a column of bubbles that rose into the cone, the sliding funnel and ultimately into the graduated cylinder, where its combined volume could be measured. When these tests were repeated three times with each nipple, the accuracy of collection was always better than 1% for each volume. (We used a 25 ml graduated cylinder to collect and measure the 14 ml gas volume, and a 250 ml graduated cylinder for the two larger volumes.) Video

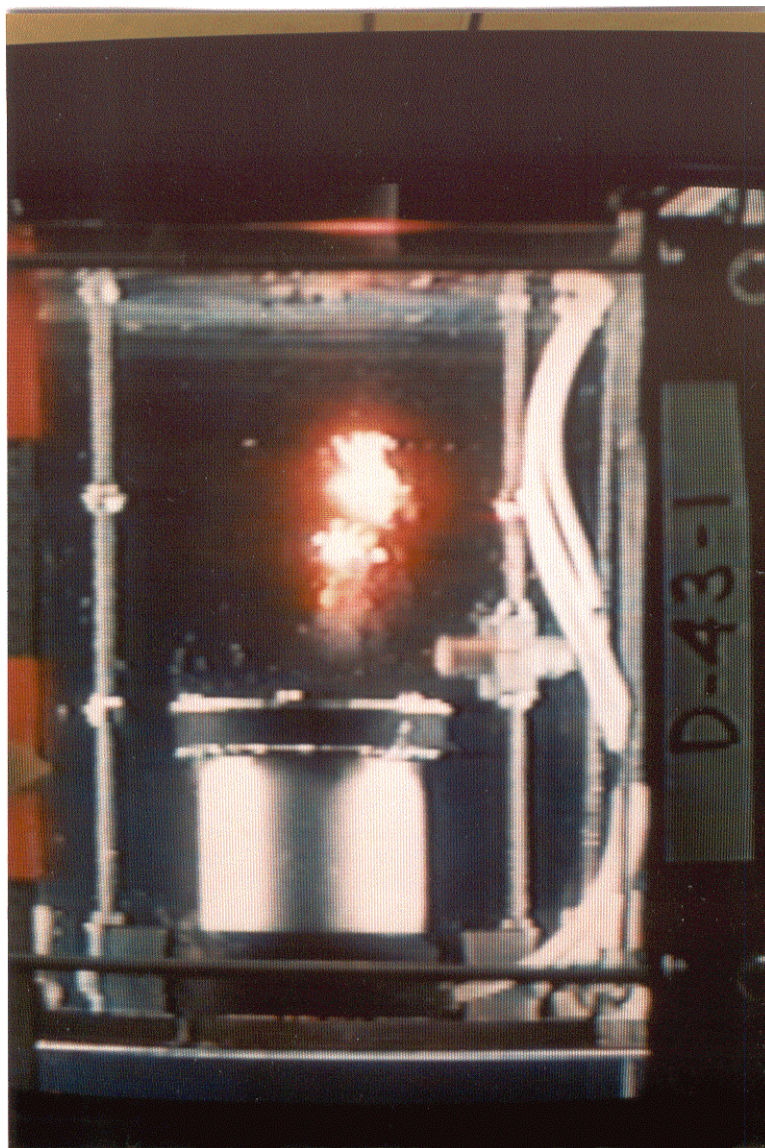


Figure 17e (+ 0.3 s). Fifth of six photographs of frames from the video screen recorded from 1 frame before to 12 frames after (-0.03 s to + 0.4 s) the trigger fired for Experiment D-43-1-2. In these images, particles of burning silicon were carried upward inside the bubbles as they rose, causing the bubbles to appear luminous. Impactor 2 was used in this experiment. Vertical fiducial bars are 185 mm apart.

imaging showed that no bubbles of gas escaped past the edges of either the cone or the funnel for any of the three gas volumes released. This observation was especially important for the largest volume, 167 ml, because the volume of the sliding funnel is only about 150 ml. This indicates that gas begins to bubble into the graduate soon after it enters the sliding funnel.

Collection of Hydrogen Bubbles. There was concern about the accuracy of our volumetric method for collecting small amounts of hydrogen (<10 ml) as bubbles from the water chamber. It has been pointed out to us that the solubility of H₂ in water is appreciable: 21.4 ml/L at 0 °C, 19.1 ml/L at 25 °C, 18.9 ml/L at 50 °C and 8.5 ml/L at 90 °C. Thus if the 90 L of water in the chamber is at room temperature (assume 25 °C) and has not been exposed to H₂ previously, the water will be able to absorb about 1700 ml of H₂ at

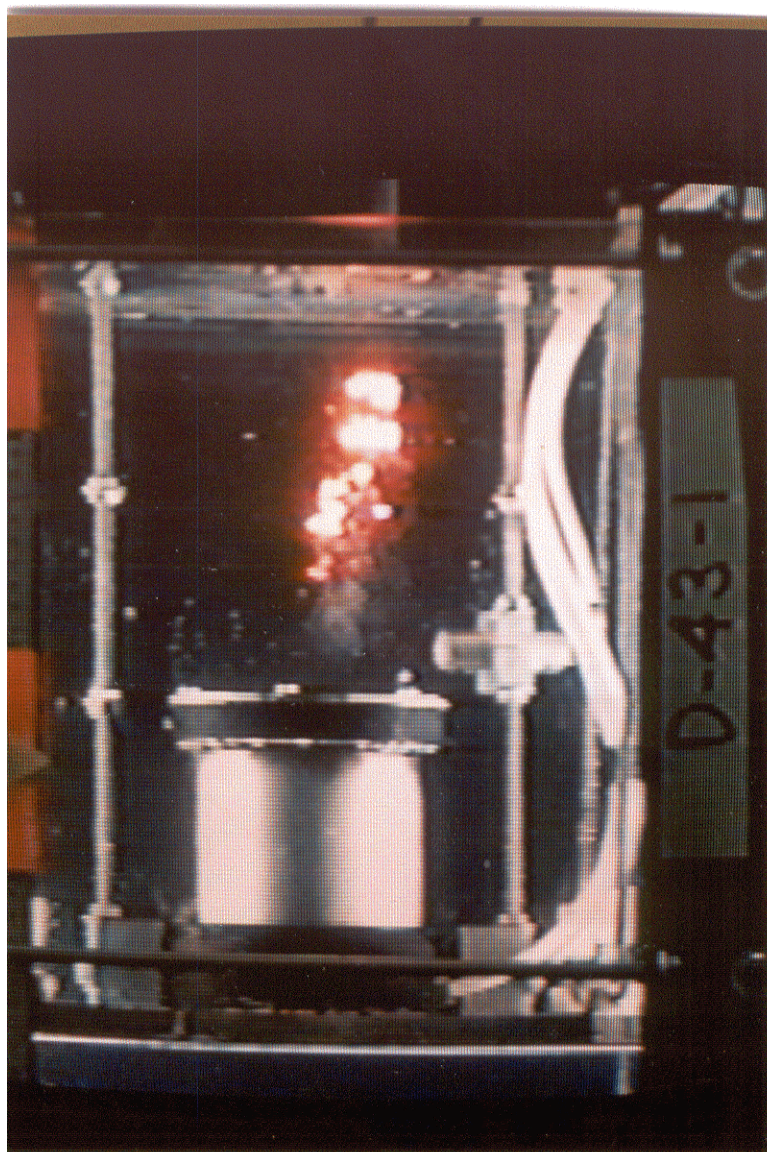


Figure 17f (+ 0.4 s). Sixth of six photographs of frames from the video screen recorded from 1 frame before to 12 frames after (-0.03 s to + 0.4 s) the trigger fired for Experiment D-43-1-2. In these images, particles of burning silicon were carried upward inside the bubbles as they rose, causing the bubbles to appear luminous. Impactor 2 was used in this experiment. Vertical fiducial bars are 185 mm apart.

equilibrium, much more than the 2-10 ml collected in our graduated cylinder. This brings into question our estimates of H_2 generation during the combustion of the silicon.

It is certainly correct that if the hydrogen bubbles were to come into equilibrium with the water in the chamber, they would completely dissolve. This should be the case when the bubbles travel long distances through the water, when the bubbles are very fine and/or when there is stirring or turbulence of the water. Therefore, it was necessary to determine the losses as hydrogen bubbles rose through about 400 mm of water with contact times of a few seconds.

In order to estimate the possible losses with minimum effort, we again used an empirical approach, namely, to release known small volumes of 3-8 ml of gaseous hydrogen in the water beneath our hydrogen collector as we did in the experiments with air-filled capped pipe nipples described in the previous section.

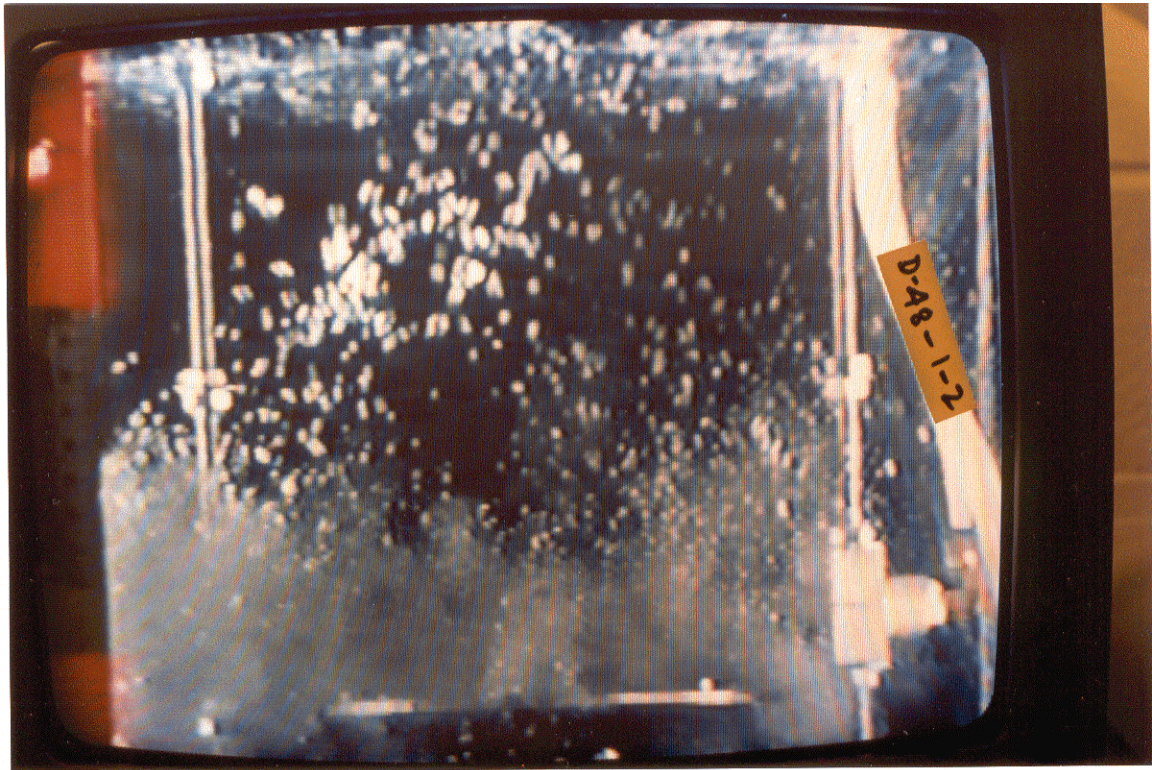


Figure 18. Photograph of a video image recorded 0.7 seconds after the trigger fired in Experiment D-48-1-2. This frame was recorded later in the explosion shown in Figure 17. In this image, many hydrogen bubbles have risen individually without coalescing and are about to break through the surface of the water. Impactor 2 was used in this experiment. Vertical fiducial bars are 185 mm apart.

We performed these experiments by releasing between 3 and 8 ml of gaseous hydrogen from a hypodermic syringe attached to a 4.2 mm-ID tube, the end of which was placed at a depth of 400 mm in the water beneath our collector. The results of four tests were:

- (1) Volume of H₂ released, 3.0 ml, volume collected, 3.0 ml;
- (2) Volume of H₂ released, 4.6 ml, volume collected, 4.5 ml;
- (3) Volume of H₂ released, 6.8 ml, volume collected, 6.9 ml; and
- (4) Volume of H₂ released, 8.1 ml, volume collected, 8.0 ml.

The differences between the amounts of hydrogen released and the amounts collected were quite small, within the uncertainty level of these experiments.

The conclusion we can draw from both sets of experiments is that there seems to be very little loss of either air or hydrogen by dissolution into the water from the bubbles in the short times during which they rise into the collector. (Note that the solubility of air in water is of the same order as H₂ (at 25 °C, the solubilities of H₂, N₂ and O₂ are about 19 ml/L, 20 ml/L and 32 ml/L, respectively).)

We must note, however, that the bubbles of both air and H₂ released in these tests were fairly large, with diameters from perhaps 4 mm to greater than 10 mm. More experiments should be performed to learn how small bubbles would compare, such as the tiny ones observed after the steam explosions of drops of molten silicon.

Hydrogen Generated by Drops of Molten Silicon

The volumes of hydrogen measured in the silicon drop experiments are summarized in Tables 1B and 1C.

When a single 9 mm-diameter drop of molten silicon was released into water at room temperature and exposed to no trigger or to a very low trigger (for example, when the drop veers to the edge of the impactor), about 1 ml of hydrogen was collected.

When the silicon drop was exposed to a trigger pulse that caused the drop only to fragment coarsely, more hydrogen was generated, 2 or 3 ml. The coarse fragments of silicon often burned luminously and rose within hydrogen bubbles for a second or so after the trigger was applied. (In fact, in some experiments, for example, D-111-1, several burning particles actually rose through the sliding funnel and into the graduated cylinder.) Particles that burn as they rise within hydrogen bubbles produce “seaweed-like” images in open shutter photographs such as Figure 15. (Similar “seaweed-like” images were produced when coarse fragments of molten ferrosilicon burned in hot water (Nelson et al., 1998).)

When the triggering transients were strong enough to initiate vigorous explosions, larger amounts of hydrogen were generated. For example, volumes of 5 ml each were collected in both experiments D-94-1-2 and D-104-1-2. (These values may be somewhat high, however, because during our earliest experiments, air trapped in crevices in the base of the impactor sometimes was released during a strong steam explosion. The crevices were eliminated as a source of spurious gas in the later experiments by covering the base of the impactor with a heavy adhesive tape.)

We also learned that when we switched from the rods in Batch A-8 to those in Batch A-7, the explosions of drops produced from Batch A-7 seemed to generate less hydrogen than those produced from Batch A-8. Thus in experiments D-107-1-1 and D-109-1-1, we collected only 3.5 ml and 1.5 ml of hydrogen, respectively, compared to 5 ml in both experiments D-94-1-2 and D-104-1-2⁴. It should be emphasized, however, that the volumes of hydrogen measured in these latter two experiments may be somewhat high because of the reasons cited in the previous paragraph.

Alloying the silicon affected the generation of hydrogen. As shown in Table 1C, the smallest amounts of hydrogen were generated in Series C by the drops of alloy C that contained only the calcium additive—about 4 ml when there was coarse fragmentation and about 2 ml when the drops did not fragment. Also, the largest amounts of hydrogen were generated by the drops of alloy D that contained both aluminum and calcium—about 7 ml when there was coarse fragmentation and again about 2 ml when the drops did not fragment. Intermediate amounts of hydrogen were collected when the alloy contained only the aluminum additive (alloy B)—about 6 ml when there was coarse fragmentation or an explosion of the drops, and again about 2 ml when the drops did not fragment.

Energetics of the Explosions

In the 1998 experiments (Nelson et al., 1999), we estimated the amounts of energy released to the water by the steam explosions of drops of molten ferrosilicon. These energies were determined from the pressure-volume products of the bubbles generated by the explosions, where the bubble volumes are determined from the photographic images of the explosions. Bubble volumes can be converted into energies as follows:

$$E \text{ (J)} = 1013 [P_{\text{amb}} \text{ (MPa)} \times V \text{ (liters)}]$$

⁴ A similarly smaller amount of hydrogen, 3.4 ml, was collected in the single transducer experiment, D-150-1 described in Appendix B. Here, the rod was also taken from Batch A-7.

Table 5. Energetics of the Explosions of 9 mm-Diameter Drops of Molten Silicon in Water at Room Temperature														
Drops were prepared from rods of Batch A-9/A-10 and were triggered with Impactor 2.														
Drop No.	Impactor	Fiducial		Bubble Diam. (mm)		Bubble Volume (cc)		PV Energy (J) ^b			Drop Wt. ^c (g)	PV Energy / Wt. of Si (J/g) ^b		
		Depth(mm)	Sepr.(mm)	#1	#2	#1	#2	#1	#2	Total		#1	#2	Total
D-56-1-4	200	86/185 ^a	30/65 ^a	None	144	None	14.5	None	14.5	0.93	15.6	None	15.6	
D-59-1-2	300	87/185 ^a	20/42.5 ^a	44/93.6 ^a	40.2	429	4.0	43.5	47.5	0.88	4.5	49.8	54.3	
D-61-1-1	400	88/185 ^a	18/37.8 ^a	44/92.5 ^a	28.3	414	2.9	41.9	44.8	0.87	3.3	48.2	51.5	

^aThe first entry is the dimension as measured on the photograph. The second is the true value.

^bCalculated from the relationship: $PV (J) = 1013 [P_{amb} (Mpa) \times V_{max} (Liters)]$.

^cAverage weight per drop based on the loss of weight of the silicon rod.

where P_{amb} is the ambient pressure against which the bubble grows and V is the volume of the bubble. We assume here that the pressure needed to blow a bubble underwater is not very different from the local barometric pressure plus that of the depth of the water. Because our experiments are performed in less than a meter of water, we can equate P_{amb} to P_{atm} , the local barometric pressure; that is, for our present purposes, $P_{amb} = P_{atm} = 0.1$ MPa.

Thus, if we can accurately determine the true dimensions of the steam explosion bubbles from our images of the interactions, we will be able to estimate the amount of energy transferred to the water.

In our work with drops of molten ferrosilicon (Nelson et al., 1998), we compared the images of steam explosions recorded by high-speed photography in reflected light with time-exposed images recorded in a darkened room by the self-luminosity of the melt particles. We learned that the time-exposed images could be used with reasonable accuracy to estimate V_{max} , the maximum volumes of the steam bubbles generated during the explosions. Because these estimates can be performed quickly and inexpensively, without the need for high-speed photography, we used this procedure exclusively during the 1998 work for determining the maximum bubble volumes produced by the explosions of molten ferrosilicon. We also applied the procedure to the explosions of drops of molten silicon in the 1999 work.

In Figure 14, we show the time-exposed image of the explosion of Drop No. D-61-1-1 that was prepared from a rod in Batch A-9,10 and triggered by Impactor 2 at a depth of 400 mm. Note that the image shows a double bubble, similar to those observed with some ferrosilicon drops in the 1998 work (Nelson et al., 1999). If we use the known horizontal separation of the fiducial bars in the image in Figure 14, we can estimate the maximum true diameters of the steam explosion bubbles to be 37.8 mm and 92.5 mm. These correspond to maximum bubble volumes of 28.3 cc and 414 cc and energies of 2.9 J and 41.9 J. For the averaged drop weight (loss of weight of the rod / no. of drops released) of 0.87g, these energies per unit weight of silicon are about 3.3 J/g and 48.2 J/g, respectively, for a total of about 51.5 J/g.

We have made similar estimates of the PV energies for the explosions of two other drops prepared from a rod in Batch A-9,10: D-56-1-4, triggered by Impactor 2 at a depth of 200 mm; and D-59-1-2, triggered by Impactor 2 at a depth of 300 mm. The total energies for these two drops are 15.6 J/g and 54.6 J/g, respectively. We have collected the energy values estimated for these three experiments in Table 5. Note that these values are on the same order as the energies of 20-50 J/g determined for the ferrosilicon drops in the 1998 work.

At present, we have analyzed only one open shutter time-exposed image of a silicon drop prepared from a rod in Batch A-7, namely, that for experiment D-114-1-1, triggered by Impactor 3 at a depth of 400 mm; this image is shown in Figure 16⁵. From the essentially spherical bubble image shown in this figure and the

⁵After the regular work was finished in 1999, a single experiment (D-150-1) was performed with a silicon drop prepared from a rod in Batch A-7; it was triggered with Impactor 3 at a dpth of 400 mm. In this experiment, transducer measurements of pressurizations vs. time were made during the explosion. Using the (RL, VCR) image of the explosion, the PV energy produced by the explosion of this drop was estimated to be about 50 J/g of melt. This experiment is summarized in Appendix B.

Table 6. Fall Distance vs. Time for Drops of Molten Silicon and Ferrosilicon in Water at Room Temperature

Drop No.	D-38-1-1	D-38-1-2	D-38-1-3	C-129-1	D-25-1-1	C-268-1	
Drop Diameter (mm)	9	9	9	9	9	11	
Crossrod	Distance (mm)	Silicon (Seconds)	Silicon (Seconds)	Silicon (Seconds)	Ferrosilicon (Seconds)	Ferrosilicon (Seconds)	Ferrosilicon (Seconds)
1	0	0	0	0	0	0	
2	311	1.23	1.03	1.53	0.72	0.87	0.48
3	635	2.67	2.17	3.30	1.64	1.80	1.17
Bottom	959	4.00	3.20	4.87	2.59	NM	2.00
	Slope(mm/s)	238.10	298.10	195.40	367.30	352.70	471.90

known separation of the vertical fiducial rods, 185 mm, we estimate the maximum diameter of the bubble to be 60.6 mm which corresponds to a maximum volume of the bubble, V_{\max} , of 0.117 L. The PV_{\max} energy transferred to the water, then, is 11.8 J. For the drop weight of 1.04 g, the energy transferred per gram of melt is $E(\text{J/g}) = 11.3 \text{ J/g}$.

This value can be compared with the analogous results obtained with 9 mm-diameter drops of molten ferrosilicon shown in Figure 19 of the final report for the 1998 work (Nelson et al., 1999). For triggering depths of 400 mm, those values ranged from about 7 J/g to about 26 J/g. Thus, the single value for the 9 mm-diameter silicon drop prepared from the rods in Batch A-7 is of similar magnitude as for the 9 mm-diameter ferrosilicon drops.

Fall Behavior of Drops of Molten Silicon

Early in the Series A experiments, we noticed that the 9 mm-diameter drops of molten silicon fell through the water more slowly than the drops of molten ferrosilicon of the same diameter studied in 1997 and 1998 (Nelson et al., 1998, 1999).

The slower fall of the silicon drops was confirmed by examining the video records for experiment D-38-1, in which the drops were allowed to fall the entire 1 m-depth of the chamber. We did this by viewing the video images frame-by-frame and noting when the drops fell behind the four reinforcing crossrods that pass horizontally across the chamber. This procedure is the same as that used for the ferrosilicon drops in the 1998 work (Nelson et al., 1999). In Table 6, we have summarized these times for the three 9 mm-diameter drops of molten silicon released during experiment D-38-1, and compared them with the analogous times for 9 mm- and 11 mm-diameter drops of ferrosilicon. These times are plotted against the fall depths of the drops in Figure 19. It should be noted that even though there is considerable scatter between their depth-time relationships, the three silicon drops always fell more slowly than their ferrosilicon counterparts.

In Table 6, we have also included the slopes of the depth-time plots calculated for the five drops. These slopes indicate that the 9 mm-diameter silicon drops fell at 200 to 300 mm/s, about $\frac{3}{4}$ as fast as the 9 mm-diameter ferrosilicon drops that fell at about 350 mm/s, and about $\frac{1}{2}$ as fast as the 11 mm-diameter ferrosilicon drops that fell at about 470 mm/s.

As the experiments in Series A progressed, we gathered more depth-time data for the 9 mm-diameter drops of molten silicon. Plots of these data are shown in Figure 20. At first, the new data seemed to indicate only poor reproducibility between experiments. But then we realized that the weights of the drops also varied somewhat when the experiments were repeated, and that the heavier drops seemed to fall faster. Therefore,

Table 7. Fall Behavior of 9 mm-Diameter Drops of Molten Silicon in Water at Room Temperature

Trial Number	Drop No.	Alloy ^a	Fall to Crossrod 2 at 311 mm			Fall to Crossrod 3 at 635 mm		
			Frames	Time (s)	v (mm/s)	Frames	Time (s)	v (mm/s)
1	D-38-1-1	A-4	38	1.254	248			
2	D-38-1-2	A-4	40	1.320	236			
3	D-38-1-3	A-4	46	1.518	205			
4	D-40-1-1	A-4	44	1.452	214			
5	D-40-1-2	A-4	43	1.419	219			
6	D-50-1-1	A-9,10	38	1.254	248	84	2.772	229
7	D-50-1-2	A-9,10	40	1.320	236	85	2.805	226
8	D-52-1-1	A-9,10	48	1.584	196			
9	D-52-1-2	A-9,10	40	1.320	236			
10	D-52-1-3	A-9,10	38	1.254	248			
11	D-61-1-1	A-9,10	No video ^b	1.499	207			
12	D-62-1-1	A-9,10	35	1.155	269			
13	D-64-1-1	A-9,10	38	1.254	248			
14	D-71-1-1	A-8	33	1.089	286	63	2.079	305
15	D-74-1-1	A-8	44	1.452	214	94	3.102	205
16	D-74-1-2	A-8	43	1.419	219	93	3.069	207
17	D-74-1-3	A-8	37	1.221	255	78	2.574	247
18	D-77-1-1	A-8	38	1.254	248			
19	D-77-1-2	A-8	34	1.122	277			
20	D-83-1-1	A-8	40	1.320	236			
21	D-83-1-2	A-8	46	1.518	205			
22	D-86-1-1	A-8	51	1.683	185			
23	D-86-1-2	A-8	48	1.584	196			
24	D-86-1-3	A-8	50	1.650	188			
25	D-90-1-1	A-8	42	1.386	224			
26	D-90-1-2	A-8	41	1.353	230			
27	D-94-1-1	A-8	39	1.287	242			
28	D-94-1-2	A-8	38	1.254	248			
29	D-97-1-1	A-8	40	1.320	236			
30	D-97-1-2	A-8	45	1.485	209			
31	D-104-1-1	A-8	40	1.320	236			
32	D-104-1-2	A-8	35	1.155	269			
33	D-107-1-1	A-7	29	0.957	325			
34	D-109-1-1	A-7	43	1.419	219			
35	D-111-1-1	A-7	40	1.32	236			
36	D-114-1-1	A-7	46	1.518	205			
37	D-115-1-1	A-7	43	1.419	219			
38	D-120-1-1	A-7	38	1.254	248			
39	D-123-1-1	A-7	42	1.386	224			

^aAlloy Compositions: A = Pure Si; B= Si + 0.4 w/o Al; C = Si + 0.04 w/o Ca;
D = Si + 0.4 w/o Al +0.04 w/o Ca

^bEstimated from the shutter wheel image.

Table 7 (continued). Fall Behavior of 9 mm-Diameter Drops of Molten Silicon in Water at Room Temperature

Trial Number	Drop No.	Alloy ^a	Fall to Crossrod 2 at 311 mm			Fall to Crossrod 3 at 635 mm		
			Frames	Time (s)	v (mm/s)	Frames	Time (s)	v (mm/s)
40	D-127-1-1	B	19	0.627	496			
41	D-130-1-1	B	18	0.594	524			
42	D-145-1-1	B	20	0.660	471			
43	D-147-1-1	C	20	0.660	471			
44	D-133-1-1	C	19	0.627	496			
45	D-135-1-1	C	20	0.660	471			
46	D-137-1-1	D	21	0.693	449			
47	D-139-1-1	D	20	0.660	471			
48	D-143-1-1	D	20	0.660	471			

^aAlloy Compositions: A = Pure Si; B= Si + 0.4 w/o Al; C = Si + 0.04 w/o Ca;

D = Si + 0.4 w/o Al + 0.04 w/o Ca

^bEstimated from the shutter wheel image.

by plotting the depth-time slopes for six new data points vs. drop weight, we obtain the reasonably linear relationship shown in Figure 21.

After the experiments performed with molten silicon in Series A, B and C were completed, we were able to examine the fall behavior of a still larger number of drops. For simplicity, we looked only at experiments in which the drops fell at least 311 mm in the water (the distance of reinforcing crossrod 2 below the surface of the water; see Table 6) and measured only the number of video frames required for the image of the drop to pass behind this crossrod. In Table 7, we show these data as both number of video frames and time (at 30 frames/s) for a number of experiments in Series A, B and C performed during 1999 with drops of molten silicon. In Figure 22, we have plotted the entire set of data as time to fall to crossrod 2 versus an arbitrary trial number; we have also identified each data point by placing this trial number beside it.

From Figure 22, we learned that the fall times were essentially the same for all drops prepared from nonalloyed silicon rods, namely, from Batches A-4, A-7, A-8 and A-9,10. But when only small amounts of Al (0.4 w/o) and/or Ca (0.04 w/o) were alloyed with the silicon in Batches B, C and D, the fall times were drastically reduced! In fact, the drops of alloyed silicon fell even faster than 9 mm-diameter drops of the denser molten ferrosilicon or ferrosilicon with an Al additive, as shown in Figure 23. (The data for the ferrosilicon drops were obtained from several video records from the 1998 experiments and are shown in Table 8.)

Brightness of the Drops of Molten Silicon

An important qualitative observation has been the significantly higher luminosity of drops of molten silicon compared to drops of molten ferrosilicon. We became aware of this brightness primarily from the erratic behavior of our photodetector, which is filtered optically to be most sensitive in the near infrared (at wavelengths of about 900 nm), as shown in Figure 3. It is also apparent as the yellow luminosity of the silicon drops and their explosions in our open shutter time-exposed photographs, for example, Figures 11 through 16, compared to the red-orange luminosity emitted by the ferrosilicon drops and their explosions (Nelson et al., 1998, 1999, 1999a).

Table 8. Fall Behavior of 9 mm-Diameter Drops of Molten Nonalloyed Ferroilicon in Water at Room Temperature

Trial No.	Drop No.	Alloy	Fall to Crossrod 2 at 311 mm			Fall to Crossrod 3 at 635 mm		
			Frames	Time (s)	v (mm/s)	Frames	Time (s)	v (mm/s)
1	D-20-1-1	FeSi	31	1.023	304			
2	D-20-1-2	FeSi	30	0.99	314			
3	D-20-1-3	FeSi	28	0.924	337			
4	D-20-1-4	FeSi	27	0.891	349			
5	D-20-1-5	FeSi	29	0.957	325			
6	D-21-1-1	FeSi	28	0.924	337			
7	D-21-1-2	FeSi	32	1.056	295			
8	D-21-1-3	FeSi	29	0.957	325			
9	D-21-1-4	FeSi	30	0.99	314			
10	D-22-1-1	FeSi	34	1.122	277	75	2.475	257
11	D-22-1-2	FeSi	31	1.023	304	63	2.079	305
12	D-22-1-3	FeSi	28	0.924	337	55	1.815	350
13	D-24-1-1	FeSi	26	0.858	362	55	1.815	350
14	D-24-1-2	FeSi	25	0.825	377	52	1.716	370
15	D-24-1-3	FeSi	27	0.891	349	57	1.881	338
Alloyed Ferrosilicon (C-34-1)								
16	C-122-2	FeSi + Al	23	0.759	410			
17	C-123-1	FeSi + Al	28	0.924	337			
18	C-125-1	FeSi + Al	22	0.726	428			
19	C-131-1-1	FeSi + Al	21	0.693	449			
20	C-131-1-2	FeSi + Al	18	0.594	524			
21	C-131-1-3	FeSi + Al	20	0.66	471			

Furnace Failures

During the Series B and C experiments, we experienced several failures of the furnace used to prepare the drops of molten silicon. These failures are described in Appendix C.

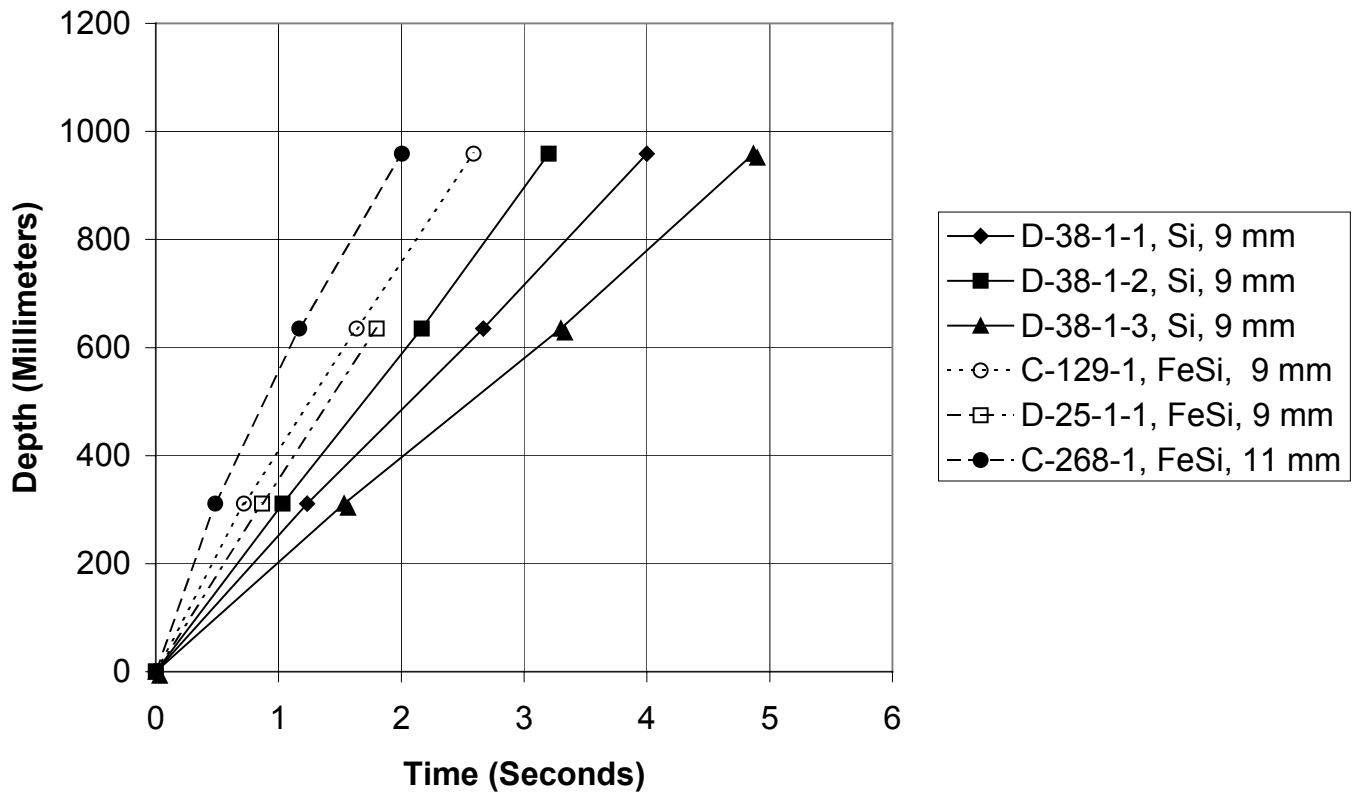


Figure 19. Fall histories of silicon and ferrosilicon drops in water at room temperature.

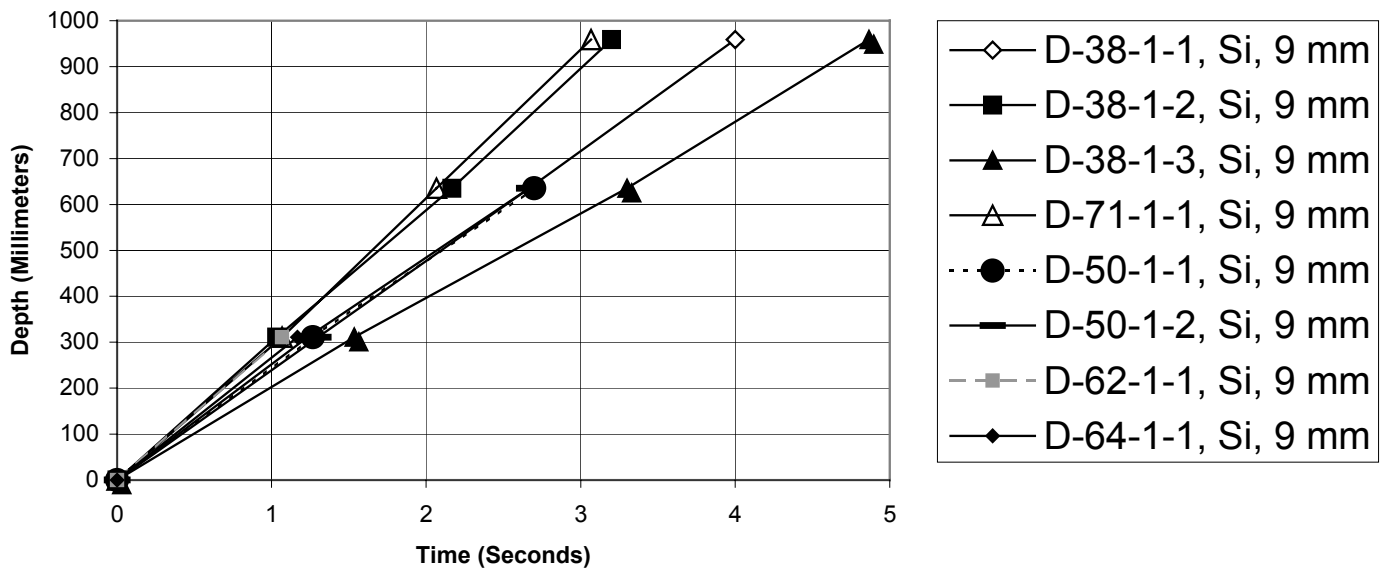


Figure 20. Fall depth-time data for nominally 9 mm-diameter drops of molten silicon released into water at room temperature.

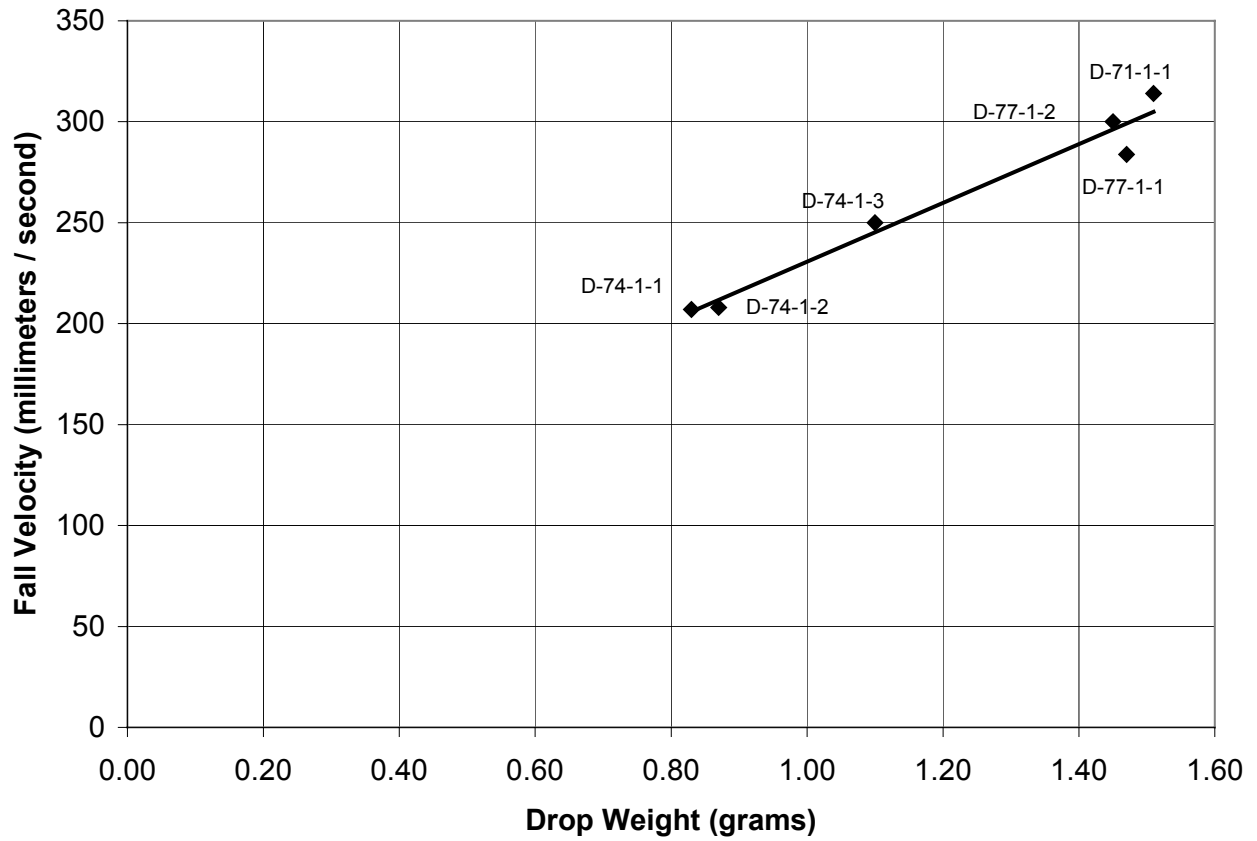


Figure 21. Plot of the slopes of depth-time data vs. drop weight for six nominally 9 mm-diameter drops of molten silicon released into water at room temperature.

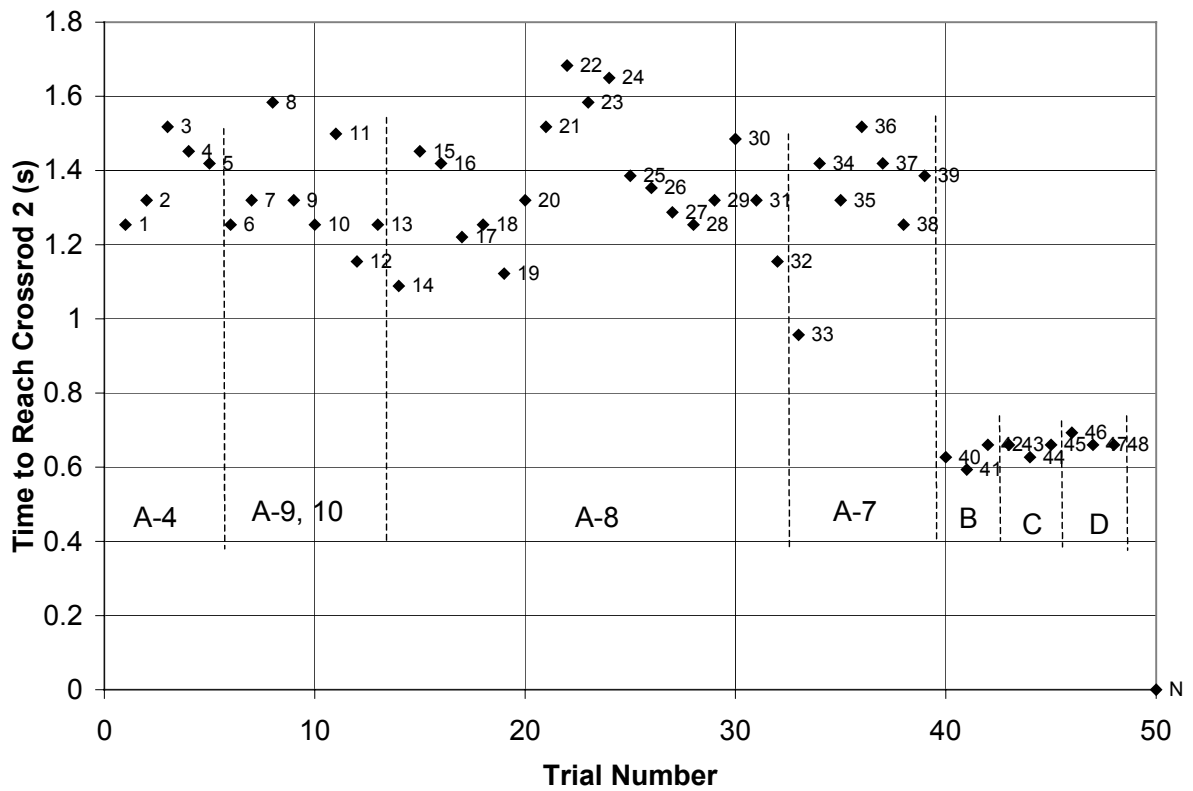


Figure 22. Time for 9 mm-diameter drops of molten silicon to reach crossrod 2 at 311 mm in water at room temperature.

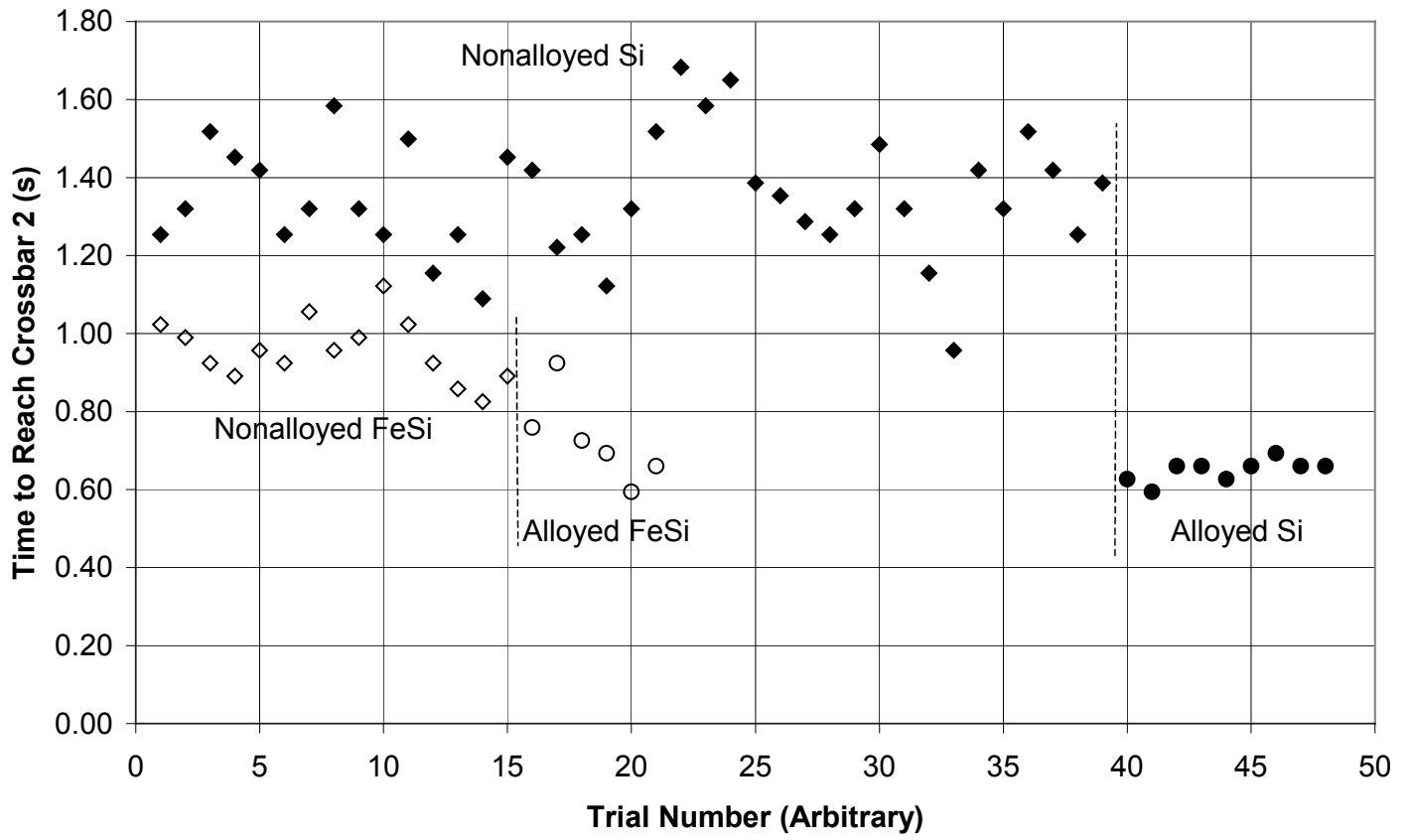


Figure 23. Time for 9 mm-diameter drops of molten silicon, alloyed silicon, ferrosilicon and alloyed ferrosilicon to reach crossrod 2 at 311 mm in water at room temperature.

DISCUSSION

The Need for a New Impactor

Although we were able to initiate steam explosions of 9 mm-diameter drops of molten silicon with Impactor 2 (the pneumatic piston device) during the experiments in Series A, we had to allow the drops to fall very close to the surface of the impactor to achieve pressure transients strong enough to produce 2.0 MPa or larger. This can be seen in experiment D-48-1-2 in Figure 10 and in experiment D-61-1-1 in Figure 14, where the drops have fallen to about 15 mm above the surface of the impactor. Based on the $1/r$ relationship applied to the value of 0.3 MPa measured at 100 mm (see Figures 7 and 9), this corresponds to an applied transient of about 2 MPa.

It should be noted in Figures 10 and 14 that when the drops explode this close to the impactor, it becomes difficult to (a) measure the volumes of the bubbles because the surface of the impactor can distort the images, and (b) accurately estimate the distance of the drop above the impactor at the time of triggering and hence determine the magnitude of the pressure transients based on the $1/r$ relationship.

It became apparent during the experiments in Series A that in order to increase the distance of the explosions above the impactor, we would need a new impactor that could deliver transients with higher peak pressures than the pneumatic impactor. Therefore, we designed and constructed an improved impactor with heavier construction to generate stronger pressure pulses.

The rationale for building a new impactor is displayed in Figure 24. This figure, a plot of pressure vs. r , the distance above the impactor, shows the triggering pressures a drop will experience as it falls toward the surfaces of the three impactors discussed here. Each curve has been calculated with the $1/r$ relationship and one fixed point, the averaged maximum pressure measured in the water 100 mm above the surface of Impactors 1, 2 and 3—0.129 MPa, 0.300 MPa and 1.963 MPa, respectively.

From the experiments performed in Series A, we obtained a preliminary estimate that pulses somewhat larger than 2 MPa are required for the successful triggering of 9 mm-diameter drops of molten silicon (see Table 3). (Note that this value is significantly larger than the threshold transient of 1.3 MPa needed to trigger 9 mm-diameter drops of molten ferrosilicon (Nelson et al., 1999).) Therefore, in Figure 24 we assume a triggering pulse of 3 MPa is required to trigger the silicon drops. This level is indicated by the dashed horizontal line. It can be seen that this pressure occurs 4 mm above Impactor 1, 10 mm above Impactor 2 and 65 mm above Impactor 3, provided the $1/r$ relationship is valid at these distances. The small distances required for Impactors 1 and 2 to successfully trigger the explosions of the silicon drops provided the impetus to build Impactor 3.

Advantages Provided by Impactor 3

Better Estimation of Triggering Pressures. As indicated in Figure 24, when r is small, the pressures generated by the impactor change much more rapidly as r changes than when r is larger. Thus, for the same uncertainty in determining r from the photographic or video images, there is greater uncertainty in the estimation of the pressure required to trigger a drop when r is smaller than when r is larger. Thus, the use of Impactor 3 to generate the pressure transients is expected to provide more accurate estimates of the triggering pulses applied to the drop than the use of either Impactor 2 or Impactor 1.

Less Distortion of the Photographic and Video Images. The other difficulty associated with triggering the steam explosion of a drop of molten silicon very close to the impactor is the interference between the surface and the image of the explosion. To illustrate this, we compare two explosions triggered with Impactor 2, shown in Figures 10 and 14 with an explosion triggered with Impactor 3, shown in Figure 16.

Notice that not only do the steam explosion bubbles impinge on the surface of the impactor in Figures 10 and 14, but also there is a confusing interference in the image between the luminous explosion and light reflected from Impactor 2 in Figure 14.

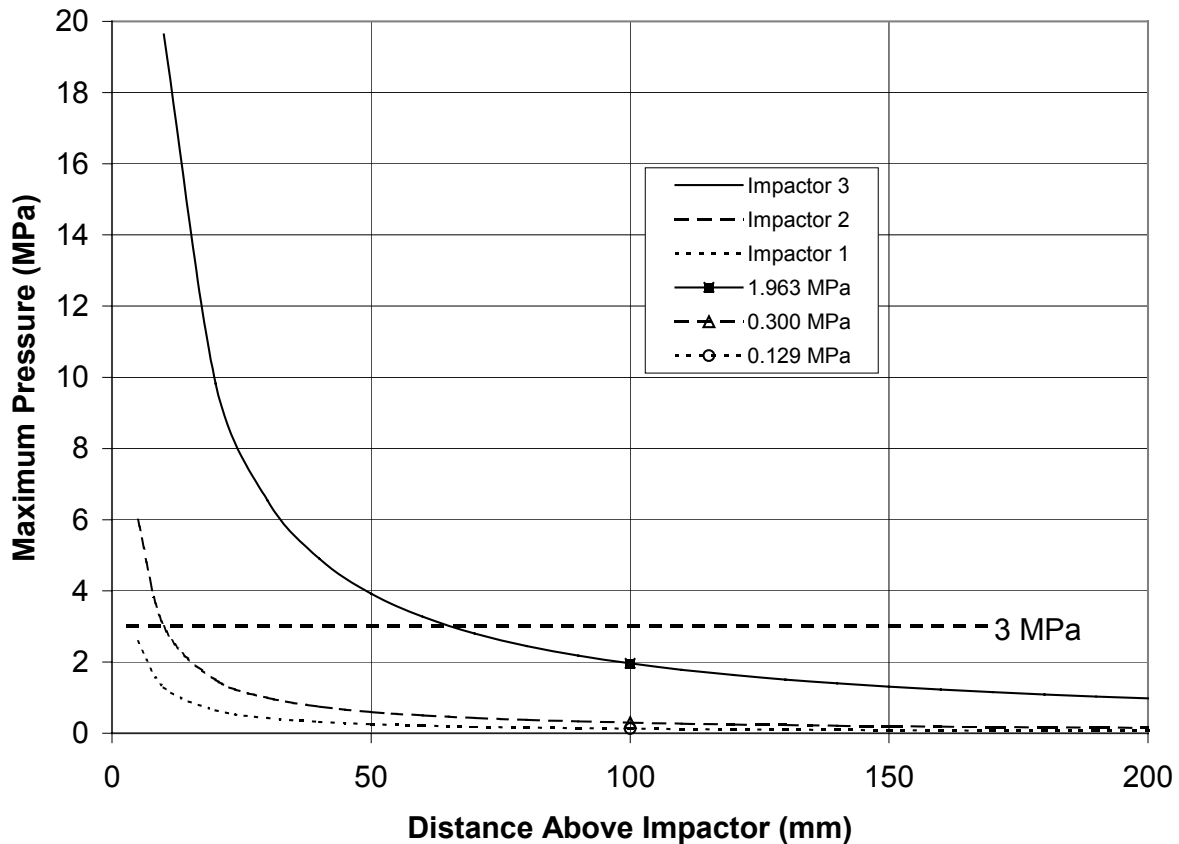


Figure 24. Plot of triggering pressures vs. r , the distance in the water above Impactors 1, 2 and 3. The curves are calculated from the $1/r$ relationship, and fixed on the averaged maximum pressures measured in water 100 mm above each impactor.

These interferences do not occur with Impactor 3. For example, to be more quantitative, we consider the spherical image of the explosion initiated in experiment D-114-1-1, shown in Figure 16. By comparison with the separation of the fiducial rods, the maximum diameter of this bubble was estimated to be 60 mm, with a maximum radius of 30 mm. Now, if the explosion of this drop had been triggered closer to the impactor than 30 mm, the bottom of the bubble would have impinged on the surface and become distorted. Thus, if a 3 MPa pulse is needed, Impactor 3 could easily trigger the explosion 65 mm above the surface, high enough to show the full growth of the bubble. But if either Impactor 1 or Impactor 2 were used to produce 3 MPa triggering pulses, this pressure would be produced 4 mm above Impactor 1 and 11 mm above Impactor 2; that is, both impactors would probably produce highly distorted bubbles.

Brightness of the Drops of Molten Silicon

As discussed earlier, drops of molten silicon seem to be much brighter than the drops of molten ferrosilicon. This brightness becomes apparent as it affects the submerged photodetector that fires that impactor. In working with the ferrosilicon drops, the photodetector fired reproducibly when the drop passed in front of it. But when the same triggering was attempted with drops of molten silicon, the drops activated the photodetector shortly after they entered the water, far above the photodetector. We avoided the problem empirically in the Series A experiments by using the time-delay relay to add a delay between activation of the photodetector and the actual firing of the impactor to allow the drop to fall to the appropriate depth for triggering. But in the Series B and C experiments, we overcame the difficulty by installing a narrow horizontal aperture over the photodetector, by positioning nonreflecting panels along the walls of the water chamber and by covering other surfaces in the chamber with a non-reflective coating. These “fixes” helped

reduce reflections that preceded the drop downward through the water and caused early activation of the photodetector.

We suggest several possible explanations for the greater overall brightness of the silicon drops compared to the ferrosilicon drops:

- The greater apparent brightness may be due in part to the differences in the drop release temperatures.

The temperature of the silicon drops upon release is higher than the temperature of the ferrosilicon drops. That is, the silicon drops are detached from the rod at approximately the melting temperature of 1410 °C, while the ferrosilicon drops were released at approximately the liquidus temperature of 1320 °C. Since the brightness ratio at a given wavelength, $I_{\text{Si}}/I_{\text{FeSi}_2}$, should be approximately equal to the 4th power of the ratio of absolute temperatures, $(T_{\text{Si}}/T_{\text{FeSi}_2})^4$, the silicon drops should be about 28% brighter than the ferrosilicon drops if temperature is the only factor involved.

- The greater apparent brightness may be due in part to differences in the response of the photodetector to the wavelengths of light emitted by the two materials.

Our photodetector, the Skan-a-Matic P33001 infrared-sensitive photosensor, was selected for these experiments because it has been filtered to activate with radiation in the near infrared, at about 900 nm (see Figure 3), to avoid spurious activation by changes of room lighting. It is possible that some peculiarity of the radiation emitted by the molten silicon makes it seem particularly intense to this particular photodetector-filter combination.

- The greater apparent brightness of the silicon may be due in part to a greater emissivity of silicon in this spectral region.

There are several aspects of the emissivity of silicon at high temperatures that may affect the radiation emitted by drops of molten silicon after their release into water:

1. At high temperatures, the emissivity of molten silicon ($e_{\text{liquid}} = 0.26$) is considerably lower than that of solid silicon ($e_{\text{solid}} = 0.55$). [These values are obtained from Guo et al. (1998), who worked with the zone refining of silicon near its melting temperature. A plot of the wavelength-dependence of solid silicon at lower temperatures is reproduced from Touloukian and Ho (1976) as our Figure 25. Note in this plot that the emissivity of solid silicon at 900 nm (0.9 micrometers) is closer to 0.7 at the lower temperatures.] Thus, if a shell of solid silicon had begun to form on the outside of the drop, it would appear considerably brighter than the completely liquid drop, even though the temperature had not changed appreciably.
2. The emissivity of silicon dioxide is probably not of concern here because in this part of the infrared it is very low. (A plot of the emittance of vitreous silica at room temperature is reproduced from Touloukian and Ho (1976) as our Figure 26. Note in this plot that the normal spectral emittance of solid silica at 900 nm (0.9 microns) is essentially zero.) Thus even if a thin layer of oxidized silicon were to coat the falling drop, as might be expected from the release of bubbles of hydrogen soon after the drop enters the water, it would probably be transparent and not significantly affect the radiation emitted by the drop at 900 nm, the wavelength of highest sensitivity of our photodetector.

We must conclude, then, that if emissivity plays an important role in the apparent brightness, it is probably because a thin shell of solid silicon begins to coat the falling drop. This might cause the silicon drop to appear brighter than the completely molten drop by perhaps a factor of two as it enters the water. But the immediate formation of a solid shell probably does not occur with the ferrosilicon; instead, it probably goes through a mushy state because of the two-component nature of the melt, during which there is little change in emissivity. Also, the higher release temperature of the silicon melt will probably increase its brightness

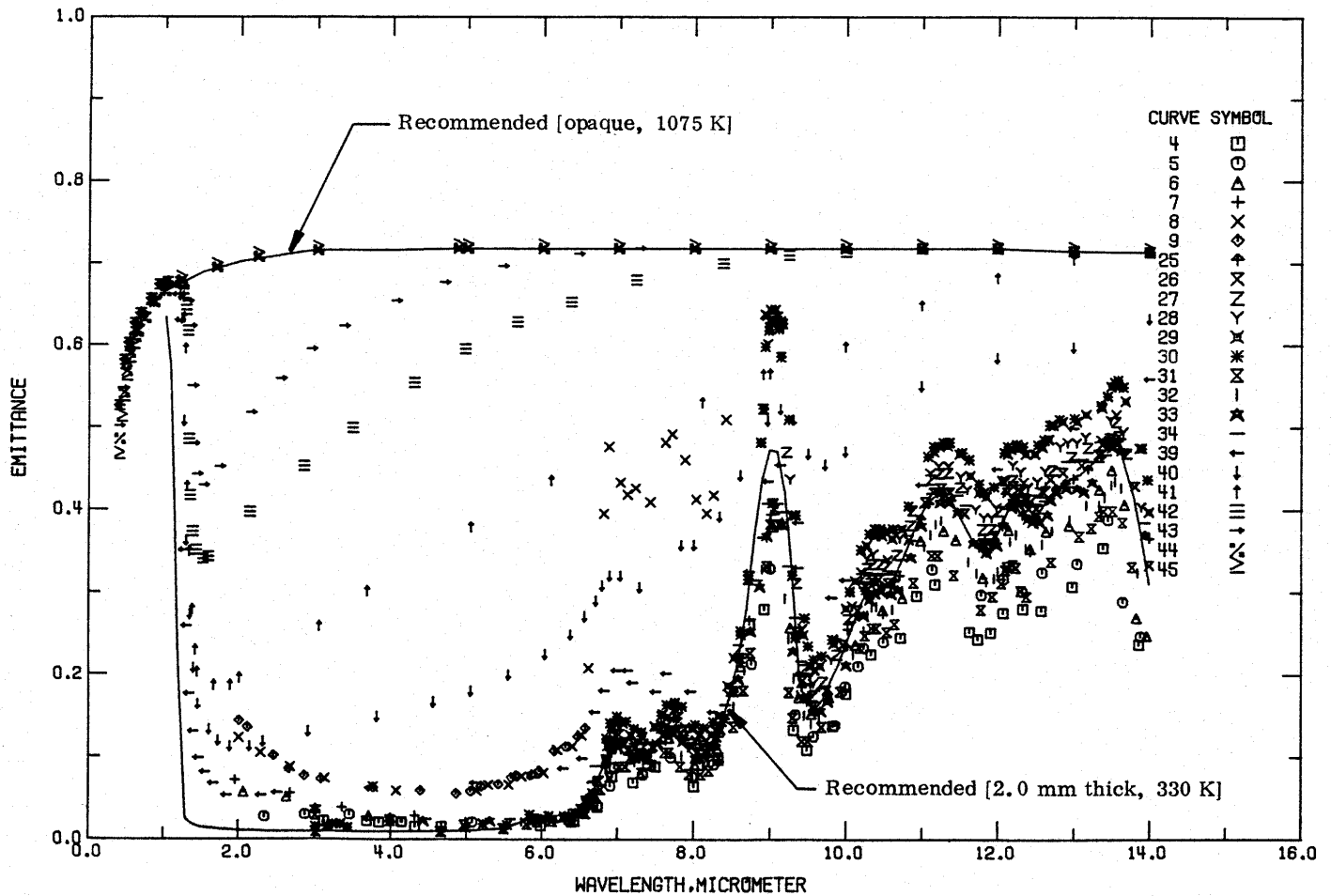


Figure 25. Wavelength-dependence of the emissivity of high resistivity solid silicon, reproduced from Touloukian and Ho (1976). Upper curve is the recommended value for 800 °C and the lower curve for 25 °C.

still further, possibly by as much as 25%, to give a total brightness at 900 nm possibly three-fold greater than the ferrosilicon drops.

Although these comments on the brightness of the silicon drops apply mostly to the operation of our photodetector, they may also be important for understanding the overall radiative heat transfer during the water granulation of molten silicon.

Effects of Alloying

As indicated in Table 1C, several trends seem to emerge as the result of alloying the silicon with small amounts of calcium (0.04 w/o) and aluminum (0.4 w/o):

- The suppression of the steam explosions seems to be in the order $Ca = (Ca + Al) > Al$.
- The amounts of colloid deposited in the water during the interactions are very small and seem to be roughly the same for the three alloys studied.
- The amounts of hydrogen generated seem to be in the order $(Ca + Al) > Al > Ca$.

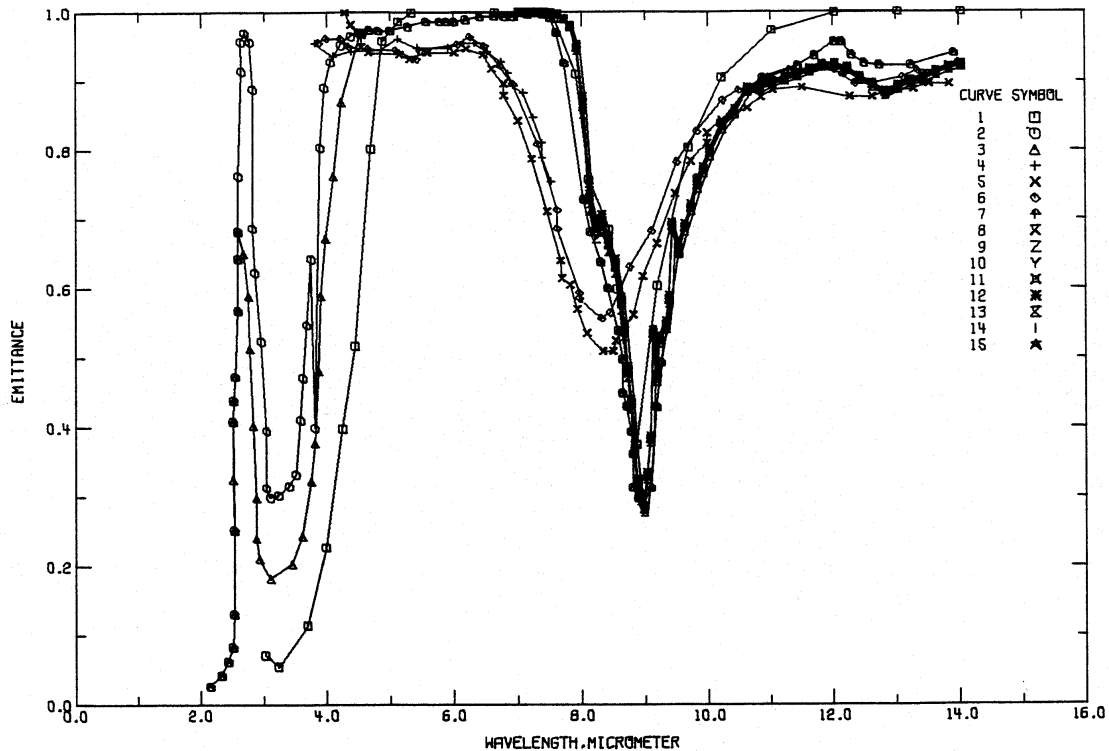


Figure 26. Wavelength-dependence of the emissivity of vitreous silica at room temperature, reproduced from Touloukian and Ho (1976).

Thus, from the standpoint of granulation safety, a preliminary judgment suggests that silicon alloyed with calcium alone may be the best of the three combinations of additives studied because it generates the least hydrogen during the interaction with water, yet is equal to or exceeds the other two alloys in its ability to suppress steam explosions. Again, we must emphasize that this judgment is very tentative because it is based on only nine experiments. But in any case, from the standpoint of steam explosions alone, each of the alloys seems safer to handle during water granulation than pure silicon.

There is another aspect of alloying molten silicon that may affect the water granulation process—the increased fall velocity of the alloyed drops compared to the nonalloyed drops. This can be seen in Figures 22 and 23 and in Table 7, where the alloyed drops fall through the water 2 or 3 times faster than the nonalloyed drops of the same diameter. This suggests that if the cooling rates of the alloyed and nonalloyed materials are about the same, considerably deeper water would be required to achieve the same cooling with the alloyed materials! Moreover, the 9 mm-diameter drops of alloyed silicon fall even faster than the 9 mm-diameter drops of the much denser ferrosilicon, as shown in Figure 23 and Tables 7 and 8.

Colloidal Material

We are still trying to understand the formation of colloidal material when molten drops of both ferrosilicon and pure silicon interact with liquid water. We have noted the following aspects of the deposition of these colloidal materials:

- The deposition of colloidal products is unusual during steam explosions. It does not seem to form when drops of other melts explode, for example, molten iron oxide (Nelson and Duda, 1982) or aluminum (Nelson, 1995).

- The fraction of the original melt that remains suspended after an interaction seems large—sometimes as much as 30% of the original weight of the drop.
- The sizes of the colloidal particles must be very small, as indicated by the long settling times—hours to days. This suggests that a gas phase process may be involved in the deposition.
- But if the process involves the gas phase, it is unlikely that it can be caused by combustion because of the small amount of hydrogen liberated—nowhere near that expected from the 30% of the mass of the drop sometimes converted into colloid.
- Moreover, our attempt to analyze the colloidal products of molten ferrosilicon indicated that the composition of the melt did not change appreciably during the explosion (Nelson et al., 1999). That is, the X-ray diffraction pattern of the colloid produced from ferrosilicon seemed to be identical to the pattern produced by the original parent material.
- There is some indication that the colloid may be related to solidification. This comment is based on the very late first appearance of colloid from a drop of silicon that did not explode or fragment; it seems to appear after the drop has almost completely solidified.

We always return to the explanation that the very fine colloidal material is formed somehow by the release of a gaseous silicon-bearing material that later condenses in the water as a colloid. The main difficulties with this explanation are (a) that we seem to have ruled out combustion with the release of hydrogen as the primary source of the gas, and (b) that significant amounts of permanent gas are never seen to form as bubbles when the colloid is released from drops that solidify without exploding.

There seems to be one gaseous material associated with the molten silicon or ferrosilicon that might cause the colloid to form without producing bubbles of permanent gas: water vapor (steam).

We propose here a new hypothesis: That the drop of silicon or ferrosilicon absorbs water vapor while it is hot and molten and then rejects it again as a metastable gaseous silicon-steam molecular combination (perhaps a hydrate) as the melt cools and solidifies. This hypothesized metastable species would then dissociate and release (a) silicon or ferrosilicon into the water as a very fine solid and (b) steam that would condense quickly and thus would not form bubbles of a permanent gas. This behavior would be somewhat analogous to the behavior of molten aluminum in the presence of moisture: it absorbs hydrogen while the metal is hot and molten but then rejects it again to form bubbles in the metal as it cools and solidifies.

We have begun a literature search to learn whether water vapor (steam) will dissolve in molten silicon, but, as yet, the search has been inconclusive.

If water vapor dissolves in molten silicon or ferrosilicon, it is possible that it might not be completely released when the melt solidifies without a steam explosion; that is, some of the silicon-steam molecular combination might remain quenched in the solid after the interaction. Thus, it would be interesting to find an analytical technique that would identify and measure water dissolved metastably in solid silicon or ferrosilicon. Possible diagnostics for water in the solid metal might be nuclear magnetic resonance (NMR) or transmission infrared spectroscopy.

Silicon monoxide, SiO, is another gaseous species that might produce colloidal material if released into the water during the interactions of drops of molten silicon or ferrosilicon with water. It is a well-known chemical species with high vapor pressure that forms readily when silicon-bearing materials at high temperatures are exposed to an oxidizing atmosphere. Of course, the production of this oxidized form of silicon would necessarily generate hydrogen when it forms, but a few milliliters of hydrogen is always generated as the a silicon drop falls through the water. It is possible that as it forms, the silicon monoxide dissolves in the molten silicon, but then is released at a high pressure when the silicon freezes. This release

might cause some of the fine fragmentation of the melt and its deposition in the water in colloidal form. It is difficult to see, however, how SiO alone could be responsible for the large percentages of the melt that remain suspended in the water without the formation of much larger amounts of hydrogen.

A new factor that has been added to this mystery during the Series C experiments is the action of small additions of Al and Ca to the silicon to almost completely suppress the deposition of colloid during coarse fragmentation and even during a moderately strong explosion, as indicated for experiment D-130-1-1 (see Table 1C).

Generation of Hydrogen

Because knowledge of the amounts of hydrogen generated during water granulation of molten silicon is important from the standpoints of both plant safety and the chemical behavior of the melt, we have made a strong effort during 1999 to estimate the volume of permanent gas produced during the quenching interactions with and without triggering.

“Guesstimate” from Video Images

During the first few experiments in Series A, we made a rough estimate of the total amount of hydrogen generated as a nominally 0.9 g drop of molten silicon quenched to room temperature in water without a trigger. We attempted to use video images to determine the diameter and number of hydrogen bubbles formed during the quenching. In this way, we estimated the diameter of each bubble to be 17 mm, which corresponds to a volume of 2.6 ml per bubble. We also determined the average number of bubbles emitted by each drop to be 19, giving a total amount of hydrogen of 49 ml, assuming the gas to be at room temperature.

After we began to make actual volumetric measurements of the volume of hydrogen generated in the experiments in Series B and C, we realized that this “guesstimate” was high by more than an order of magnitude. Instead of 49 ml, the value measured at room temperature was about 1 ml.

There were two major sources of uncertainty in our “guesstimate” of the volume:

- (a) The volume of each bubble, which was determined from a bubble diameter measured on a video image (with its poor resolution and tendency toward overexposure) and raised to the 3rd power; and
- (b) The temperature of the gas in the bubble, which could be between the melt temperature and room temperature. (In experiment D-48-1-1, the bubbles generated during the interaction ignited and exploded when they broke through the surface of the water, indicating that the hydrogen must have been at a temperature of at least 500 °C, the spontaneous ignition temperature of hydrogen in air (Conti and Hertzberg, 1988).)

Once we learned that the true total volume of hydrogen produced as these drops quenched was about 1 ml, we could correct our volume to 0.053 ml per bubble. This would correspond to a bubble diameter of about 5 mm instead of the 17 mm estimated from the video images. But even with these large uncertainties, this “guesstimate” of the amount of hydrogen was important early in 1999 to place at least an upper limit on the extent of oxidation of the silicon drops as they quenched in water without exploding.

Effects of Gas Solubility on the Volumetric Measurements

After we modified our apparatus as shown in Figure 3 and 4 to allow the collection and measurement of hydrogen after the release of silicon drops into water with or without triggers, we tested the system for the effects of dissolution of the gas from the bubbles into the water. These tests showed that when known volumes of either air or hydrogen were released underwater in the form of bubbles with diameters of about a centimeter, the gas was recovered quantitatively with our collection system. This indicates that during travel of about 400 mm through water at room temperature, loss of the gas from the bubbles into the water

by dissolution is negligible. Thus, our measurements shown in Tables 1B and 1C indicating that 1 or 2 ml of hydrogen is produced when 9 mm-diameter drops of silicon quench and solidify without a trigger are probably accurate because the bubbles were about a centimeter in diameter.

This does not eliminate our concern about the effects of gas dissolution from smaller bubbles, however. For example, very small bubbles are formed during the steam explosions of the drops of molten silicon, where the surface area for diffusion is much larger for a given volume of hydrogen. These tiny bubbles have diameters of a millimeter or less, where the dissolution may be much faster. This should be checked in future experiments.

Probably the best way to test for the effects of dissolution on small bubbles would be again to use a hypodermic syringe to force known volumes of hydrogen through tubing of various smaller diameters. Again, the tip of the tube would be placed at an appropriate depth underwater and beneath our collection system. Another way to test would be to force the hydrogen through a porous metal disc to simulate the cluster of tiny bubbles produced in an explosion. If the losses by diffusion from the small bubbles into the water are not too great, we should be able to correct for them.

One aspect of the release of hydrogen from the silicon drops might be interesting to simulate in side experiments: that the hydrogen is probably hot when the bubbles are released. We believe this will actually favor the accuracy of our collection system because the solubility of gases normally decreases in hot water. We would expect the water surrounding the bubbles to be heated significantly when hydrogen is being released from a silicon drop near its freezing temperature of 1410 °C.

Amounts of Hydrogen Generated

The amounts of hydrogen generated in these interactions were never large. As indicated in Table 1B, about 1 ml was generated when a drop of nonalloyed silicon quenched benignly and perhaps 2 or 3 ml when the drop was exposed to a small trigger and fragmented coarsely. Even in the most vigorous explosions of drops of nonalloyed silicon, the volumes never exceeded about 5 ml (all at room temperature and a local atmospheric pressure of 0.1 MPa).

When the silicon was alloyed with small amounts of Al and/or Ca, the amounts of hydrogen generated were somewhat larger. As indicated in Table 1C, about 2 ml was generated when a drop of alloyed silicon quenched benignly and perhaps 6 or 7 ml when the drop was exposed to a small trigger and fragmented coarsely. And in the most vigorous explosion of a drop of alloyed silicon, the volume was only about 6 ml (all at room temperature and a local atmospheric pressure of 0.1 MPa).

In order to provide a conservative estimate of the explosion hazards involved, we assume that 6 ml is generated during a vigorous steam explosion. This volume corresponds to $6 / 22,400 = 2.7 \times 10^{-4}$ moles of H_2 . If we assume the reaction $Si + 2 H_2O \rightarrow SiO_2 + 2H_2$, the formation of this amount of hydrogen would indicate that 1.4×10^{-4} moles of silicon had been oxidized. Since a 1 g drop of Si = $1 / 28 = 0.036$ moles, the fraction of the drop oxidized is at most about 0.004, or 0.4 %.

Although the amount of hydrogen generated per drop is not large, it must be multiplied by the total number of drops involved at a given time during industrial granulation. Thus every 1000 drops of molten silicon that quench in water at room temperature without fragmentation or explosion will generate 1 or 2 liters of hydrogen; that is, 1 or 2 L of H_2 / kg of melt for 9 mm-diameter drops. Considering the easy ignition and explosiveness of gaseous hydrogen when mixed with air, this is a hazard that requires appropriate precautions.

Because the amounts of hydrogen generated per drop are small, they allow us to draw two basic conclusions about the explosive interactions of drops of molten silicon with water:

- The colloidal material deposited in the water during a steam explosion cannot be a combustion product. This statement is supported by the great difference between the amount of silicon that remains suspended in the water as colloid after a vigorous explosion (as much as 30% of the original mass of the drop), and the amount of combustion that occurs during the interaction (less than 1%).
- Combustion does not play a significant role in the energy released during the steam explosion of drops of molten silicon. Again, this statement is based on the small amount of hydrogen generated compared to the total mass of silicon involved in an explosion. As yet, this conclusion applies only to the conditions we have studied here: the interaction between molten silicon at or below its melting temperature (1410 °C) and water at room temperature and atmospheric pressure. It is possible that if the molten silicon is hotter, the steam explosion may be accompanied by a stronger chemical component that will greatly augment the energy release, as has been observed to occur with molten aluminum and molten zirconium (Nelson, 1995; Cho et al., 1995, Cho et al., 1998).

We can compare the amounts of hydrogen generated after single drops of molten silicon and a molten aluminum-3 w/o lithium alloy were released into water at room temperature. When drops of molten silicon at a temperature of about 1410 °C fell into water without explosion, 1 or 2 ml of hydrogen was produced per gram of melt, while the drops of the molten Al-Li alloy at a temperature of about 1000 °C, also without explosion, produced about 9 ml / g (Nelson et al., 1994).

Fall Behavior of Molten Silicon Drops

We have discovered several aspects of the fall behavior of drops of molten silicon that seem important for understanding the water granulation process:

- Drops of nonalloyed silicon fall more slowly through the water than drops of ferrosilicon of the same diameter, as shown in Figures 19 and 23. Several factors may influence these fall rates: the lower density of the silicon, its higher melting temperature and the faster generation of hydrogen by the silicon drops than by the ferrosilicon drops.
- Heavier drops of nonalloyed silicon fall faster than lighter drops, as shown in Figure 21, with velocities roughly proportional to their masses. A theoretical discussion of this behavior will be given in the next section.
- If the molten silicon is alloyed with small amounts of aluminum (0.4 w/o) and/or calcium (0.04 w/o), the drops fall roughly twice as fast as drops of nonalloyed silicon of the same diameter and about 30% faster than drops of molten ferrosilicon of the same diameter, as shown in Figures 22 and 23. It will be difficult to explain these effects with a similar theoretical discussion, however, because only small changes in dimensions, weights and physical properties of the drops are expected with these small additives.

Theoretical Discussion of Fall Velocities

The fall velocities for molten Si-drops have been measured using video imaging. It is assumed that the drops fall with a constant velocity in the water, and the effect of the entrance is neglected, as the time scale for the entrance event is small compared to the total time elapsed. For a molten drop falling in water with a constant velocity, the drag force must equal the drop weight. The drag force and weight are given by

$$\text{Drag force} = C_D \cdot \pi \cdot R^2 \cdot \frac{1}{2} \cdot \rho_{\text{water}} \cdot V^2 \quad (1)$$

where C_D is the drag coefficient, R is the radius of the drop and V is the drop velocity. It is assumed here that the drop is spherical. This is not completely true, as the experimental results indicate. For other

geometries, the drag coefficient will take another value, so will the term πR^2 , which describes the frontal area of the drop.

The weight of the drop, again assuming spherical shape, is given by

$$Weight = \frac{4}{3} \pi R^3 \cdot \rho_{sphere} \cdot g \quad (2)$$

where g is the acceleration of gravity and ρ_{sphere} is the density of the molten silicon minus the density of the water, to account for buoyancy. Combining equation (1) and (2) we get

$$V = \sqrt{\frac{8g\rho_{sphere}}{3C_D\rho_{water}}} \cdot \sqrt{R} \quad (3)$$

The mass for a spherical drop is given by

$$M = \rho_{sphere} \cdot \frac{4}{3} \pi R^3 \quad (4)$$

Combining (3) and (4), we get the velocity as a function of the mass of the molten drop

$$V = \sqrt{\frac{8g\rho_{sphere}}{3C_D\rho_{water}}} \cdot \left(\frac{3M}{4\pi\rho_{sphere}} \right)^{1/6} \quad (5)$$

In other words, the velocity is not very sensitive to changes in the mass, $V = \text{constant} \cdot M^{1/6}$.

Figure 21 shows experimental data for the velocity as a function of drop mass. In this plot, the velocity shows approximately a linear dependence of the mass. This suggests other geometries than the assumed spherical one. The form of the solidified globules, which take a disk-like form, also indicates this. However, the theoretical plot (V vs. $M^{1/6}$) for a sphere fits reasonably well with the experimental data, scattering and uncertainties taken into account. So a spherical molten drop is a reasonable first approximation for the fall velocity of the molten Si-droplet.

Theoretical Heat Transfer Studies

A preliminary theoretical discussion of the heat balance for a single drop after its release from the rod and an analysis of the debris and the change in surface energy after a drop explodes has been prepared by Mr. Kjetil Hildal during his stay during 1999 at the Department of Engineering Physics, University of Wisconsin in Madison. This document is included in this report as Appendix D.

CONCLUSIONS

During 1999, we have studied the release of 9 mm-diameter drops of molten silicon into water at room temperature.

In a first series of experiments (Series A), we compared their behavior with the 9 mm-diameter drops of molten ferrosilicon studied previously. From these initial experiments, we concluded that:

- There are no catastrophic effects when 9 mm-diameter drops of either molten silicon or molten ferrosilicon fall onto ice or into liquid water at room temperature.
- Neither silicon nor ferrosilicon drops explode spontaneously as they fall through water at room temperature or when they strike an underwater steel surface.
- Drops of molten silicon generate bubbles of hydrogen as they quench in water; ferrosilicon drops do not.
- Silicon drops fall through the water more slowly than ferrosilicon drops.
- Steam explosions of both silicon and ferrosilicon drops can be triggered by exposing them to pressure transients generated in the water with a mechanical impactor.
- Silicon drops require stronger pressure transients for initiation of the explosions than the ferrosilicon drops.
- Silicon drops cannot be triggered at depths as great as the ferrosilicon drops.

In a second series of experiments (Series B), we redesigned our impactor to operate with a slug fired upward to strike an underwater steel surface and thereby increased the triggering pressure transients generated about 5-fold over our previous design. The new device provided the stronger pulses needed to initiate steam explosions of drops of molten silicon at a distance above the impactor that permitted good imaging and accurate measurements of triggering pressures.

In this second series of experiments, we also added a gas collector to our system to measure the amounts of hydrogen generated during molten metal-water interactions. Drops of molten silicon 9 mm in diameter that quench quiescently in water at room temperature generate about 1 ml of hydrogen per gram of melt. But if the drops are triggered to explode, not more than 6 ml/g is produced. (Volumes are measured at room temperature and a local atmospheric pressure of 0.1 MPa). These volumes indicate that, at most, only about 0.4 % of the silicon oxidizes during even the most vigorous explosions.

The small amounts of hydrogen generated in these interactions at the melt and water temperatures involved in our experiments allow us to conclude that combustion does not:

- Add significantly to the energy released during explosive molten silicon-water interactions.
- Play an important role in causing the large fractions of the melt to remain suspended in the water as a colloid after the drops explode.

In a third series of experiments (Series C), we performed nine experiments with alloyed silicon and saw these preliminary trends:

- Additions of small amounts of calcium (0.04 w/o) and/or aluminum (0.4 w/o) to the silicon seem to reduce the tendency for drops of melt to explode.

- Both alloys that contained calcium seemed less inclined to explode than the alloy that contained only aluminum.
- Additions of small amounts of calcium (0.04 w/o) and/or aluminum (0.4 w/o) reduced the tendency to deposit colloid in the water during triggered interactions.
- Less hydrogen seemed to be generated when the alloy contained only the calcium additive.
- The fall velocities of the alloyed drops through the water were more than twice those of nonalloyed silicon drops.

In a single exploratory experiment performed at the end of 1999, a drop of nonalloyed molten silicon was triggered to explode at a known distance from a transducer. The energy released by the explosion generated a steam bubble that collapsed and produced a pressure transient as strong as the original triggering pulse.

The new results obtained with drops of molten silicon during 1999 are both important and provocative to the understanding of quenching and steam explosions during water granulation. It is apparent that more experimentation is needed to clarify many of these observations.

FINAL NOTES

This document originally was submitted to the sponsor, SINTEF Materials Technology, Trondheim, Norway, on March 15, 2000, as the draft final report that describes the research performed at the University of Wisconsin-Madison during 1999. Three informal letter reports that describe this work also have been submitted to the sponsor on July 1, 1999 (Nelson et al., 1998b), October 1, 1999, (Nelson et al., 1999c) and on January 15, 2000 (Nelson et al., 2000).

Related research has been performed at NTNU, the Norwegian Technological University, Trondheim, Norway, under the direction of Professor Johan Kr. Tuset, and has been described in the thesis “Steam explosions during granulation of Si-rich alloys: Effect of Ca- and Al-additions” by Kjetil Hildal, dated 25 March, 2002. It may be accessed via the Internet link <http://www.ub.ntnu.no/dravh/000057.pdf>.

REFERENCES

- Cho, D. H., Armstrong, D. R., and Anderson, R. P., 1995, "Combined Vapor and Chemical Explosions of Metals and Water," *Nuclear Engineering and Design* 155, 405 – 412.
- Cho, D. H., Armstrong, D. R., and Gunther, W. H., 1998, Experiments on Interactions Between Zirconium-Containing Melts and Water, U. S. Nuclear Regulatory Commission, Washington, D. C., NUREG/CR-5372.
- Conti, R. S., and Hertzberg, M., 1988, "Thermal Autoignition Temperatures for Hydrogen-Air and Methane-Air Mixtures," *J. Fire Sciences* 6, 349-355.
- Guo, Z., Maruyamam, S., and Togawa, S., 1998, "Combined Heat Transfer in Floating Zone Growth of Large Silicon Crystals with Radiation on Diffuse and Specular Surfaces," *J. Crystal Growth* 194, 321-330.
- Nelson, L. S., and Duda, P. M., 1982, "Steam Explosion Experiments with Single Drops of Iron Oxide Melted with a CO₂ Laser," *High Temperatures-High Pressures*, 14, 259-281.
- Nelson, L. S., Duda, P. M., and Hyndman, D. A., 1994, "Interactions Between Drops of a Molten Aluminum-Lithium Alloy and Liquid Water," *Metallurgical and Materials Transactions B*, 25B, 623-625.
- Nelson, L. S., 1995, "Steam Explosions of Single Drops of Pure and Alloyed Molten Aluminum," *Nuclear Engineering and Design* 155, 413-425.
- Nelson, L. S., Bonazza, R., and Corradini, M. L., 1995, Formation of 10-20 mm Drops of Molten Ferrosilicon, University of Wisconsin-Madison, Report UWFD-1027, June, 1995.
- Nelson, L. S., Bonazza, R., Brooks, P. W., and Corradini, M. L., 1997, Quenching 10-20 mm-Diameter Drops of Molten Ferrosilicon in Water and on Solids, Draft Final Report to SINTEF Materials Technology, Trondheim, Norway, March 13, 1997.
- Nelson, L. S., Brooks, P. W., Bonazza, R., and Corradini, M. L., 1998, Steam Explosions of Molten Ferrosilicon Drops Released into Water: Effects of Triggering, Alloying and Water Temperature, Draft Final Report to SINTEF Materials Technology, Trondheim, Norway, March 15, 1998.
- Nelson, L. S., Brooks, P. W., Bonazza, R., Corradini, M. L. and Hildal, K., 1999, Triggered Steam Explosions of Molten Ferrosilicon Drops: Behavior of Solenoid-Driven and Pneumatic Impactors; Ability to Trigger the Explosions at Various Water Depths; Energetics of the Explosions; Fall Histories; Colloidal Material Deposited During the Explosions, Draft Final Report to SINTEF Materials Technology, Trondheim, Norway, March 15, 1999.
- Nelson, L. S., Brooks, P. W., Bonazza, R., and Corradini, M. L., 1999a, "Triggering Steam Explosions of Single Drops of a Molten Ferrosilicon Alloy with a Simple Encapsulated Mechanical Impactor," *Metallurgical and Materials Transactions B*, 30B, 1083-1088, December, 1999.
- Nelson, L. S., Brooks, P. W., Bonazza, R., Corradini, M. L. and Hildal, K., 1999b, The Quenching and Steam Explosions of Drops of Molten Silicon Released into Water, Informal Letter Report to SINTEF Materials Technology, Trondheim, Norway, Submitted July 1, 1999.
- Nelson, L. S., Brooks, P. W., Bonazza, R., Corradini, M. L. and Hildal, K., 1999c, The Release of Drops of Molten Silicon into Water: Quenching, Steam Explosions and Hydrogen Generation, Informal Letter Report to SINTEF Materials Technology, Trondheim, Norway, Submitted October 1, 1999.

Nelson, L. S., Brooks, P. W., Bonazza, R., Corradini, M. L. and Hildal, K., 2000, The Release of Drops of Molten Silicon into Water: Effects of Alloying; Collection of Hydrogen; Pressure Transients Generated by a Steam Explosion, Submitted January 15, 2000.

Touloukian, Y. S., and Ho, C. Y., Editors, 1976, Thermophysical Properties of Selected Aerospace Materials. Part I: Thermal Radiative Properties, CINDAS, Purdue University, West Lafayette, IN.

APPENDIX A

Synopsis of reports and articles prepared for SINTEF Materials Technology, Trondheim, Norway, by the University of Wisconsin-Madison

1. L.S. Nelson, R. Bonazza and M.L. Corradini; "Formation of 10-20 mm Drops of Molten Ferrosilicon", University of Wisconsin-Madison Report No. UWFD 1027, June, 1995.
2. Lloyd S. Nelson, Riccardo Bonazza, Paul W. Brooks and Michael L. Corradini; "Quenching 10-20 mm-Diameter Drops of Molten Ferrosilicon in Water and on Solids", Draft, March 1997.
3. Lloyd S. Nelson, "Review of Steam Explosions Emphasizing Single Drops", Seminar at Mo-I-Rana, Norway, April 8, 1997.
4. Lloyd S. Nelson, "Results from Explosion Tests", Seminar at Mo-I-Rana, Norway, April 8, 1997.
5. Lloyd S. Nelson, Paul W. Brooks, Riccardo Bonazza and Michael L. Corradini; "Generation of Pressure Transients for the Initiation of Steam Explosions of Single Drops of Melt", Informal Letter Report (Draft), June 30, 1997.
6. Lloyd S. Nelson, Paul W. Brooks, Riccardo Bonazza and Michael L. Corradini; "Release of Molten Ferrosilicon Drops into Water: Effects of Triggering and Alloying", Informal Letter Report (Draft), September 1, 1997.
7. Lloyd S. Nelson, Paul W. Brooks, Riccardo Bonazza and Michael L. Corradini; "Release of Molten Ferrosilicon Drops into Water: Part 2 Effects of Triggering, Alloying and Water Temperature", Informal Letter Report (Draft), December 31, 1997.
8. Lloyd S. Nelson, Paul W. Brooks, Riccardo Bonazza and Michael L. Corradini; "Generation of Pressure Transients in Water for Triggering Steam Explosions of Single Drops of Melt: A Simple and Inexpensive Mechanical Impactor", Paper intended for publication (Draft), March 11, 1998.
9. Lloyd S. Nelson, Paul W. Brooks, Riccardo Bonazza and Michael Corradini; "Steam Explosions of Molten Ferrosilicon Drops Released into Water: Effects of Triggering, Alloying and Water Temperature", Final Report (Draft), March 15, 1998.
10. Lloyd S. Nelson, Paul W. Brooks, Riccardo Bonazza and Michael L. Corradini; "Release of Molten Ferrosilicon Drops into Water: Effects of Triggering and Alloying", SINTEF/UW Review and Discussions, May 27 and 28, 1998.
11. Lloyd S. Nelson, Paul W. Brooks, Riccardo Bonazza and Michael L. Corradini; "Pressure Transients Generated by Solenoid-Driven and Pneumatic Impactors for Triggering Steam Explosions of Single Drops of Molten Ferrosilicon Alloys", Informal Letter Report (Draft), July 1, 1998.
12. Lloyd S. Nelson, Paul W. Brooks, Riccardo Bonazza and Michael L. Corradini; "A Simple Encapsulated Mechanical Impactor for Triggering Steam Explosions of Single Drops of a Molten Ferrosilicon Alloy", Paper intended for publication (Draft), August 17, 1998.
13. Lloyd S. Nelson, Paul W. Brooks, Riccardo Bonazza, Michael L. Corradini and Kjetil Hildal; "Triggered Steam Explosions of Molten Ferrosilicon Drops: Explosiveness as Water Depth Increases; Colloidal Material Deposited in the Water During the Explosions", Informal Summary Report (Draft), October 1, 1998.

14. Lloyd S. Nelson, Paul W. Brooks, Riccardo Bonazza, Michael L. Corradini and Kjetil Hildal; "Triggered Steam Explosions of Molten Ferrosilicon Drops", Presentation at Ferrolegeringsseminar, Trondheim, Norway, October 21, 1998.
15. Lloyd S. Nelson, Paul W. Brooks, Riccardo Bonazza, Michael L. Corradini and Kjetil Hildal; "Triggered Steam Explosions of Molten Ferrosilicon Drops: Ability to Trigger the Explosions at Various Water Depths; Energetics of the Explosions; Fall Histories; Colloidal Material Deposited During the Explosions", Informal Letter Report (Draft), December 31, 1998.
16. Lloyd S. Nelson, Paul W. Brooks, Riccardo Bonazza and Michael L. Corradini and Kjetil Hildal, "Triggered Steam Explosions of Molten Ferrosilicon Drops: Behavior of Solenoid-Driven and Pneumatic Impactors; Ability to Trigger the Explosions at Various Water Depths; Energetics of the Explosions; Fall Histories; Colloidal Material Deposited During the Explosions," Final Report (Draft), March 15, 1999.
17. Lloyd S. Nelson, Paul W. Brooks, Riccardo Bonazza and Michael L. Corradini, "The Quenching and Steam Explosions of Drops of Molten Silicon Released into Water," Informal Letter Report, [Draft (Revised)], July 1, 1999.
18. Lloyd S. Nelson, Paul W. Brooks, Riccardo Bonazza, Michael L. Corradini and Kjetil Hildal, "The Release of Drops of Molten Silicon into Water: Quenching, Steam Explosions and Hydrogen Generation," Informal Letter Report (Draft), October 1, 1999.
19. Lloyd S. Nelson, Paul W. Brooks, Riccardo Bonazza, Michael L. Corradini, Kjetil Hildal and Trond Bergstrom, "Steam Explosions of Single Drops of a Molten Ferrosilicon Alloy," Paper presented at The Minerals, Metals and Materials Society, Fall 1999 Meeting, November 1, 1999, Cincinnati, Ohio.
20. L. S. Nelson, P. W. Brooks, R. Bonazza and M. L. Corradini, "Triggering Steam Explosions of Single Drops of a Molten Ferrosilicon Alloy with a Simple Encapsulated Mechanical Impactor," Metallurgical and Materials Transactions B, 30B, 1083-1088, December, 1999.
21. Lloyd S. Nelson, Paul W. Brooks, Riccardo Bonazza, Michael L. Corradini and Kjetil Hildal, "The Release of Drops of Molten Silicon into Water: Effects of Alloying; Collection of Hydrogen; Pressure Transients Generated by a Steam Explosion," Informal Letter Report (Draft), January 15, 2000.

APPENDIX B

The Transducer Experiment

Introduction

Pressure transients emitted by an exploding drop of melt may trigger the explosions of neighboring drops and thus initiate a self-propagating large-scale steam explosion. Therefore, there is much to gain by carefully measuring and understanding the pressurizations generated by individual drops as they explode.

To investigate these transient phenomena, we performed one exploratory experiment (D-150-1) in which a drop of nonalloyed molten silicon was triggered to explode at a known distance from a transducer. In this experiment, the explosion generated a steam bubble that collapsed and produced a pressure transient as strong as the original triggering pulse.

Experimental

In experiment D-150-1, the surface of Impactor 3 was placed in the water at a depth of 400 mm, with the optical axis of the photodetector aimed horizontally 50 mm above it at a depth of 350 mm. We used no delay in the photodetector control circuit in order to trigger the drop at the depth of the photodetector—350 mm. We placed the tourmaline pressure transducer 325 mm below the water surface and 94 mm behind the centerline of the impactor, near the back wall of the water chamber; that is, the transducer was located in a horizontal plane 75 mm above the surface and 30 mm horizontally behind the rear edge of the impactor (OD = 127 mm).

The output of the transducer was recorded with the Hewlett Packard Infinium oscilloscope as described in previous reports (see, for example, Nelson et al., 1999). The oscilloscope was triggered with the electrical signal used to fire the impactor.

Results

The drop of molten silicon used in experiment D-150-1 was 9 mm in diameter, produced from a 10 mm-diameter rod from Batch A-7. We released the drop into water at room temperature (22 °C). The drop triggered about 40 mm above the impactor and produced a powerful explosion slightly to the left of the centerline. The explosion threw considerable water from the chamber and generated many tiny hydrogen bubbles and lots of white colloidal material that remained suspended in the water after the experiment. The parameters and experimental results of experiment D-150-1 are summarized in Table B-1.

Photographs of several single frames from the video record of experiment D-150-1 are shown in Figures B-1a through B-1d. Figure B-1a was recorded 14 frames before the explosion and Figure B-1b one frame before. Figure B-1c shows the explosion and Figure B-1d shows the frame just after the explosion. At a video imaging rate of 30 frames/s, the images shown in Figures B-1a, b, c, and d were recorded at the times -0.467 s, -0.033 s, 0 s (the frame with the explosion), and + 0.033 s, respectively.

Schematic side and top views of the orientation of the impactor, photodetector, transducer, and the explosion are shown in Figures B-2a and b, respectively. As indicated in these figures, the center of the explosion was about 90 mm from the transducer, diagonally below it and somewhat to the left of the centerline of the impactor.

Pressure-Time Traces

The pressure-time trace recorded by the oscilloscope during the interaction is shown in Figure B-3a. There were three major spikes in the trace: PT 1 with $P_{\max}=1.44$ MPa occurred 0.7 ms after the oscilloscope record began. About 2.3 ms later, PT 2 with $P_{\max}=0.8$ MPa occurred. And then, 2.8 ms after PT 1, there was a third stronger and wider pulse, PT 3, with $P_{\max}=2.2$ MPa. Pulses PT 1 and PT 2 but not PT 3 appear in the

Table B-1. Summary of Release of 9 mm-Diameter Drop of Nonalloyed Molten Silicon into Water ^a																
Interaction was triggered with Impactor 3; air pressure was 1.3 Mpa.																
The silicon rod was supported in the furnace on a graphite cross-rod.																
Drop No.	Alloy	T(water) (°C)	T(furnace) (°C)	Furnace Atm.	Rod Loss Wt (g)	Debris Wt. (g)	Difference (g)	Depths (mm)		Delay (s)	Trigger ^b (mm)	Trigger ^b (Mpa)	Imaging	V(H ₂) (ml)	Remarks	
								Impactor	Photodetr							
D-150-1-1	A-7	22	1430	Ar + 1%H₂	1.03	0.81	Loss 0.22	400	350	0	40	5	RL, VCR	3.4???	Transducer experiment.	
															Powerful explosion, threw water. Much colloid deposited in the water.	
^a Drops that exploded are indicated by this symbol: 																
^b The magnitude of the triggering pulse was estimated from the distance of the drop above the impactor at the time of triggering . This distance was determined from the video image.																

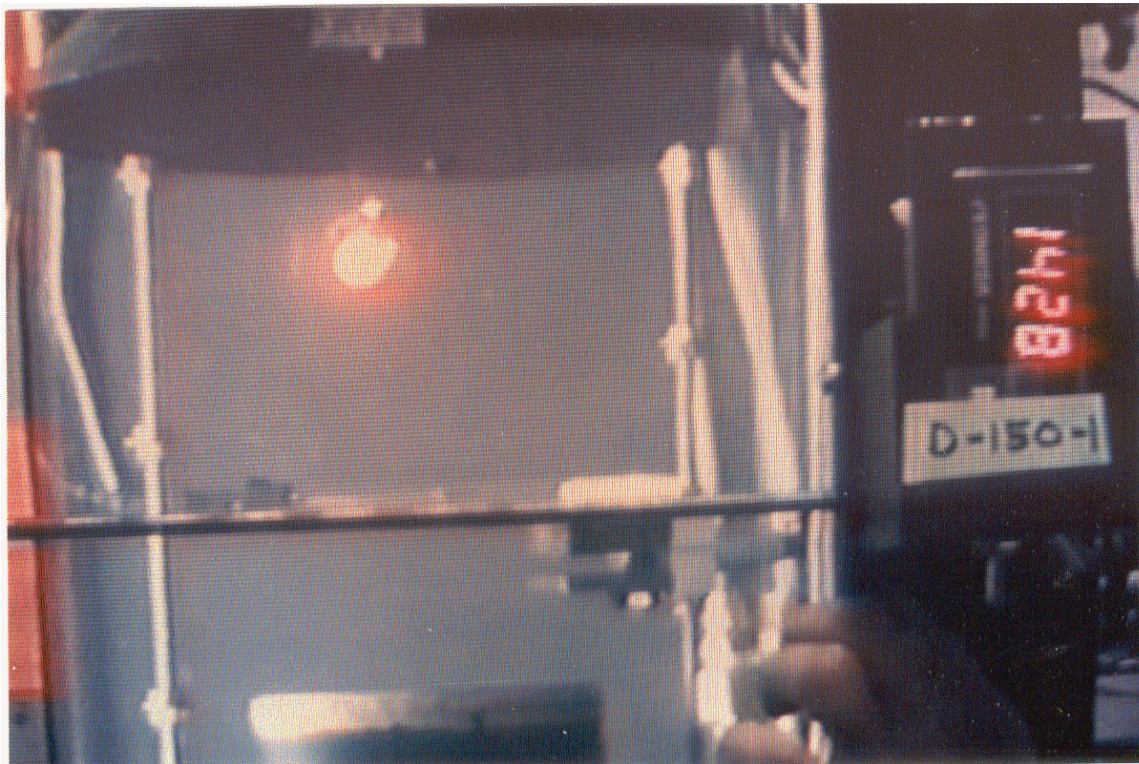


Figure B-1a. Photograph of a single image from the video record of Experiment D-150-1-1. This image was recorded 14 frames before the explosion (-0.467 s). Imaging rate was 30 frames/s. Impactor 3 was used in this experiment. The horizontal separation of the vertical fiducial bars is 185 mm.

baseline trace shown in Figure B-3b, which was generated by firing the impactor alone, without a silicon drop.

By comparison of the traces in Figures B-3a and B-3b, we can conclude that the impactor produced the spikes PT1 and PT 2 and that the steam explosion produced PT 3. It is also important to note that there is no appreciable difference between the pressure records near PT 1 in Figures B-3a and B-3b. This indicates that the initiation of the steam explosion does not generate a significant pressurization! (A similar absence of pressurization at the time drops of molten iron oxide were triggered to explode was also observed by Nelson and Duda (1982).)

From our previous experience with simultaneous transducer recording and high-speed photography during steam explosions of drops of molten iron oxide (Nelson and Duda, 1982), we attribute PT 3 to the collapse of the steam bubble generated by the explosion. We believe this bubble started to grow immediately after the pulse PT 1 destabilized the boiling film and initiated the explosion. The bubble then grew and collapsed 2.8 ms later, with the impact of the collapse generating the pressure pulse PT 3. It is not possible to tell from the pressure trace or the video record (time resolution 33 ms/frame) whether a small bubble grew and collapsed before the major spike, PT 3, occurred at 2.8 ms. (Double bubble growths and collapses have been observed in the triggered steam explosions of single drops of molten ferrosilicon (see Figures 16b and 17b in Nelson et al., 1999) and aluminum (Nelson, 1995) and several bubble growths and collapses in the case of molten iron oxide (Nelson and Duda, 1982).) Only single bubbles seem to have been produced during explosions of drops prepared from rods in Batch A-7, however, as observed in the open shutter time-exposed photographs of experiment D-114-1-1 (shown in Figure 16 in the main body of this report) and of experiment D-123-1-1. Open shutter time-exposed photography (or better, high-speed photography) should



Figure B-1b. Photograph of a single image from the video record of Experiment D-150-1-1. This image was recorded 1 frame before the explosion (-0.033 s). Imaging rate was 30 frames/s. Impactor 3 was used in this experiment. The horizontal separation of the vertical fiducial bars is 185 mm.

be used to resolve whether one or more bubbles form and collapse during future transducer experiments with drops of molten silicon.

The height of PT 3 in Figure B-3a is 2.2 MPa, measured by the transducer 90 mm from the explosion (see Figures B-2a and B-2b). This peak pressure should be compared to the maximum pressures generated along the centerline of the impactor alone. In Figure 9 in the main body of this report, we showed that the averaged maximum pressure recorded 100 mm above the surface of Impactor 3 was 1.96 MPa. If we assume the $1/r$ relationship applies to PT 3 in Figure B-3a, the maximum pressure at 100 mm would be 1.98 MPa. Note that this value is essentially identical to the peak pressure of 1.96 MPa produced by Impactor 3 at 100 mm. This indicates that, at equal distances, the collapse of a steam explosion bubble can produce a pressure pulse as strong as Impactor 3! (Impactor 3 is the most powerful of the three impactors we have built; see Figure 9 in the main body of this report.) At present, we do not know whether the equality of the impactor and bubble collapse pulses is only a coincidence or represents some more fundamental behavior, where the explosion returns a pressure pulse as strong as the pulse that triggers it (although delayed by several milliseconds).

The underlined statement above suggests, then, that if two drops of molten silicon, A and B, are separated by a distance equal to or less than the distance above the impactor required to trigger a drop explosion, and if somehow drop A should explode, the collapse of its bubble will trigger neighboring drop B. For 9 mm-diameter drops of molten silicon, this distance above Impactor 3 is about 50 mm (see Table 1b in the main body of this report). This behavior might start the propagation of a large-scale steam explosion through an array of drops of molten silicon that are spaced in the water on average 50 mm apart or closer.

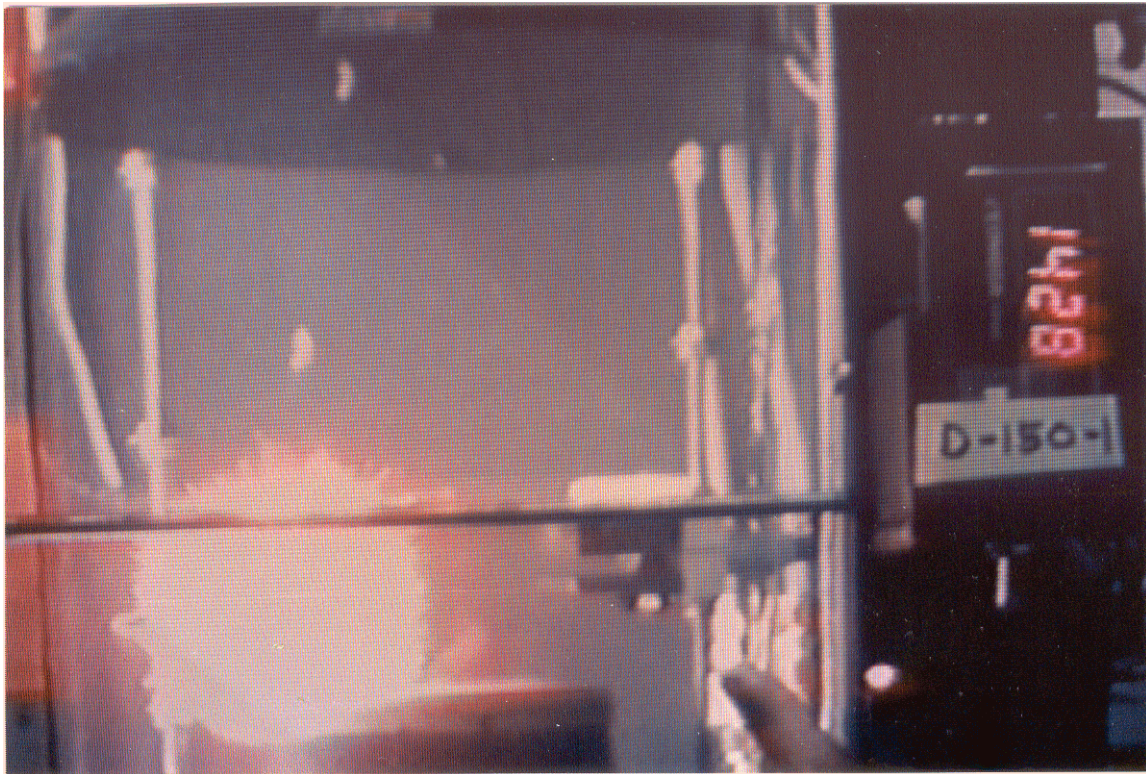


Figure B-1c. Photograph of a single image from the video record of Experiment D-150-1-1. This image shows the explosion (0 s). Imaging rate was 30 frames/s. Impactor 3 was used in this experiment. The horizontal separation of the vertical fiducial bars is 185 mm.

In Figure B-3c, we show a view of PT 2 and PT 3 enlarged from the trace in Figure B-3a. As noted above, PT 2 was generated by the impactor and PT 3 by the steam explosion. The widths of these pulses should be compared. The second spike, PT 2, is very narrow, perhaps only a few microseconds wide, while the third spike, PT 3, is about 0.1 ms wide. This difference is probably due to the actions that produce them: perhaps a mechanical impact of solid materials for PT 2 and the collapse of a steam bubble for PT 3.

We believe the second pulse, PT 2, does not participate in the triggering process. It seems to occur after the steam explosion bubble has grown to maximum and has almost completed its collapse. It is probably an artifact that accompanies the impact of the slug against the undersurface of the impactor, rather than, for example, a pulse reflected from some location in the chamber. Using the velocity of sound in water of 1.5 m/ms, and a depth of 400 mm for the impactor, reflection of the pressure wave from the upper surface of the water and return would require travel of 800 mm and take 0.5 ms. The spike PT 2 at 2.3 ms would correspond to at least 3 m of travel, a distance that does not exist in our 1 m-tall chamber. We therefore conclude tentatively that PT 2 at 2.3 ms, the second spike in the triggering pulse, is somehow generated internally in the impactor and does not participate in the initiation of the steam explosion of the drop of molten silicon.

Hydrogen Generation

We collected 3.4 ml of hydrogen in this experiment (D-150-1-1). But on the video record, it is seen that several bubbles may have escaped to the left of the bubble collection cone, perhaps as much as 50% of the hydrogen produced during the explosion. But the agreement between the volumes of hydrogen collected in

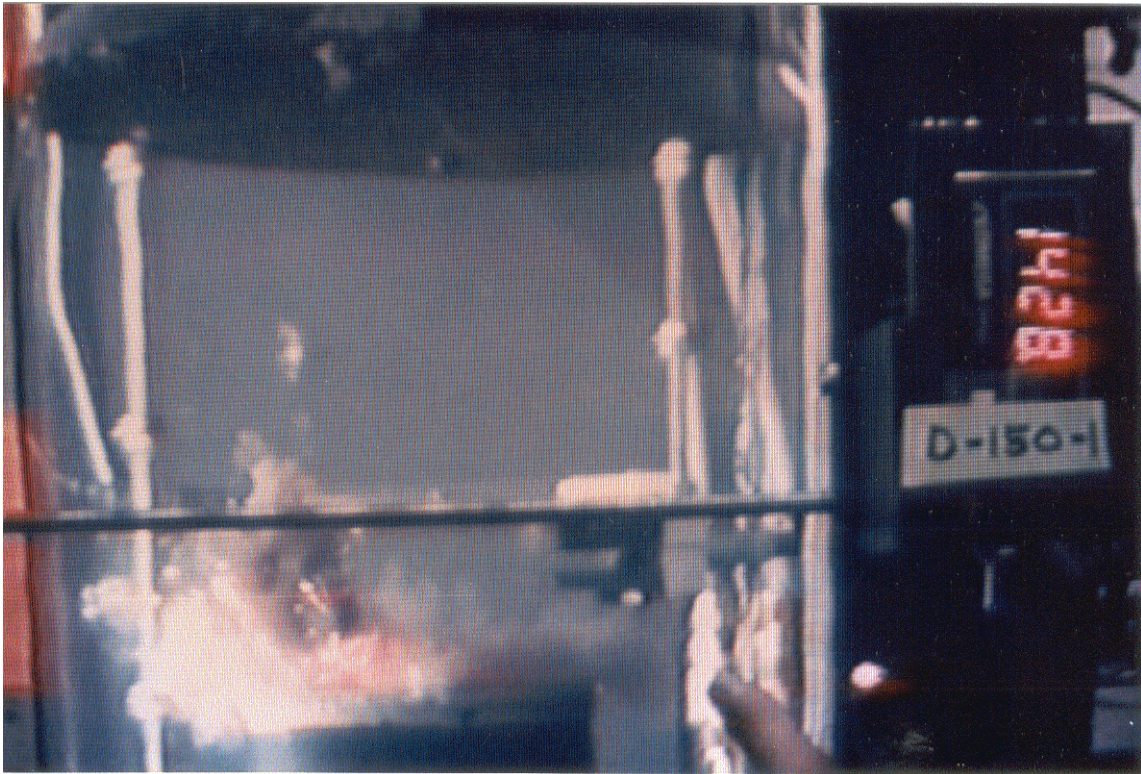


Figure B-1d. Photograph of a single image from the video record of Experiment D-150-1-1. This image shows the frame just after the explosion (+ 0.033 s). Imaging rate was 30 frames/s. Impactor 3 was used in this experiment. The horizontal separation of the vertical fiducial bars is 185 mm.

other similar experiments with drops produced from rods in Batch A-7 (2 or 3 ml) make a loss this large seem unlikely (for example, experiment D-107-1-1, which had essentially identical experimental parameters, generated 3.5 ml of hydrogen; see Table 1B).

Colloidal Material

When the drop of molten silicon was released into the water, it weighed 1.03 grams (determined from the loss of weight of the rod). The dried weight of the granular debris recovered from the impactor and the debris catcher several hours after the experiment weighed 0.81 g. Thus, 0.22 g of the original 1.03 g drop remained suspended in the water as colloid after the explosion, about 21% of the initial weight of the drop.

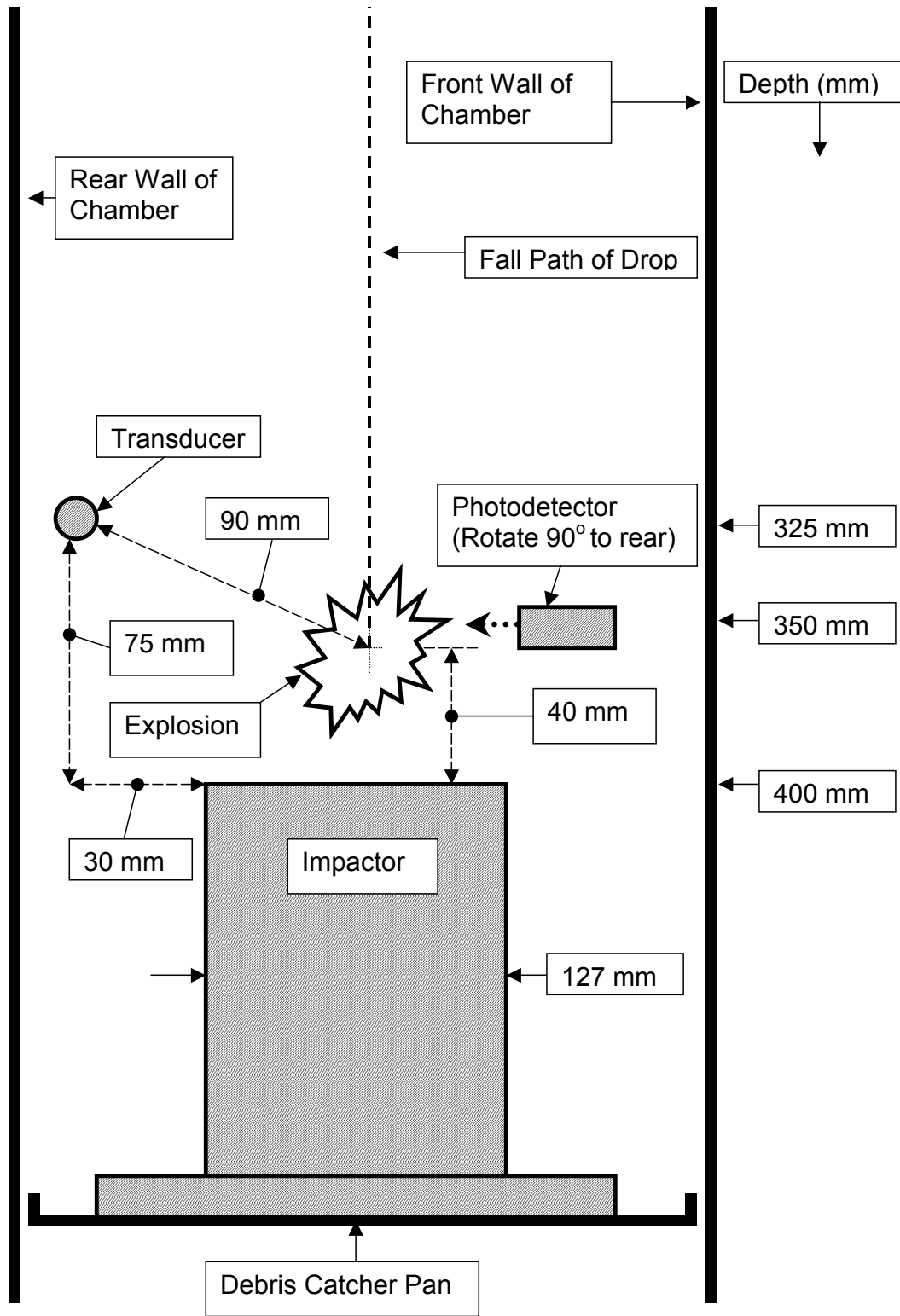


Figure B-2a. Schematic side view of the explosion and placement of components in Experiment D-150-1-1. Impactor 3 was used in this experiment.

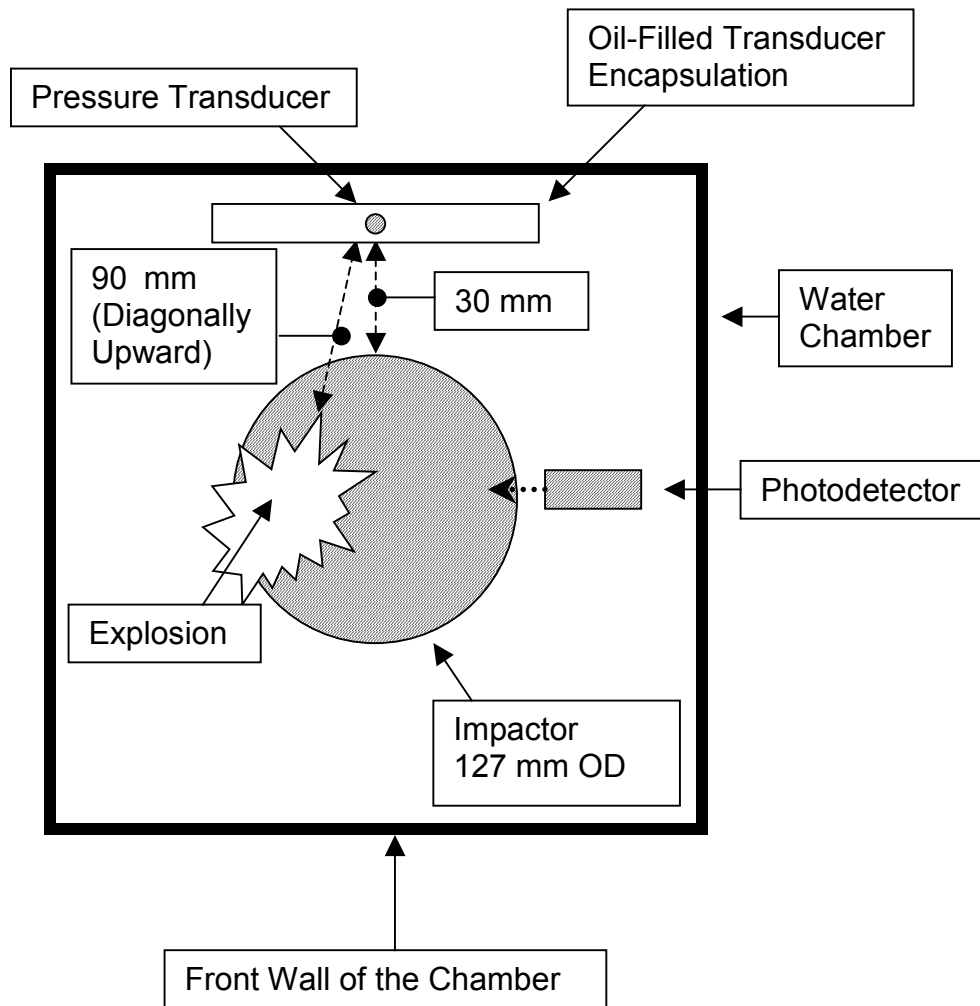


Figure B-2b. Schematic top view of the explosion and placement of components in Experiment D-150-1-1. Impactor 3 was used in this experiment.

Energetics of the Explosion

We have examined the video image shown in Figure B-1c to estimate the pressure-volume energy released into the water by the explosion in experiment D-150-1. We determined that the maximum diameter of the steam explosion bubble was 99 mm, using the known separation of the fiducial bars of 181 mm to calibrate distances on the photograph. The maximum volume of the bubble, V_{\max} , then, is 0.51 L. Using the equation

$$E(\text{J}) = 1013 P_{\text{amb}} (\text{MPa}) V_{\max} (\text{L}) = 51.4 \text{ J.}$$

For the drop of melt that weighed 1.03 g upon release into the water, the energy released per gram of molten silicon was

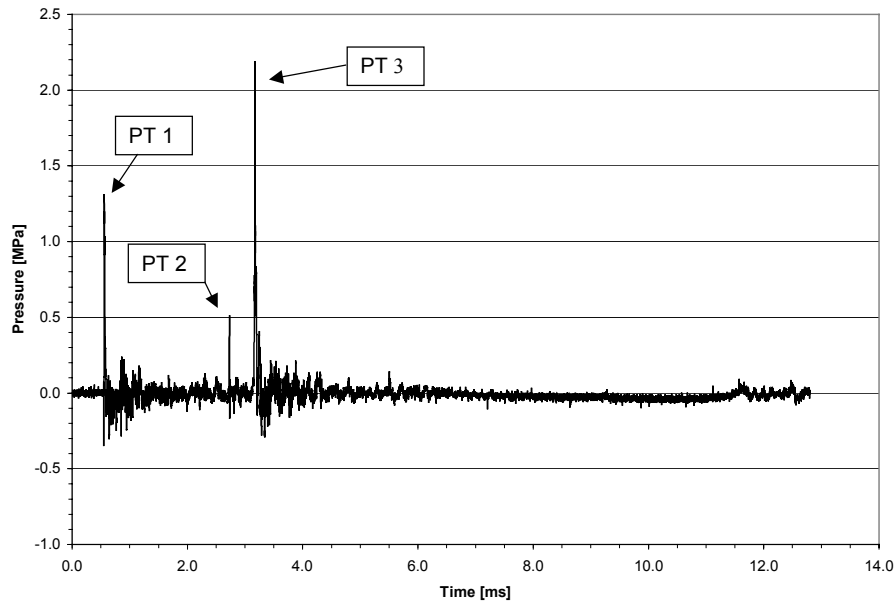


Figure B-3a. Pressure-time trace recorded during Experiment D-150-1-1. Impactor 3 was used in this experiment.

$$E(\text{J/g}) = 49.9 \text{ J/g.}$$

Although previously we have analyzed only one open shutter time-exposed image of a silicon drop prepared from rods in Batch A-7, namely, that for experiment D-114-1-1, shown in Figure 16 in the main body of this report, the energy transferred per gram of melt was only $E(\text{J/g}) = 11.3 \text{ J/g}$. This value was compared to the analogous results obtained with 9 mm-diameter drops of molten ferrosilicon shown in Figure 19 of the final report for 1998 (Nelson et al., 1999). For triggering depths of 400 mm, those values ranged from about 7 J/g to about 26 J/g. Thus, the single value for the energy transferred from the 9 mm-diameter silicon drop in experiment D-114-1-1 prepared from a rod in Batch A-7 seemed to be of similar magnitude as those energies transferred from the 9 mm-diameter ferrosilicon drops.

Now with experiment D-150-1-1, we are confronted with a new level of energy transfer for molten silicon that is larger than any value observed at triggering depths of 400 mm for 9 mm-diameter ferrosilicon drops (50 J/g for the drop of molten silicon vs. 26 J/g for the drops of molten ferrosilicon) and of the same order of the largest energies transferred from the 9 mm-diameter ferrosilicon drops, namely, at 200 mm triggering depths (see Figure 19 of the final report for 1998 (Nelson et al., 1999a)).

Several features emerge from the bubble analysis in experiment D-150-1:

- The energy transferred per gram of molten silicon may be larger than that transferred per gram of molten ferrosilicon, especially at shallower triggering depths.
- This larger energy transfer may generate steam explosion bubbles that are even larger than the bubble observed in experiment D-150-1.
- The collapse of larger steam explosion bubbles may generate even stronger pressure transients than PT 3 shown in Figures B-3a and B-3c (>2 MPa at 100 mm).

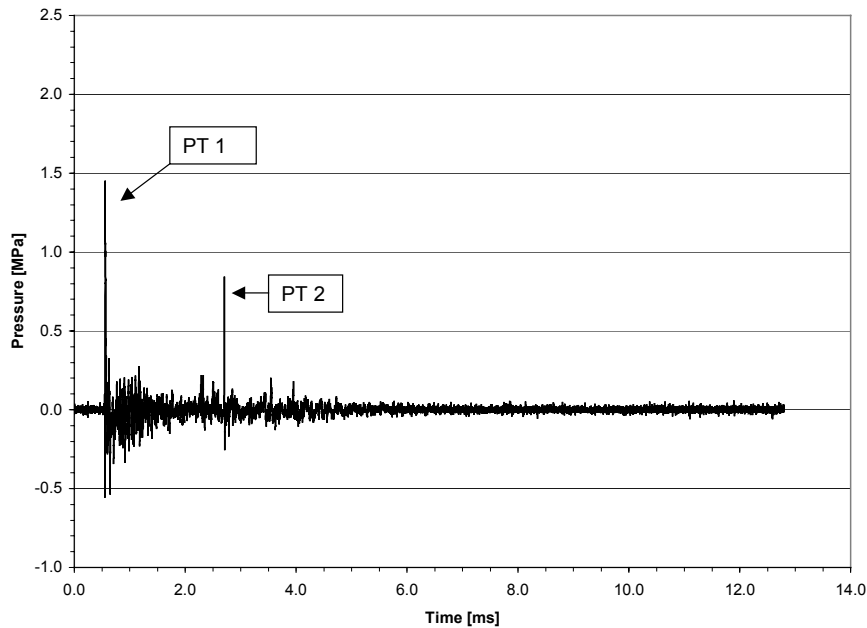


Figure B-3b. Pressure-time trace recorded when the trigger was fired alone. Impactor 3 was used in this experiment.

Conclusions

The collapse of the bubble produced by the steam explosion of a 9 mm-diameter drop of molten silicon returned a pressure transient to the water that was as strong as the original trigger, but delayed by 2.8 ms. This observation suggests a way for the explosion of a single drop of molten silicon to propagate into a large scale steam explosion of an array of many drops in water.

The energy transferred to the water by this explosion was estimated to be 50 J/g of molten silicon. By analogy with earlier work with molten ferrosilicon, it seems that if the drop of molten silicon explodes in shallower water, even larger energies may be released. Because larger bubbles are produced when the energies released are larger, their collapse may generate pressure transients with larger peak pressures.

REFERENCES FOR APPENDIX B

Nelson, L. S., and Duda, P. M., 1982, "Steam Explosion Experiments with Single Drops of Iron Oxide Melted with a CO₂ Laser," *High Temperatures-High Pressures*, 14, 259-281.

Nelson, L. S., 1995, "Steam Explosions of Single Drops of Pure and Alloyed Molten Aluminum," *Nuclear Engineering and Design* 155, 413-425.

Nelson, L. S., Brooks, P. W., Bonazza, R., Corradini, M. L. and Hildal, K., 1999, Triggered Steam Explosions of Molten Ferrosilicon Drops: Behavior of Solenoid-Driven and Pneumatic Impactors; Ability to Trigger the Explosions at Various Water Depths; Energetics of the Explosions; Fall Histories; Colloidal Material Deposited During the Explosions, Draft Final Report to SINTEF Materials Technology, Trondheim, Norway, March 15, 1999.

APPENDIX C

Furnace Failures

Although it is common to report only successful results, we feel it is important also to document troubles for the future experimenter, especially when they affect a major component of our apparatus that had operated reliably for more than five years.

During this reporting period, we have encountered four failures of our silicon carbide-heated furnace, as summarized in Table C-1.

Experiment D-77-1

In this experiment, we attempted to use a rod that was too short. Prior to the failure, we already had released two drops from a rod from Batch A-8 and in this experiment, we tried for a third drop while the furnace was still hot. In this third attempt, we lowered the rod and its graphite support too far into the hot zone of the mullite furnace tube. This initiated a chemical reaction between the silicon, graphite and mullite, causing the graphite to expand into the tube and fracture it. The result was a delay of 8 working days.

A photograph of a typical silicon rod in a graphite holder before an experiment is shown in Figure C-1. Photographs of the damaged tube are shown in Figure C-2. Note that no silicon remained in the graphite afterward, even though we estimate that at least 3 g of the rod had been present in the holder just before the failure.

Experiment D-101-1

In this experiment, the mullite furnace tube and the hot zone of the original silicon carbide heating element may have come into contact, possibly due to a particle of the firebrick insulation falling between the helix and the furnace tube. There was a chemical reaction in the hot zone of the furnace that caused the heating element to fail catastrophically. Photographs are shown in Figure C-3. This heating element had been in use continually since 1995 without difficulty (Nelson et al., 1995).

This failure delayed us 2 working days.

Experiment D-117-1

We replaced the original silicon carbide heating element that failed in experiment D-101-1 with a new one. Seven experiments were performed with it (D-103-2, D-104-1, D-107-1, D-109-1, D-111-1, D-114-1 and D-115-1) until again the mullite furnace tube and the new silicon carbide heating element somehow came into contact. This time, the reaction did not cause the helix to break, but did increase its resistance and prevented it from heating properly. Photographs are shown in Figure C-4. We believe the failure may have been the result of a slight misalignment of the element during manufacture. (This misalignment caused the element to stand at a slight angle when photographed, as can be seen in Figure C-4a.)

Date	Expt. No.	Description of Failure	Delay
22 Jul '99	D-77-1	Reaction between Si and graphite rod support fractured mullite furnace tube.	8 days
6 Aug '99	D-101-1	Reaction with mullite furnace tube caused catastrophic failure of SiC element.	2 days
7 Sep '99	D-117-1	Reaction with mullite furnace tube increased resistance of SiC element.	7 days
27 Sep '99	D-126-1	Reaction with mullite furnace tube caused failure of SiC element.	10 days

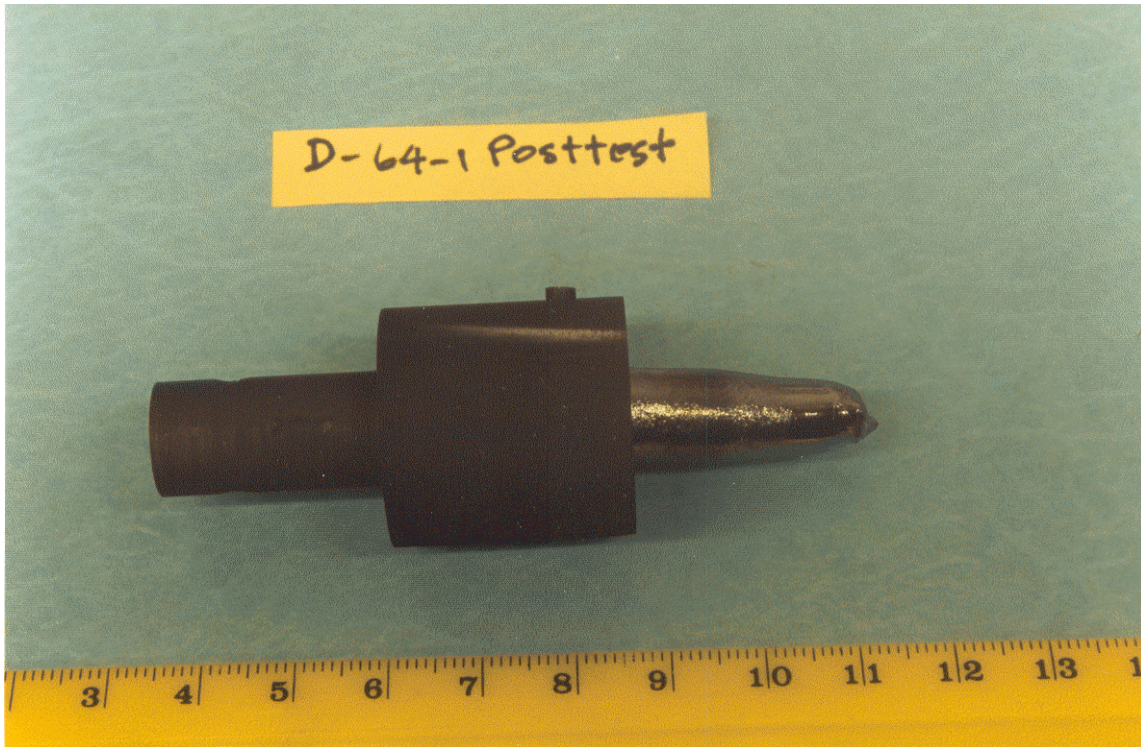


Figure C-1. Photograph of a typical silicon rod in a graphite holder.

This failure caused a delay of 7 working days.

Experiment D-126-1

This failure was essentially identical to that in Experiment D-117-1, with the helix somehow again contacting the side wall of the furnace tube. This was unexpected, because we had changed from a 32 mm OD to a smaller 29 mm OD mullite furnace tube to avoid contact of this sort. Photographs of the failed element and furnace tube are shown in Figure C-5. This failure caused a delay of 10 working days.

Final Note

On September 30, 1999, we discussed the failures of the silicon carbide elements with their manufacturer, I Squared R Element Company of Akron, NY. It is their opinion that we have been operating the elements at current densities that are too high. Apparently this can cause a very hot spot to form on the element and initiate combustion. This produces silicon dioxide, which condenses nearby, and carbon dioxide, which diffuses away. This explanation is consistent with the white deposits seen on the furnace tubes in several of the photographs shown in the figures of this Appendix.

The manufacturer suggests that we try insulation around the element that is thicker and more efficient than the firebrick currently being used in order to reduce the current needed to achieve the same high temperature. We are currently modifying our furnace insulation accordingly.



Figure C-2a. Photograph of the damaged mullite tube after Experiment D-77-1, overall side view.



Figure C-2b. Photograph of the damaged mullite tube after Experiment D-77-1, close-up side view.



Figure C-2c. Photograph of the damaged mullite tube after Experiment D-77-1, close-up end view. In this view, note that no silicon remained in the graphite afterward, even though at least 3 g was present before the failure.



Figure C-3a. Photograph of the failed silicon carbide heating element and mullite furnace tube after Experiment D-101-1.

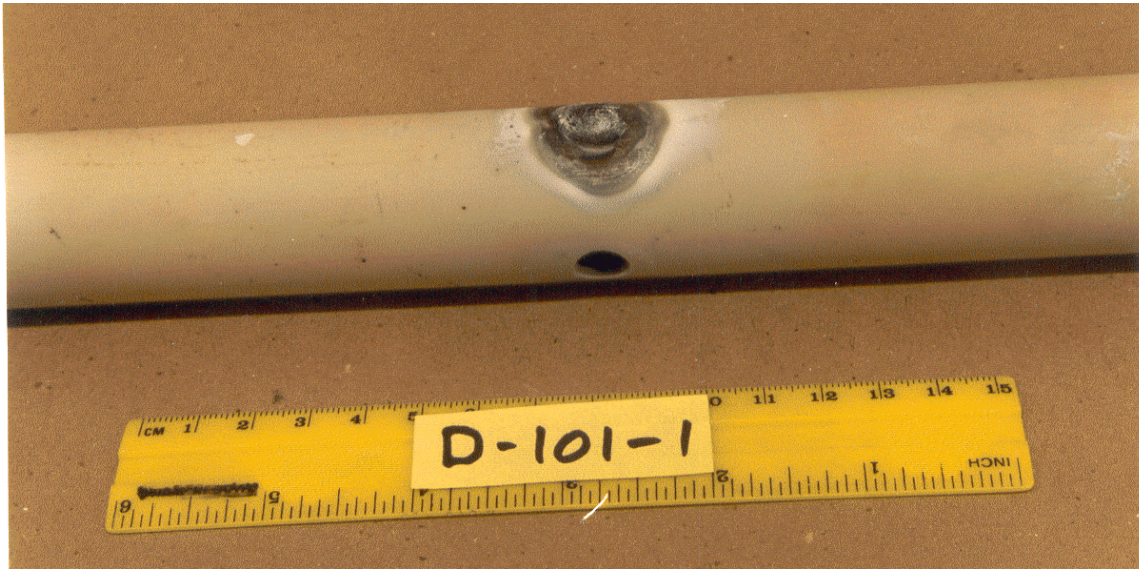


Figure C-3b. Photograph of the failed mullite furnace tube after Experiment D-101-1.



Figure C-4a. Photograph of the failed silicon carbide heating element and mullite furnace tube after Experiment D-117-1.



Figure C-4b. Photograph of the failed mullite furnace tube after Experiment D-117-1.



Figure C-4c. Photograph of the failed silicon carbide heating element after Experiment D-117-1.



Figure C-5a. Photograph of the failed silicon carbide heating element and mullite furnace tube after Experiment D-126-1.

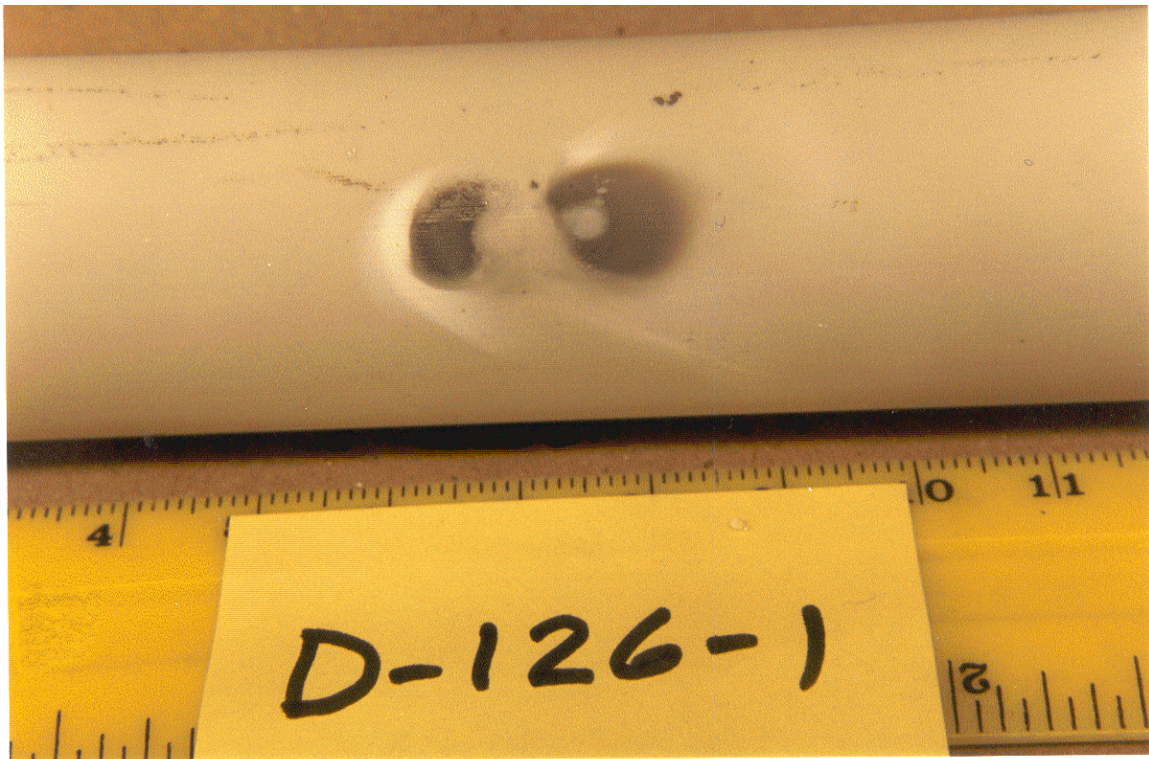


Figure C-5b. Photograph of the failed mullite furnace tube after Experiment D-126-1.

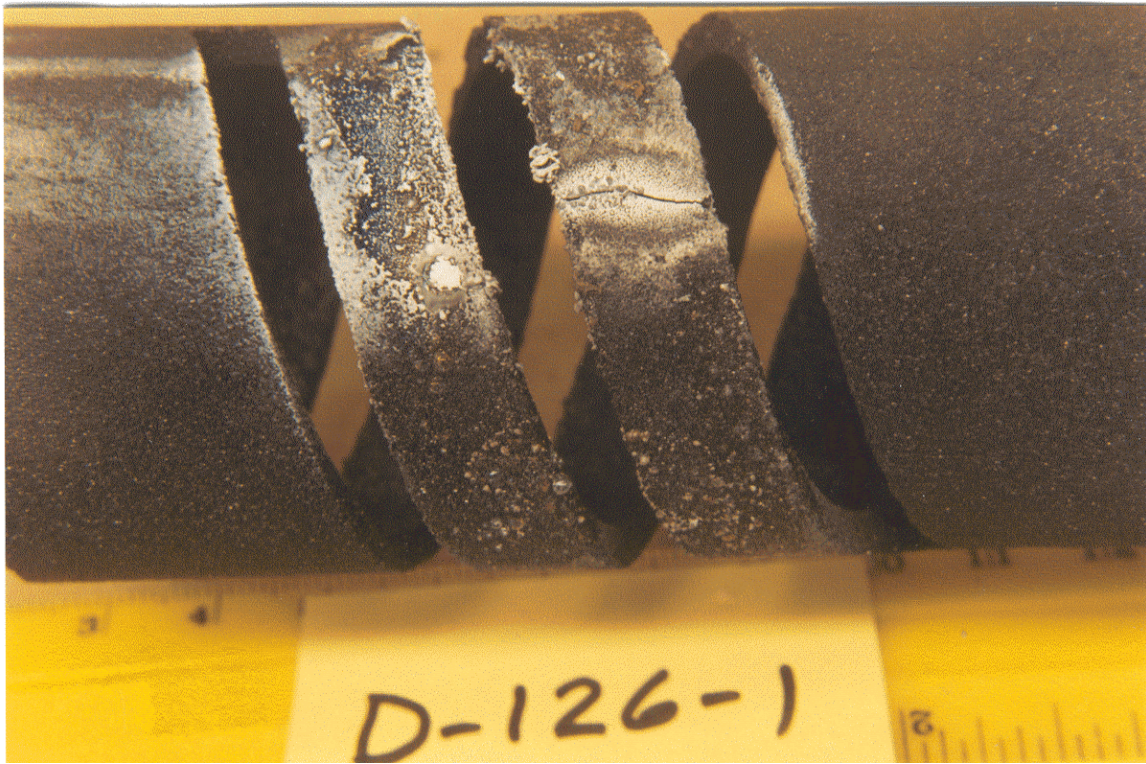


Figure C-5c. Photograph of the failed silicon carbide heating element after Experiment D-126-1.

APPENDIX D

Theoretical Heat Transfer Studies

Kjetil Hildal
Institute of Metallurgy
Norwegian University of Science and Technology
N-7016 Trondheim, Norway

This preliminary document has been prepared by Mr. Kjetil Hildal during his stay during 1999 at the Department of Engineering Physics, University of Wisconsin in Madison.

2.4 The heat balance for a single drop

In the experiments performed at the University of Wisconsin, Madison (UW), the drop is released from the furnace at its melting temperature, approximately 1412 °C. Its heat transfer history can be divided into three parts, the fall through the gas atmosphere, the fall in the water, and the explosion event. We will in this section estimate the heat transfer for each one of these stages. A number of assumptions are made:

- neglecting air resistance during free fall
- the molten drop behaves like a gray radiant object, with emissivity less than one
- the initial drop temperature is equal to the melting temperature of silicon, i.e. 1412 °C.
- the calculations are based on a drop mass of 1 gram.

Other assumptions are also made, which will be clarified for each stage.

Silicon properties used in the calculations are given in table 2.1.

Table 2.1. Silicon properties.

<i>Enthalpy, 1685 K, liquid Si</i>	$\Delta H=86\ 187\ J/mol$
<i>Specific heat, 1690 K</i>	$C_p=0.2476\ cal/K*gram$
<i>Surface tension, xxxx K</i>	$\sigma=7.25*10^{-7}\ J/cm^2$
<i>Latent heat of fusion</i>	$H_f=50.208\ J/K*mol$
<i>Exothermic energy from the reaction $Si+2H_2O=SiO_2+2H_2$</i>	$\Delta H_{reaction}=155\ kJ/mol\ H_2$

The gas mixture used for flushing the furnace was argon+1% hydrogen. This mixture prevents the silicon to oxidize. The properties for this mixture were taken to be the same as for pure argon. The properties used in the calculations are given in table 2.2.

Table 2.2. Argon properties.

<i>Thermal conductivity, 400 K</i>	$k_{Ar}=0.226\ W/m*K$
<i>Dynamic viscosity, 400 K</i>	$\mu_{Ar}=28.9*10^{-6}\ Pa*s$
<i>Density, 400 K, 1 atm</i>	$\rho_{Ar}=1.217\ kg/m^3$
<i>Specific heat, 400 K, 1 atm</i>	$C_{p,Argon}=20.81\ J/K*mol$

The calculations were done in EES. All of the details and the code used are in appendix A.

2.4.1 Heat transfer during fall through gas mixture

The fall from the furnace to the water furnace gives off heat in two ways, convection and radiation. For the estimate it is assumed that the drop is spherical, with a diameter equal to the rod specimen diameter (9 mm).

However, being able to calculate the mass of the drop, one can easily do the heat transfer calculation for each drop, knowing the density of molten silicon. The argon flow velocity is constant and equal to 0.274 m/s, based on the flowmeter measurements and calibration data from the manufacturer. It is acknowledged that the gas temperature rises close to the molten sphere. As the thermodynamic data are somewhat limited, a value of 400 K has been used for the mean boundary layer temperature. All parameters used are included in appendix A, where the equations and solutions are posted.

To estimate the heat transfer coefficient, Ranz and Marshall's model for freely falling liquid drops was used [50]. The Nusselt number in their model is correlated by

$$Nu=2+0.6*Re^{1/2}*Pr^{1/3} \quad (16)$$

Re is the Reynolds number and Pr the Prandtl number for the flowing argon around the molten sphere. The heat transfer coefficient is $h=k_{Ar}*Nu/D_{drop}$.

It was found that the heat loss due to convection was negligible. This was not surprising, taken the short fall and the poor heat transfer characteristics of argon into account. For important calculated values, see table 2.3.

Table 2.3. Results from the heat transfer calculation, convection in the gas mixture.

<i>Heat transfer coefficient</i>	$H=9.1 \text{ W/m}^2*\text{K}$
<i>Reynolds number</i>	$Re=958$
<i>Heat loss from molten sphere</i>	$Q=0.7 \text{ J}$
<i>Prandtl number</i>	$Pr=6.65*10^{-4}$
<i>Temperature drop associated with calculated heat loss</i>	0.7 K

The contribution from radiation heat transfer is expected to be higher, as the temperatures in question are fairly high. It is assumed that the surface temperature is constant and equal to the bulk temperature of the molten silicon. The last one is a good approximation, as the Biot number of the system ($Bi=h*D/k_{silicon, molten}$) is much less than 1. It turns out that the surface temperature does not change much during the fall in the gas, and the temperature differences are large, so the error involved in the assumption of a constant surface temperature is small. As mentioned above, the molten sphere is approximated as a gray object, with an emissivity less than one. The value of this emissivity is not known accurately. Therefore I have not compensated for gray object behavior, and have treated the sphere as a black body, with an emissivity equal to 1. This will give a upper limit to the heat loss and temperature drop in the sphere during the free fall.

The radiation heat loss is governed by Stefan-Boltzman's radiation law:

$$\text{Heat loss} = \text{Area of the drop} * \text{fall time} * \sigma * (T_{drop}^4 - T_{gas}^4) \quad (17)$$

σ is Stefan-Boltzman's constant, $5.67*10^{-8} \text{ W/K}^4*\text{m}^2$. Details for the calculations are in appendix B. The results are given in table 2.4.

Table 2.4. Results from heat transfer calculations, radiation during free fall in gas mixture.

<i>Heat loss due to radiation</i>	$Q_{radiation}=32.95 \text{ J}$
<i>Temperature drop associated with radiation heat transfer</i>	$dT=31.78 \text{ K}$

Since the heat loss is only a small fraction of the latent heat of fusion, the amount of solidification is negligible. For the rest of the calculation, it is assumed that the drop enters the water supercooled due to heat losses during the free fall. The subcooling is the temperature drop given in table 2.4.

2.4.2. Heat transfer during fall through water

There have been a number of investigations on the cooling of hot spheres in water, a review of the work done was given by Kalinin et al. [51]. However, none of the models described in this review covered subcooled heat transfer from spheres, so a newer correlation has been used, namely that of Dhir and Purohit [27]. Their correlation for the Nusselt number is

$$Nu = Nu_0 + 0.8Re^{0.5}(1 + S_cPr_v/ShPr_1\mu) \quad (17)$$

where

$$Nu_0 = 0.8(g_0\rho_v(\rho_l-\rho_v)h_{fg}D^3/(\mu_vk_v\Delta T_w))^{1/4} \quad (18)$$

For explanation of the symbols, see the nomenclature list (appendix B). This Nusselt number takes into account both convection and radiation heat transfer. The details for the calculations are given in appendix A. Important values are listed in table 2.5.

Table 2.5. Calculated thermophysical properties for the heat transfer during free fall in water for a molten sphere of silicon.

<i>Heat transfer coefficient</i>	$H=466.2 \text{ W/m}^2\text{K}$
<i>Heat loss</i>	$Q=210.4 \text{ J}$
<i>Reynolds number</i>	$Re=2696$

Comparing the heat losses during these different stages, we find as expected that the fall in the water is the far most important one. The contribution from the forced convection in the argon-1% hydrogen atmosphere is negligible. So the heat loss from the release of the drop to the point where it explodes is basically a combination of radiation and forced convection in the water.

2.4.3. The energy release due to oxidation of the surface

The oxidation of Si is exothermic, and heat will be released as the drop sinks in the water. The excess heat for the reaction $Si_{(l)} + 2H_2O_{(l,g)} = SiO_{2(s)} + 2H_{2(g)}$ is calculated by Tuset [52] to be 155 kJ/mole H_2 at 1500 °C. This is a temperature somewhat higher than in the actual case, nevertheless, this value is used here. It is assumed that this value will change considerably due to the temperature difference. Since we can measure the amount of hydrogen released in the reaction, the excess heat is directly found by multiplying the number of moles of hydrogen with 155/2, which will give the total heat released in kJ. For an amount of 5 ml H_2 , the heat release is approximately 30 J. See section 2.6 for a summary of the heat balance.

2.4.4 Increased surface energy

After the drop has experienced the trigger pulse, an explosion might occur. If the drop explodes, this is associated with a huge increase in the surface area, and therefore some of the energy of the molten drop will be used for the surface expansion work. For the estimate of the surface energy, we need to know the surface tension. It is assumed that the drop fragments when it is molten. This is not completely correct, as a thin solid shell surrounds the molten metal. However, this is neglected here. From [53], the surface tension for molten Si is given as

$$\gamma=\gamma_0+(T-T_0)(d\gamma/dT) \quad (19)$$

where $\gamma_0=865$ mN/m, T_0 is the melting point (1410 °C), T the temperature of the melt and $d\gamma/dT$ is equal to -0.13 mN/m*K. This value is used in section 4.3 when we consider the fragmentation of the drop.

The surface energy is now found by a simple mass balance. The total number of particles with a mean size yet to be decided experimentally, is given by

$$\#particles=M/(V*\rho) \quad (20)$$

where M is the mass of the drop, V the average volume of a fragment and ρ the density of solid silicon. The total surface area is now simply the number of particles multiplied by the average area of a fragment. This number is then multiplied with the surface tension to give the surface energy. It is noted that since the density of liquid and solid silicon differs considerably ($\rho_l=2.51$ g/cm³, $\rho_s=2.33$ g/cm³), this will introduce an error by overestimating the molten surface area slightly. The density difference is close to 8 % (relative to the solid density). Since mass is conserved, this suggests that the volume of the molten fragments is 8 % less than the corresponding solid volume. Since volume is proportional to r^3 , the error in the radius is 2.7 %, giving an error in the surface area of 5.3 %. But this error is small compared to the uncertainty in the measured fragment size, so it will be neglected in these calculations. However, for a more precise measurement of the debris, we would have to take this error into account. The calculated surface energy follows naturally in section 4.3, where the debris measurements are described.

4.3 Debris analysis

In order to get an estimate of the debris distribution and sizes, a sample of the debris from experiment D-107-1#2 was analyzed with a light microscopy. Sample pictures are shown in Figure 4.1 and 4.2.

Figure 4.1 shows pieces of a solid crust that has formed around the molten drop prior to the triggering. However, the shell has not been thick (or dense) enough to prevent water-melt contact after the triggering. It is believed that a combination of the strong pressure pulse applied from the impactor and the water jets following the collapse of the vapor film contributed to the break of the shell. It is also possible that water drops can have passed through the shell, and vaporized inside the oxide layer, thereby breaking up the crust. It has been confirmed in experiments performed by Hildal [58] that an oxide layer consisting of SiO₂ only is very porous, and it is possible that water can penetrate through this layer. Since the oxide layer has a higher melting point than the pure Si, solidification of this surface crust takes place rapidly after the drop enters the water.

The size of the pieces shown on figure 4.1 was measured using ImageTool, and the mean (projected) area was found to be 2.15 mm², with a standard deviation of 0.73 mm². These numbers were obtained from measurements from 7 pieces, judged to be fairly representative for the total number of pieces. This would correspond to a shell fragmented to 80-150 pieces, a relatively fine fragmentation. The thickness of the shell was not measured due to inadequately techniques, however, this will be done at the facilities of the Norwegian University for Technology and Science, Trondheim, next spring.

In Figure 4.2, a light microscopy picture of the fine debris resulting from a steam explosion is shown. The distribution and the mean particle size are highly dependent of the strength of the explosion, and the example here is mainly chosen as it was judged to be representative for a fairly strong explosion.

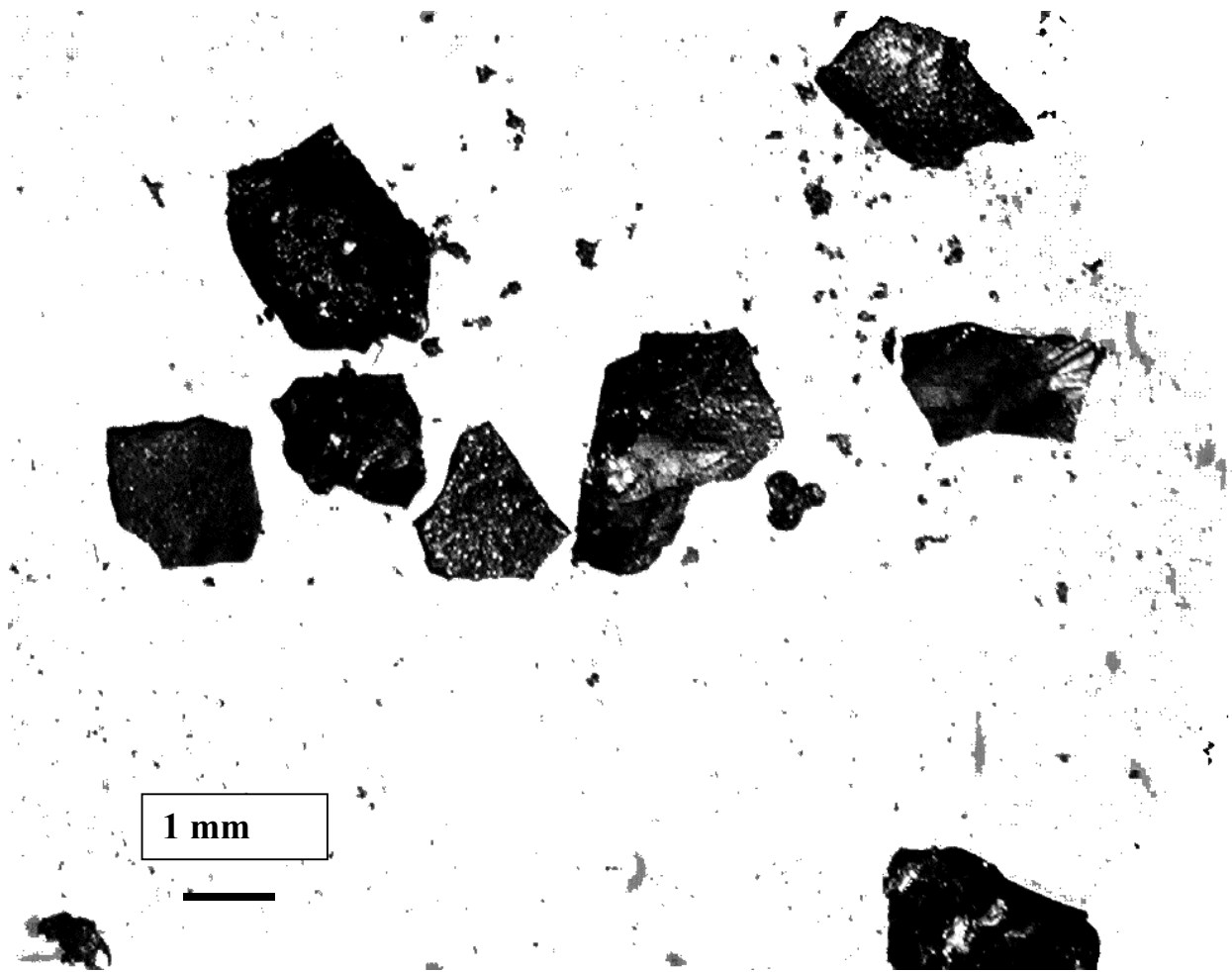


Figure 4.1. Light microscope picture of pieces of the solid shell forming around the drop as solidification proceeds.

The debris varies considerably in size, in figure 4.2 the smallest particles are about $5\ \mu\text{m}$ in diameter (assumed spherical), but the larger ones are as much as $150\ \mu\text{m}$. Still, it is easy to separate solidified material resulting from the interior of the drop from the early solidified shell. The latter one being on the order of $1\ \text{mm}$ in diameter. In order to get a good estimate of the particle size and distribution, it is necessary to use some computer program. For a quick estimate I used ImageTool, however, the process is very time-consuming. A more sophisticated way would be to create some computer code that then would help the program to scan the picture automatically and give both mean size and distribution. This was not done for these experiments, so there might be a considerably error in the mean particle size. The selection of the photos used was based on the author's best judgement, trying to get a representative distribution.

4.3.1 The surface energy

As explained in section 2.4.4, the increase in surface area uses some of the stored energy of the drop. If we take the average diameter of the debris to be $100\ \mu\text{m}$, we can estimate the surface energy. In section 2.4 we calculated the heat transfer coefficient for the droplet. Since the cooling time is known, we can estimate the energy loss, and thereby the associated temperature drop. We assume that the melt does not solidify, merely supercooles. A upper limit of this temperature drop is found to be $190\ ^\circ\text{C}$. Inserting this value for T in equation (19), we find the surface tension, and it is a simple matter of calculating the surface energy. This energy is found to be very small, on the order of $0.02\ \text{J}$. So this energy can be neglected, it is very small compared to the other energies involved. Even if we assume mean debris sizes of the order $1\ \mu\text{m}$, the surface energy is only of the $1\ \text{J}$ order.

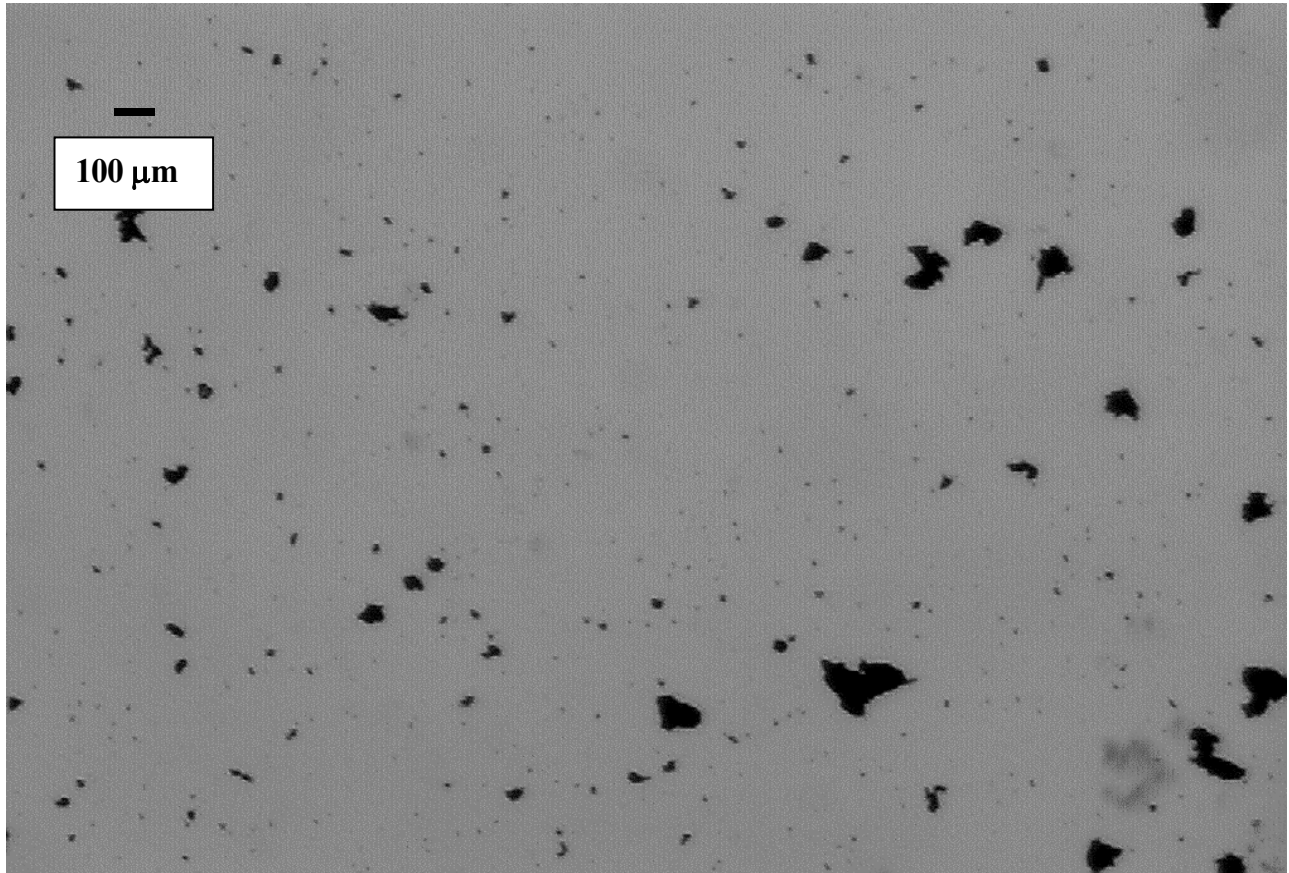


Figure 4.2. A typical sample picture for the debris collected from a steam explosion.

5. References

1. Colgate, S.A. and Sigurgeirsson, T. (1973). *Dynamic mixing of water and lava*. Nature 244, 552-555.
2. Francis, P. and Self, S. (1983). *The eruption of Krakatau*. Sci. Am. 249, 146-159.
3. Reid, R.C. (1983). *Rapid phase transitions from liquid to vapor*. Adv. in Chem. Engr. 12, 105-208.
4. Long, G. (1957). *Explosions of molten metal in water - causes and prevention*. Met. Prog. 71, 107-112.
5. Page, F.M., Chamberlain, A.T., and Grimes, R. (1987). *The safety of molten aluminium-lithium alloys in the presence of coolants*. J. de. Phys. Colloq. C3, 48, 63-73.
6. Epstein, S.G. (1992). *Molten aluminum-water explosions: An update*. Light Metals 1993, pp. 845-853, Metallurgical Society of AIME.
7. Lipsett, S.G. (1966). *Explosions from molten metal and water*. Fire Tech. 2, 118-126.
8. Anonymous (1976). *The explosion at Appleby-Frodingham Steelworks, Scunthorpe, 4 November 1975*. Health and Safety Executive Report, HMSO, ISBN 011880331X.
9. Fletcher, D.F. and Theofanous, T.G. (1997). *Explosive melt-water interactions*. Advances in Heat Transfer, 29, 129-212.

10. Corradini, M.L., Kim, B.J. and Oh, M.D. (1988). *Vapor explosions in light water reactors: A review of theory and modeling*. Prog. in Nuc. Energy, 22, No.1, 1-117.
11. Fletcher, D.F. (1994). *A Review of the Available Information on the Triggering Stage of a Steam Explosion*. Nuclear Safety, vol.35, no.1.
12. Fletcher, D.F. (1995). *Steam explosion triggering: A review of theoretical and experimental investigations*. Nuc. Engr. Design, vol. 155, 27-36.
13. Sallach, R.A., Elrick, R.M., Douglas, S.C. and Ouellette, A.L. *Reactions Between Some Cesium-Iodine Compounds and the Reactor Materials 304 Stainless Steel, Inconel 600 and Silver, Volume I. Cesium Hydroxide Reactions*, Report NUREG/CR-2921 (SAND 83-0395), U.S. Nuclear Regulatory Commission, June 1984.
14. Dufresne, J. et al. *Presentation of the ESCADRE system together with a practical application*. International Symposium on Severe Accidents in Nuclear Power Plants, Sorrento, Italy, March 1988.
15. Drumheller, D.S. *The initiation of melt fragmentation in fuel-coolant interactions*, Nucl. Sci. Engr., vol. 72, 347-356, 1979.
16. Inoue, A., Ganguli, A. and Bankoff, S.G. *Destabilization of film boiling due to arrival of a pressure shock: Part II analytical*, J. Heat Transfer, vol. 103, 465-471, 1981b.
17. Inoue, A. et al. *Study on transient heat transfer of film boiling due to arrival of pressure shock*, Paper FB39, Proc. 4th Int. Heat Transfer Conf., Munich, Germany, 1982.
18. Corradini, M.L. *Modeling film boiling destabilization due to a pressure shock arrival*, Nuc. Sci. Engr., vol. 78, 154-170, 1983.
19. Knowles, J.B., *A mathematical model of vapor film destabilization*, Report AEEW-R-1933, 1985.
20. Naylor, P., *Film boiling destabilization*, Ph.D. Thesis, University of Exeter, 1985.
21. Inoue, A. and Bankoff, S.G., *Destabilization of film boiling due to arrival of a pressure shock: Part I. Experimental*, J. Heat Transfer, vol. 103, 459-464, 1981.
22. Corradini, M.L., *Phenomenological modeling of the triggering phase of small-scale steam explosion experiments*, Nucl. Sci. Engr., vol. 78, 154-170, 1981.
23. Nelson, L.S., Brooks, P.W., Bonazza, R., Corradini, M.L. and Hildal, K., *Triggered steam explosions of molten ferrosilicon drops....*, Final Report to SINTEF, Norway, March 1999.
24. Henry, R.E., Hohmann, H. and Kottowski, H., *The effect of pressure on NaCl-H₂O explosions*, Proc. of the 4th CSNI Spec. Meet. On FCI in Nuc. React. Saf., Bournemouth, U.K, CSNI report no. 37, vol.1, 308-323., 1979.
25. Hohmann et al., *Experimental investigations of spontaneous and triggered vapor explosions in the molten salt/water system*, Proc. Int. Meet. Therm. Nuc. React. Safety, Chicago, 1982.
26. Bergstrom, T. *A review of molten metal-water reactions*. Unpublished work. SINTEF Materials Technology, Trondheim, Norway, 1988.
27. Dhir, V.K. and Purohit, G.P. *Subcooled film-boiling heat transfer from spheres*, Nuc. Engr. Design, vol.47, 49-66, 1978.

28. Nelson, L.S., Eatough, M.J., and Guay, K.P. *Initiation of explosive molten aluminum-water interactions at wet or underwater surfaces*. ANS Proc. Nat. Heat Transfer Conf., 24-27 July, Houston, vol.3, 219-227, 1988.
29. Flory, K., Paoli, R., and Mesler, R. *Molten metal-water explosions*. Chem. Engr. Prog., vol. 65, 50-54, 1969.
30. Nelson, L.S., and Guay, K.P., *Suppression of steam explosions in tin and Fe-Al₂O₃ melts by increasing the viscosity of the coolant*. High Temp.-High Pressures, vol. 18, 107-111, 1986.
31. Kim, H., Krueger, J., and Corradini, M.L., *Single droplet vapor explosions: Effect of coolant viscosity*. Proc. 4th Int. Top. Meet. on Nuc. React. Therm.-Hydr., 10-13 October, Karlsruhe, Germany, vol. 1, 261-267, 1989.
32. Kowal, M.G., Dowling, M.F., and Abdel-Khalik, S.I., *An experimental investigation of the effects of surfactants on the severity of vapor explosions*, Nucl. Sci. Engr., vol. 115, 185-192, 1993.
33. Skelton, W.T.W., Kowal, M.G., and Abdel-Khalik, S.I., *Effect of borid acid on the severity of vapor explosions in pure water and surfactant solutions*, Nucl. Eng. Design, vol. 155, 359-368, 1995.
34. Dowling, M.F., Ip, B.M., and Abdel-Khalik, S.I., *Suppression of vapor explosions by dilute aqueous polymer solutions*, Nucl. Sci. Engr., vol. 113, 300-313, 1993.
35. Becker, K.M. and Lindland, K.P., *The effect of surfactants on hydrodynamic fragmentation and steam explosions*, Dep. Of Nucl. Engr., RIT, Stockholm, Sweden, Report KTH-NEL-50, 1991.
36. Fauske, H.K., *On the mechanism of uranium dioxide-sodium explosive interactions*, Nucl. Sci. Engr., vol. 51, 95-101, 1973.
37. Board, S.J., Hall, R.W., and Hall, R.S., *Detonation of fuel coolant explosions*, Nature, vol. 254, 319-321, 1975.
38. Carslaw, H.S., and Jaeger, J.C., *Conduction of heat in solids*, Clarendon Press, Oxford, 1959.
39. Skripov, V.P., *Metastable liquids*, Wiley, New York, 1974.
40. Cronenberg, A.W., *Recent developments in the understanding of energetic molten fuel-coolant interactions*, Nucl. Safety, vol. 21, 319-337, 1980.
41. Fauske, H.K., *Some aspects of liquid-liquid heat transfer and explosive boiling*, Proc. 1st Conf. On Fast Reactor Safety, 2-4 April, Beverly Hills, CA, 992-1005, ANS, 1974.
42. Henry, R.E., and Fauske, H.K., *Nucleation processes in large scale vapor explosions*, ASME, J. Heat Transfer, vol. 101, 280-287, 1979.
43. Hohmann, H., Magallon, D., Schins, H. and Yerkess, A., *FCI experiments in the aluminium oxide/water system*, Nucl. Eng. Design, vol. 155, 391-403, 1995.
44. Board, S.J. and Hall, R.W., *Propagation of thermal explosions, Part I: Tin-water experiments*, Central Electricity Generation Board Report RD-B-N2850, 1974.
45. Board, S.J. and Hall, R.W., *Propagation of thermal explosions, Part 2: Theoretical Model*, Cent. El. Gen. Board Rep. RD-B-N3249, 1974.

46. Courant, R. and Friedrichs, K.O., *Supersonic flow and shock waves*, Interscience, London, 1948.
47. Zeldovich, I.B., and Kompaneets, A.S., *Theory of detonations*, Academic Press, London, 1960.
48. Simpkins, P.G., and Bales, E.L., *Water drop response to sudden accelerations*, J. Fluid Mech., vol. 55, 629-639, 1972.
49. Fletcher, D.F., and Anderson, R.P., *A review of pressure-induced propagation models of the vapour explosion process*, Prog. Nucl. Energy, vol. 23, 137-179, 1990.
50. Ranz, W. and Marshall, W. (1952). Chem. Engr. Prog., vol. 48, 141.
51. Kalinin, E.K., Berlin, I.I. and Kostyuk, V.V. *Film boiling heat transfer*, Adv. Heat Transfer, vol. 11, 51-198, 1975.
52. Tuset, J.C., *Private communication*, 1999.
53. Brandes, E., *Smithells metals reference book*, 6.ed, 1983
54. Nelson, L.S. and Duda, P.M., *Steam Explosion Experiments with single drops of iron oxide melted with a CO₂ laser*, High Temperatures-High Pressures, vol.14, 259-281, 1982.
55. Nelson, L.S., Brooks, P.W., Bonazza, R., Corradini, M.L. (1997-199). Informal Letter Reports to SINTEF. Restricted.
58. Hildal, K. *Oxide layer formation around molten Si, with or without Al/Ca additives*. Internal report, NTNU, Norway, 1999.
56. Nelson, L.S., Brooks, P.W., Bonazza, R. and Corradini, M.L., *Triggering steam explosions of single drops of a molten ferrosilicon alloy with a simple encapsulated mechanical impactor*, Metallurgical and Materials Trans. B., vol.30B, 1999.
57. Handbook of Chemistry and Physics, 63rd ed., p. B-103, 1983.
58. Hildal, K. *Oxide layer formation around molten Si, with or without Al/Ca additives*. Internal report, NTNU, Norway, 1999.

APPENDIX E

Analyses of Alloyed Silicon Rods

The alloyed silicon rods used in the experiments at the University of Wisconsin-Madison during 1999 were analyzed by Lilleby Metall, Trondheim, Norway. The results are shown in Table E-1.

Table E-1. Analyses of Alloyed Silicon Rods					
(Weight Percent)					
Batch					
Element	B	C	D		
Fe	0,028	0,033	0,032		
Ca	0,011	0,043	0,032		
Al	0,51	0,064	0,57		
C					
V	<0,001	<0,001	<0,001		
Cr	<0,001	<0,001	<0,001		
Ni	<0,001	<0,001	<0,001		
Cu	<0,001	<0,001	<0,001		
Mo	0,001	0,002	0,002		
Ti	0,005	0,006	0,005		
Mn	0,001	0,001	0,001		
Mg	0,002	0,002	0,002		
Co	0,003	0,002	0,002		
Zn	0,002	0,001	0,001		
Zr	0,001	0,001	0,001		
Pb	0,001	0,001	0,001		
Sn	0,001	<0,001	<0,001		